Electronic Supplementary Information for:

Waterproof Architectures through Subcomponent Self-Assembly

Edmundo G. Percástegui, Jesús Mosquera, Tanya K. Ronson, Alex J. Plajer, Marion Kieffer and Jonathan R. Nitschke*

Department of Chemistry, University of Cambridge, Lensfield Road, Cambridge CB2 1EW, United Kingdom

Table of Contents

1. General Experimental Procedures

Reagents were purchased from commercial suppliers and used without further purification. All manipulations were carried out in dry glassware under an inert atmosphere using standard Schlenk techniques. All solvents were distilled prior to use. Flash column chromatography was performed using Silica Gel high purity grade (pore size 60 Å, 230-400 mesh particle size, Sigma-Aldrich). TLC analyses were performed on Merck TLC Silica Gel 60 F254 Glass plates. Product spots were visualized under UV light (λmax = 254 nm). Centrifugation of samples was carried out using a Grant-Bio LMC-3000 low speed benchtop centrifuge.

NMR spectra were recorded on a Bruker Advance DPX 400 MHz Avance III HD Smart Probe (routine ^{1}H, ^{1}H wide-sweep, ^{13}C, and ^{19}F NMR) or Bruker Advance Cryo 500 spectrometer unless otherwise specified. Chemical shifts for ^{1}H, ^{13}C, and ^{19}F are reported in ppm on the δ scale; all coupling constants are reported in Hz. Signals on ^{1}H and ^{13}C spectra recorded in D_2O were referenced to an internal standard of tert-Butanol (δ = 1.24 ppm for ^{1}H and 30.29 ppm for $^{13}C\{^{1}H\}$) dissolved in D_2O at a concentration of 1.0 mM. Signals on ^{1}H spectra recorded in CD_3CN were referenced to the residual solvent peak (δ = 1.94 ppm). Chemical shifts (δ) for ^{19}F NMR spectra are reported relative to C_6F_6 (as an external standard in a capillary tube) at –164.9 ppm. DOSY experiments were performed using a maximum gradient strength of 6.57 G/cmA. The standard Bruker pulse program, ledbpgp2s, employing a stimulated echo and longitudinal eddy-current delay (LED) using bipolar gradient pulses for diffusion using 2 spoil gradients was utilized. Rectangular gradients were used with a total duration of 1.5 ms. Gradient recovery delays were 950–1400 μs. Diffusion times were 100 ms. Individual rows of the S4 quasi-2D diffusion databases were phased and baseline corrected. Hydrodynamic radii were calculated through the Stokes-Einstein equation by using the viscosity value of $\eta H_2O = 0.890 \times 10^{-3}$ kg/m·s, 298 K.

The ^{1}H wide-sweep paramagnetic NMR spectra were recorded in the analogue digitization mode with a spectral width (SW) of 372.98 ppm, a transmitter frequency offset (O1P) of 100.00 ppm and the line width set to 10.0 Hz. Due to the experimental difficulties associated with collecting NMR data for ^{1}H nuclei with vastly different relaxation times,

differences between measured and theoretical integration values were in some cases observed. While the paramagnetic nature of the complex precluded complete assignment of the proton environments, we suggest that the extent of downfield shifting of each resonance can be associated to the bond proximity of the proton environment to the Co^{II} centres; this has been proposed and observed in previous reports.[1,2]

Electrospray ionization (ESI-MS) mass spectra were obtained on a Micromass Quattro LC mass spectrometer infused from a Harvard syringe pump at a rate of 10 μL min^{-1}. The diverse sulfate derivatives of metal-organic capsules were dissolved in distilled H_2O (unless otherwise specified) and filtered prior to acquisition using different experimental conditions according to each metal ion: Co^{II}: cone voltage 22 eV; desolvation temp. 313 K; ionization temp. 313 K. Ni^{II}: cone voltage 33 eV; desolvation temp. 353 K; ionization temp. 353 K. Zn^{II}: cone voltage 22 eV; desolvation temp. 353 K; ionization temp. 353 K. Cd^{II}: cone voltage 22 eV; desolvation temp. 353 K; ionization temp. 353 K. The diverse acetonitrile-soluble metal-organic capsules (obtained as triflate, triflimide or tetrafluoroborate salts) were dissolved in acetonitrile and filtered prior to acquisition using different experimental conditions according to each metal ion: Co^{II}: cone voltage 22 eV; desolvation temp. 313 K; ionization temp. 313 K. Ni^{II}: cone voltage 33 eV; desolvation temp. 313 K; ionization temp. 313 K. Zn^{II}: cone voltage 18 eV; desolvation temp. 313 K; ionization temp. 313 K. Cd^{II}: cone voltage 18 eV; desolvation temp. 313 K; ionization temp. 313 K.

The construction of the diverse metal-organic capsules reported in this study entailed the *in situ* formation of dynamic imine bonds resulting from condensation of 2-formylpyridine with aniline-based subcomponents **A–C**. Likewise, reaction of formylpyridine-based subcomponents **D–H** with *p*-methoxy-aniline (anisidine), tris(2-aminoethyl)amine (TREN), or tris(3-aminopropyl)amine (TRPN) afforded the target ligand fragments (L). The different subcomponents **A–H** (Charts S1 and S2) employed in this study were prepared following previously reported methods:

(**A**) zinc(II) 5,10,15,20-tetrakis(4-aminophenyl)-21H, 23H-porphine[3]

(**B**) 1,3,5-tris(4'-aminophenyl)benzene[4]

(**C**) 4,4'-diaminobiphenyl[5]

(**D**) 1,3,5-tris(4’,4’’,4’’’-formylpyridine)benzene[6]

(**E**) 6,6’-diformyl-3,3’-bipyridine[7]

(**F**) 5,5′-(1,4-Phenylene)bis-2-pyridinecarboxaldehyde[8]

(**G**) 2,2'-(2,5-dimethyl-1,4-phenylene)bis-2-pyridinecarboxaldehyde[9]

(**H**) 5,5'-(Perfluoro-1,4-phenylene)bis-2-pyridinecarboxaldehyde.[10]

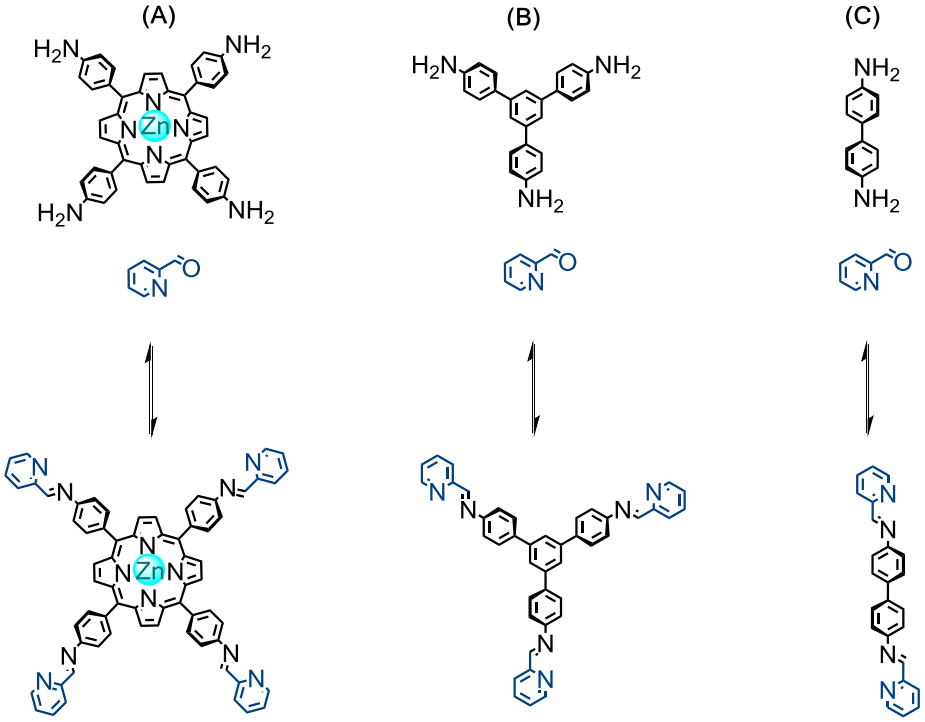

Chart S1. Aniline-based subcomponents **A–C** used to make metal-organic cages.

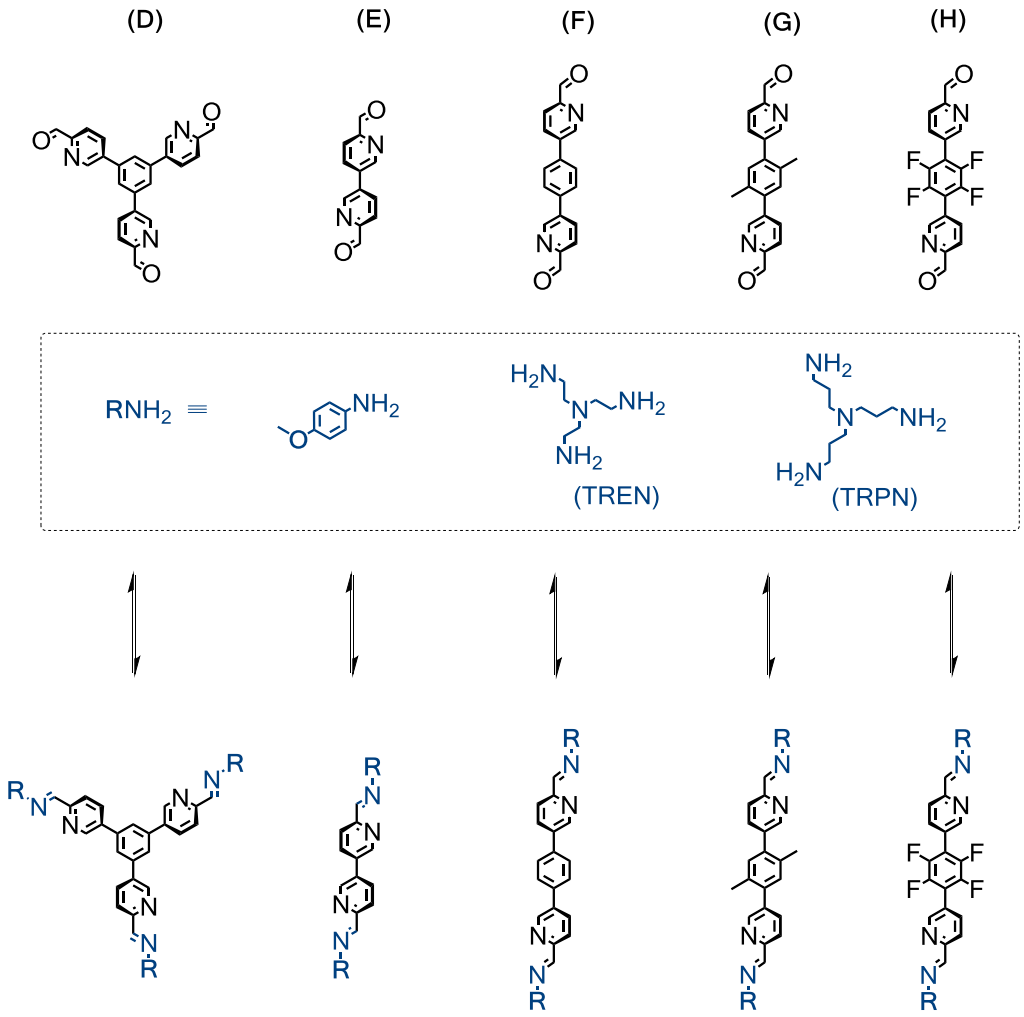

Chart S2. Formyl-pyridine subcomponents **D–H** used to make metal-organic cages.

2. Synthesis of acetonitrile-soluble cobalt(II)–based capsules and their anion-exchange sequences

The direct self-assembly of the cobalt(II)-based sulfate cages was attempted with porphyrin **A** and $CoSO_4$ in DMF or DMF/H_2O without success. Similarly, $CoSO_4$ was treated with subcomponents **B–E** in 1:1 CH_3CN/H_2O, 1:1 CH_3OH/H_2O, or 1:1:1 $CH_3CN/CH_3OH/H_2O$ solvent systems in order to prepare the corresponding water-soluble capsules; it was not possible to obtain the target sulfate salts of the cages. Hence, the preparation of the sulfate salts of Co^{II}-based cages was only accessible via anion exchange with sulfate from preformed acetonitrile-soluble subcomponent self-assembled cages.

The outcome of the diverse self-assembly reactions with Co^{II} ions to form the acetonitrile-soluble cages was sensitive to the identity of the counter anions involved. The reaction of aniline **B** with $Co(OTf)_2$ resulted in a mixture containing insoluble materials that could not be characterized as well as a products in solution, a $\mathbf{Co_2L_3}$ helicate and the $\mathbf{Co_4L_4}$ tetrahedral structure. Although the reaction of **B** and $CoSO_4$ afforded the target water-soluble capsule $\mathbf{Co–2{\bullet}SO_4}$ as the major product, some amount of a $\mathbf{Co_2L_3}$ water-soluble helicate was also formed and it could not be separated. Conversely, reaction of subcomponent **B** and $Co(NTf_2)_2$ gave tetrahedron $\mathbf{Co–2{\bullet}NTf_2}$ as a clean product.

Aniline **C** reacted with diverse CoX_2 (X = OTf^-, NTf_2^-, BF_4^-) salts to give a mixture of diastereomers of Co_4L_6 cages (**Co-3•**X). We previously observed **C** to self-assemble with Fe^{II} salts to produce mixtures of *T*, C_3, and S_4 diastereomers in different ratios depending on the anion.[5,11] The use of $Co(BF_4)_2$ provided the simplest NMR spectrum where seven intense signals could be distinguished that are consistent with the presence of the *T*-symmetric diastereomer as the major product, as when BF_4^- was used in the construction of the analogous Fe^{II}-based cage to yield the *T*-symmetric diastereomer.

Likewise, cage **Co–5** was obtained through the reported method1 that uses $Co(OTf)_2$ as the metal salt, whereas other salts produced different structures to the tetrahedral capsule.[12]

*2.1 Synthesis of the water-soluble **Co–1•SO$_4$** cube and its reversible conversion into acetonitrile-soluble **Co–1•OTf***

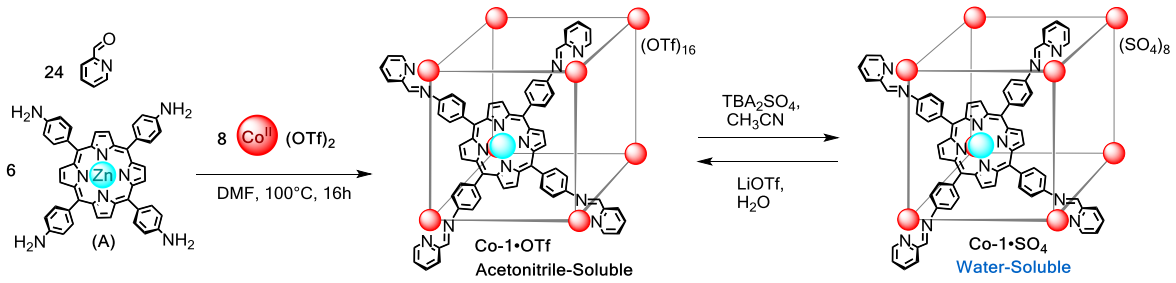

Subcomponent **A** (10.0 mg, 0.014 mmol, 6 equiv), 2-formylpyridine (5.2 µL, 0.054 mmol, 24 equiv), cobalt(II) triflate dihydrate (7.1 mg, 0.019 mmol, 8 equiv), and 2.0 mL of DMF were placed in a Schlenk flask. The mixture was degassed by three evacuation/nitrogen fill cycles and heated to 100°C overnight. After this time, the mixture was cooled to room temperature and diethyl ether (5 mL) was added leading to precipitation of a dark purple solid that was inferred to contain cube **Co-1•OTf**, the mixture was centrifuged and the supernatant DMF/Et_2O was decanted. The product was then twice dissolved in MeCN (2 mL) and precipitated with Et_2O (5 mL). **Co-1•OTf** was recovered as a purple solid (19.6 mg, yield 92%). Then, **Co-1•OTf** was dissolved in CH_3CN and tetrabutylammonium sulfate (TBA_2SO_4) solution 50wt % in H_2O (24 equivalents per cage) was added leading to precipitation of a purple solid, which was washed with CH_3CN:H_2O (9:1) and then with CH_3CN. Cube **Co-1•SO$_4$** was recovered as a dark purple solid (14.6 mg, yield 90%). ^{1}H NMR (400 MHz, D_2O, 298 K): δ = 245.2, 91.2, 75.5, 53.5, 17.8, 14.0, 8.7, 0.3, –3.4, –4.8, –63.9. ESI-MS (5:1 H_2O/CH_3CN): *m/z* = 635.6 [**Co-1**$(OTf)_4]^{+12}$, 707.5 [**Co-1**$(OTf)_5]^{+11}$, 793.0 [**Co-1**$(OTf)_6]^{+10}$, 897.8 [**Co-1**$(OTf)_7]^{+9}$, 1028.4 [**Co-1**$(OTf)_8]^{+8}$, 1196.7 [**Co-1**$(OTf)_9]^{+7}$, 1421.3 [**Co-1**$(OTf)_{10}]^{+6}$. Elemental analysis (%) calcd for $C_{408}H_{264}Co_8N_{72}O_{32}S_8Zn_6$•$8H_2O$•$CH_3CN$: C 61.61, H 3.57, N 12.79; found: C 61.82, H 3.54, N 12.70.

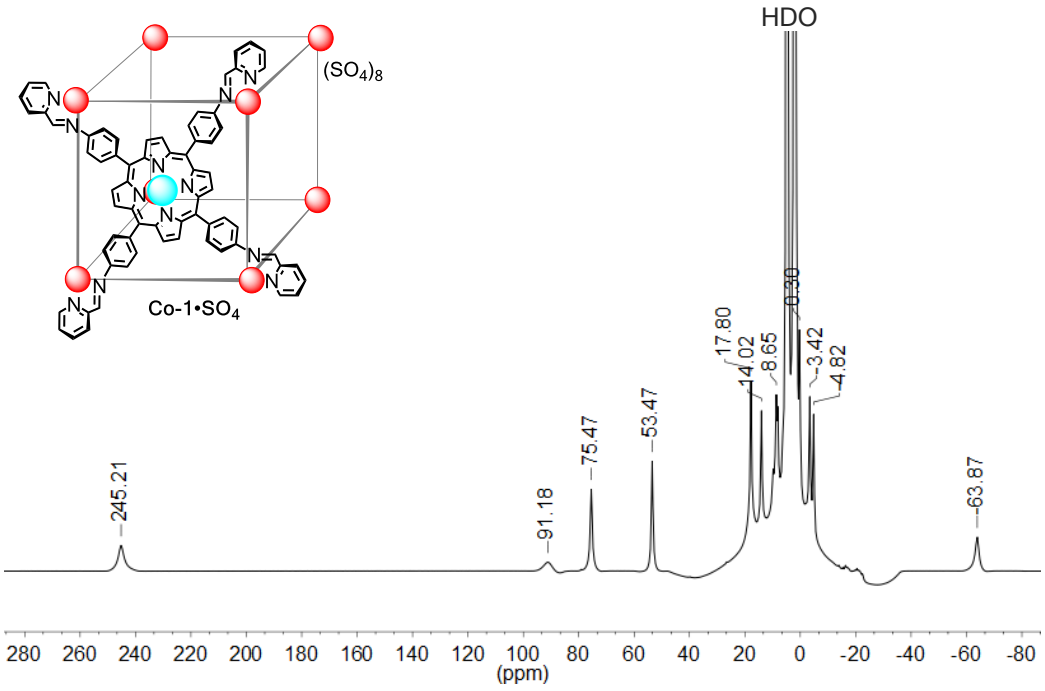

Figure S1. Wide sweep ^{1}H NMR spectrum (400 MHz, D_2O, 298 K) of cube **Co–1•SO$_4$**.

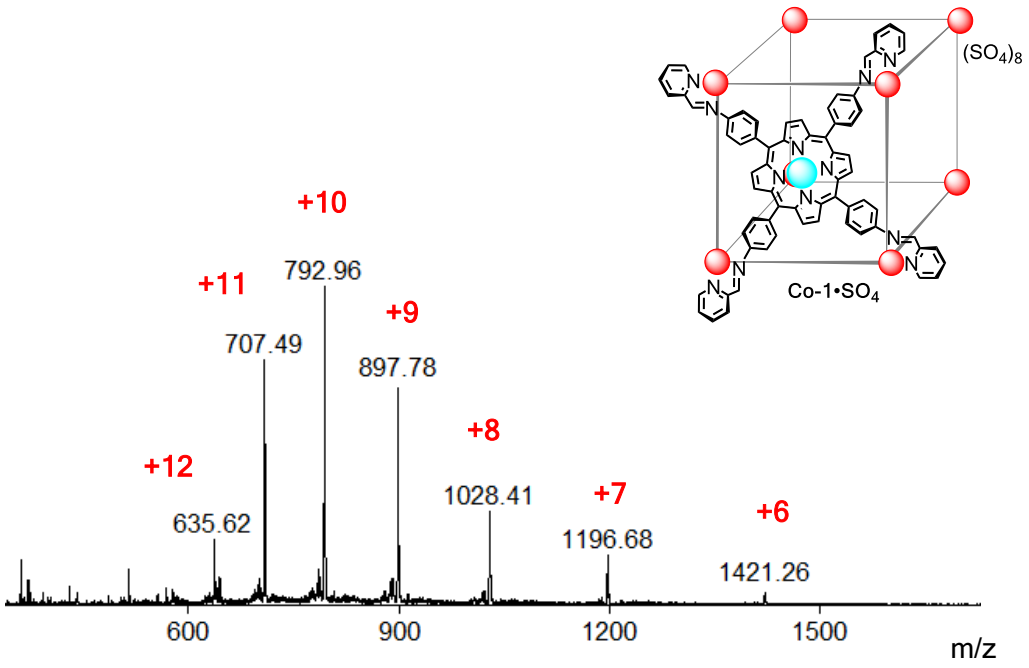

Figure S2. ESI-MS spectrum of cube **Co–1•SO$_4$** (5:1 H_2O/CH_3CN).

Addition of 24 equivalents of LiOTf (3 equiv per sulfate) to a D_2O solution of **Co-1•SO$_4$** (3.2 mg in 500 μL) induced precipitation of a purple solid in quantitative yield (3.5 mg, yield 92%), the mixture was centrifuged and the supernatant H_2O:D_2O was decanted; this

process was repeated two times with H_2O. NMR and ESI-MS analyses in CH_3CN confirmed that this solid corresponded to the former **Co-1•OTf** complex (Figures S3 and S4); spectroscopic details as follows: ^{1}H NMR (400 MHz, CD_3CN, 298 K): δ = 246.3, 90.0, 75.3, 53.1, 17.8, 14.0, 7.9, 0.2, –3.3, –5.1, –64.5. ESI-MS (CH_3CN): *m/z* = 524.0 [**Co-1**$(OTf)_2]^{+14}$, 575.7 [**Co-1**$(OTf)_3]^{+13}$, 636.0 [**Co-1**$(OTf)_4]^{+12}$, 707.4 [**Co-1**$(OTf)_5]^{+11}$, 793.0 [**Co-1**$(OTf)_6]^{+10}$, 897.7 [**Co-1**$(OTf)_7]^{+9}$, 1028.9 [**Co-1**$(OTf)_8]^{+8}$, 1197.0 [**Co-1**$(OTf)_9]^{+7}$, 1421.4 [**Co-1**$(OTf)_{10}]^{+6}$. Elemental analysis (%) calcd for $C_{424}H_{264}Co_8F_{48}N_{72}O_{48}S_{16}Zn_6$•$3H_2O$: C 53.03, H 2.98, N 10.50; found: C 53.17, H 2.84, N 10.48. Notably, X-ray quality crystals were obtained from this solution corroborating the molecular structure of the **Co-1** framework and further confirming the reversibility of the anion exchange process to regenerate the original **Co-1•OTf** complex (see X-ray crystallography section, *vide infra*).

Further addition of TBA_2SO_4 to an acetonitrile solution of this freshly regenerated **Co-1•OTf** induced precipitation of the water-soluble **Co-1•SO_4**. The complete **Co-1•OTf→Co-1•SO_4→Co-1•OTf** anion exchange cycle was carried twice out multiple times, with 90-94% recovery by weight per cycle.

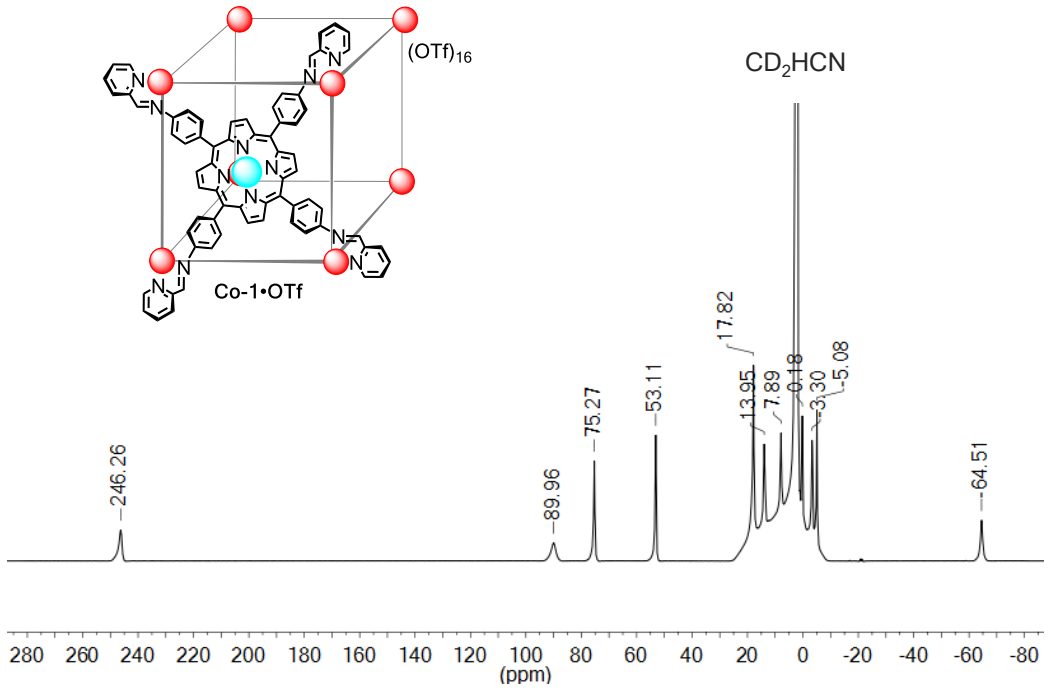

Figure S3. Wide sweep ^{1}H NMR spectrum (400 MHz, CD_3CN, 298 K) of cube **Co–1•OTf** obtained upon reversible anion exchange from **Co–1•SO_4**.

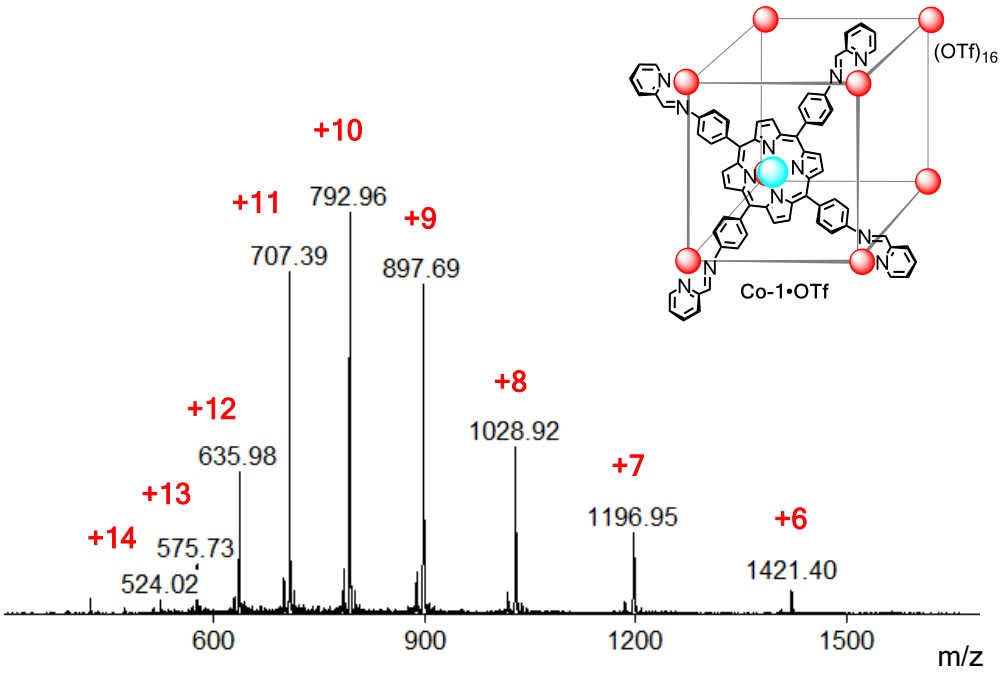

Figure S4. ESI-MS spectrum of cube **Co–1•OTf** (CH_3CN) obtained upon reversible anion exchange from **Co–1•SO_4**.

2.2 Synthesis of the water-soluble ***Co–2•SO₄*** *cage and its reversible conversion into the acetonitrile-soluble* ***Co–2•NTf₂***

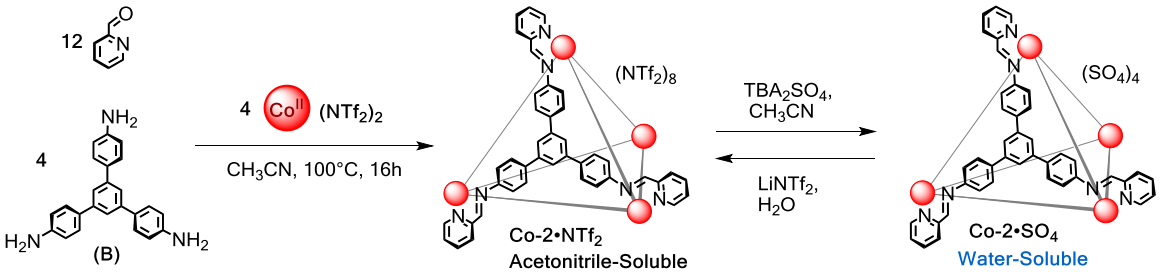

Subcomponent **B** (8.7 mg, 0.025 mmol, 4 equiv), 2-formylpyridine (6.9 µL, 0.075 mmol, 12 equiv), cobalt(II) triflimide (15.3 mg, 0.025 mmol, 4 equiv), and 2.0 mL of CH_3CN were placed in a thick-walled 25 mL sealed Schlenk tube. The mixture was degassed by three evacuation/nitrogen fill cycles and heated to reflux overnight. Cage **Co-2•NTf₂** was precipitated from the crude solution by addition of diethyl ether (5 mL), this suspension was centrifuged and the supernatant CH_3CN/Et_2O was decanted; the product was again dissolved in MeCN (2 mL) and precipitated with Et_2O (5 mL). Clean **Co-2•NTf₂** tetrahedron was recovered as an orange solid (27.9 mg, yield 91%). Then, **Co-2•NTf₂** cage was dissolved in CH_3CN and tetrabutylammonium sulfate (TBA_2SO_4) 50wt % solution in H_2O (12 equiv per cage) was added, inducing precipitation of a red solid, the mixture was centrifuged and the supernatant was decanted; this process was repeated with CH_3CN:H_2O (9:1), then with CH_3CN, and the excess solvent was removed with N_2. Cage **Co-2•SO₄** was obtained as a dark orange solid (16.00 mg, yield 92%). ^{1}H NMR (400 MHz, D_2O, 298 K): δ = 241.2, 87.3, 72.7, 51.3, 15.2, 1.5, –13.4, –19.6. ESI-MS (5:1 H_2O/CH_3CN): *m/z* = 426.9 [**Co-2**(NTf_2)]$^{+7}$, 545.1 [**Co-2**$(NTf_2)_2$]$^{+6}$, 710.3 [**Co-2**$(NTf_2)_3$]$^{+5}$, 957.9 [**Co-2**$(NTf_2)_4$]$^{+4}$, 1370.4 [**Co-2**$(NTf_2)_5$]$^{+6}$. Elemental analysis (%) calcd for $C_{168}H_{120}Co_4N_{24}O_{16}S_4$•2.5$H_2O$: C 64.26, H 4.01, N 10.71; found: C 64.46, H 3.98, N 10.76.

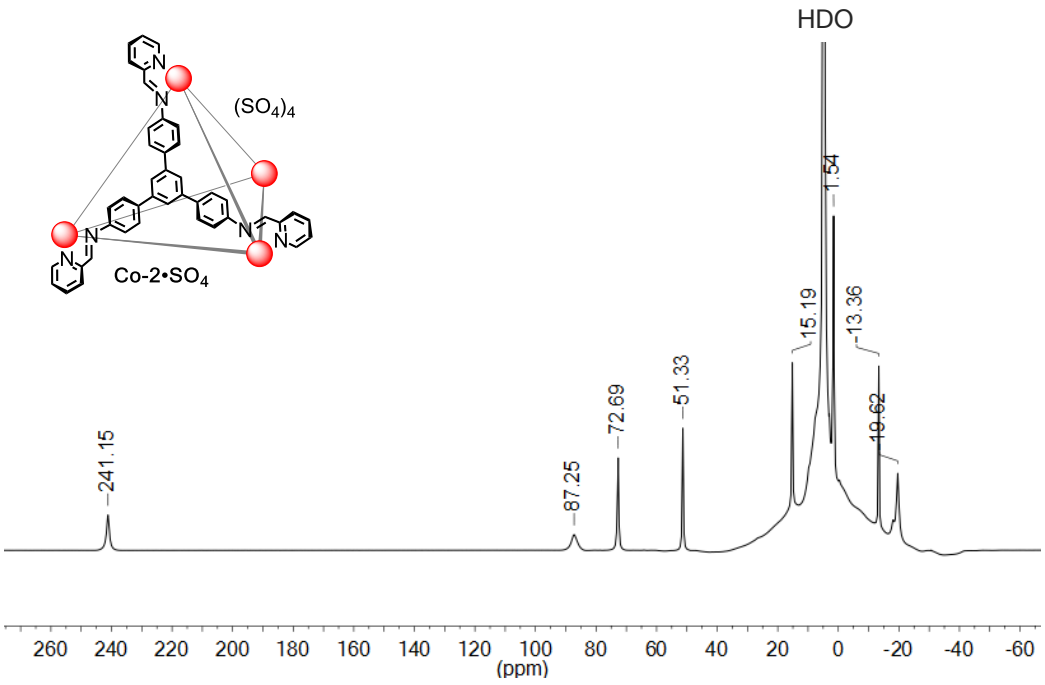

Figure S5. Wide sweep ^{1}H NMR spectrum (400 MHz, D_2O, 298 K) of **Co–2•SO$_4$**.

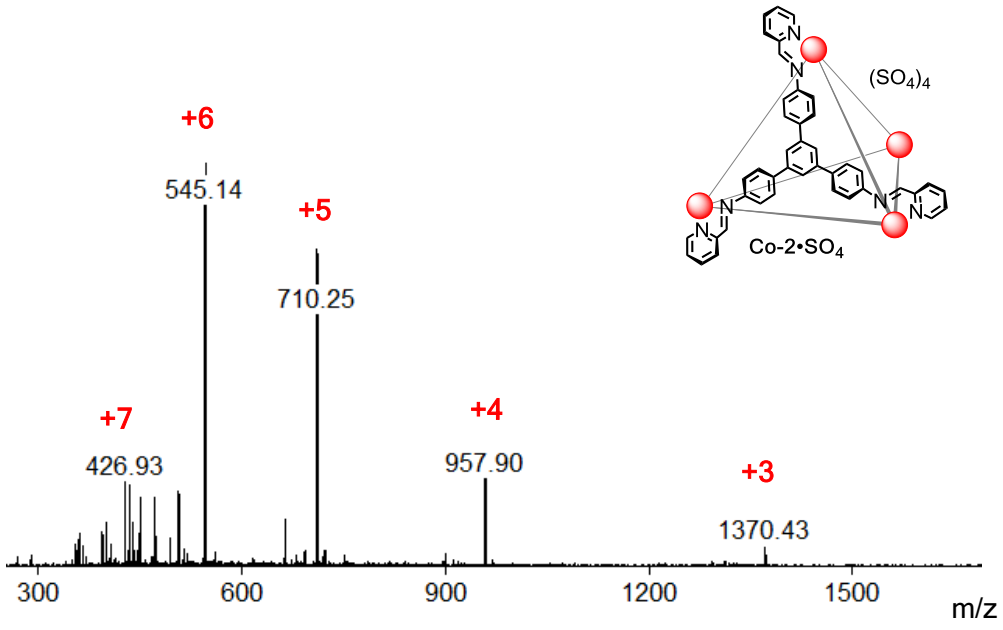

Figure S6. ESI-MS spectrum of cube **Co–2•SO$_4$** (5:1 H_2O/CH_3CN).

Addition of 12 equivalents of $LiNTf_2$ (1.5 equiv per sulfate) to a D_2O solution of **Co-2•SO$_4$** (4.2 mg in 500 μL) induced precipitation of a bright orange solid; the mixture was centrifuged and the solvent decanted (6.4 mg, yield 95%). NMR and ESI-MS analyses in CH_3CN confirmed that this solid corresponded to the former **Co-2•NTf$_2$** complex (Figures S7–S8); spectroscopic details as follows: ^{1}H NMR (400 MHz, CD_3CN, 298 K): δ = 240.2, 86.3, 72.3, 50.8, 15.0, 1.44, –13.3, –20.2. ESI-MS (CH_3CN): *m/z* = 338.1 [**Co-2**]$^{+8}$, 426.9 [**Co-2**(NTf_2)]$^{+7}$, 545.1 [**Co-2**$(NTf_2)_2$]$^{+6}$, 710.2 [**Co-2**$(NTf_2)_3$]$^{+5}$, 957.9 [**Co-2**$(NTf_2)_4$]$^{+4}$, 1370.5 [**Co-2**$(NTf_2)_5$]$^{+3}$. Elemental analysis (%) calcd for $C_{184}H_{120}Co_4F_{48}N_{32}O_{32}S_{16}$•$H_2O$: C 44.47, H 2.47, N 9.02; found: C 44.96, H 2.61, N 9.11.

Further addition of TBA_2SO_4 to an acetonitrile solution of this **Co-2•NTf$_2$** induced a second precipitation of the water-soluble **Co-2•SO$_4$**. The complete **Co-2•NTf$_2$→Co-2•SO$_4$→Co-2•NTf$_2$** anion exchange cycle was carried out multiple times, with 90-95% recovery by weight per cycle.

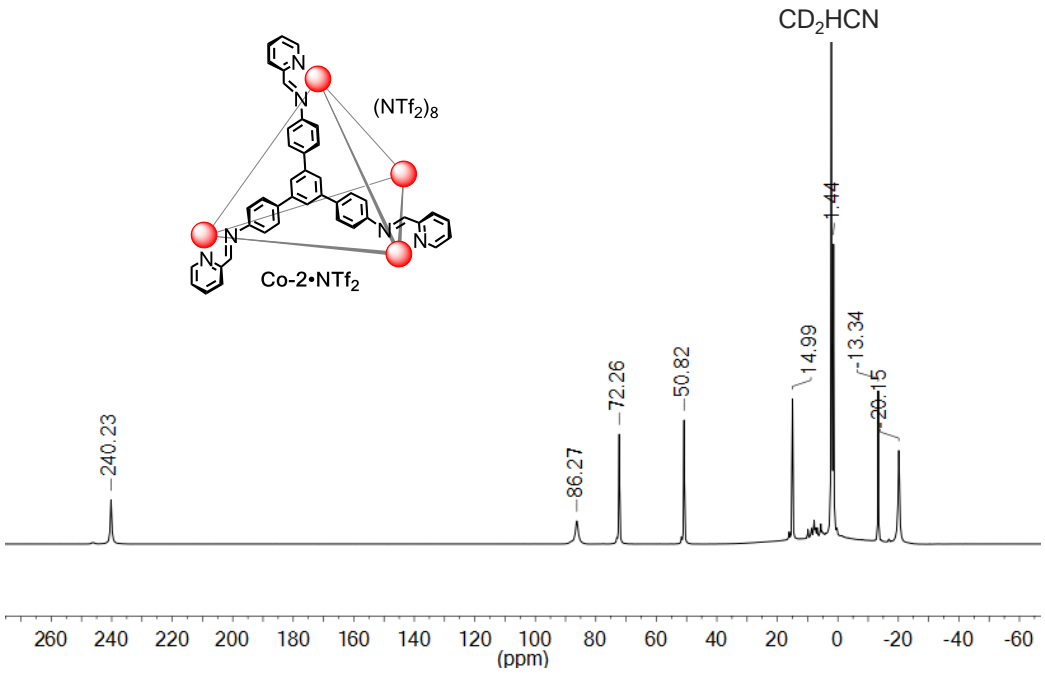

Figure S7. Wide sweep ^{1}H NMR spectrum (400 MHz, CD_3CN, 298 K) of **Co–2•NTf$_2$** obtained upon reversible anion exchange from **Co–2•SO$_4$**.

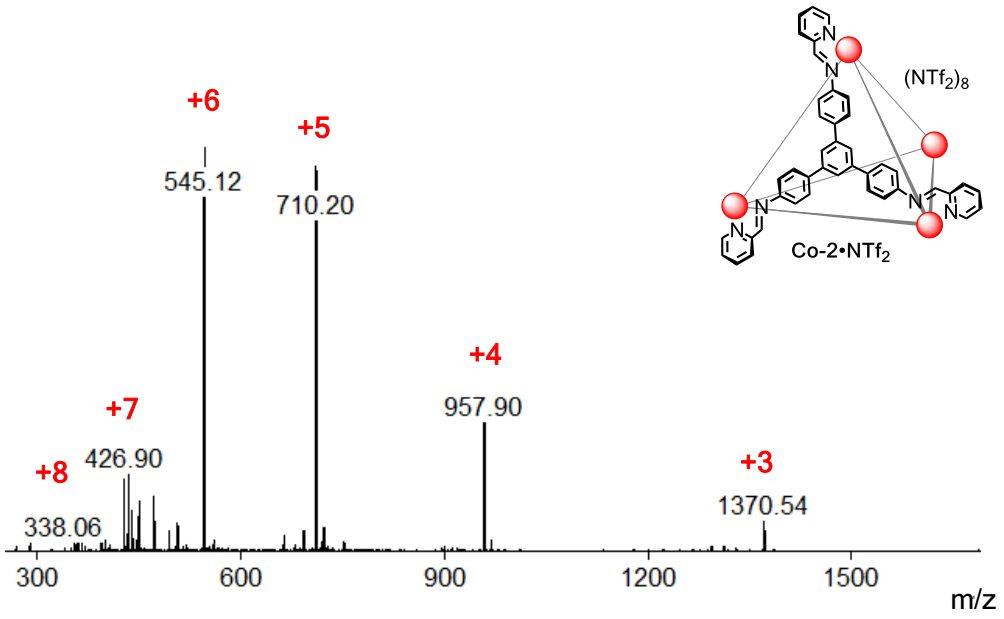

Figure S8. ESI-MS spectrum of **Co–2•NTf$_2$** (CH_3CN) obtained upon reversible anion exchange from **Co–2•SO$_4$**.

*2.3 Synthesis of acetonitrile-soluble **Co–3•BF$_4$** and its disassembly as **Co–3•SO$_4$** in water*

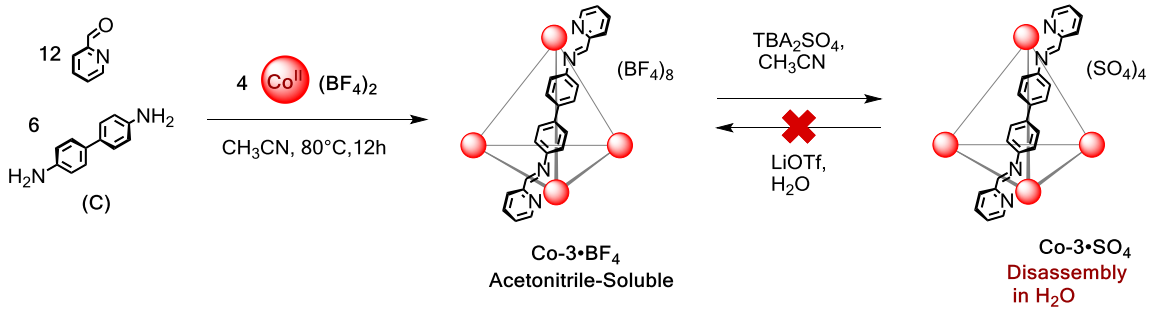

Subcomponent **C** (3.6 mg, 0.019 mmol, 6 equiv), 2-formylpyridine (3.6 μL, 0.039 mmol, 12 equiv), cobalt(II) tetrafluoroborate hexahydrate (4.4 mg, 0.013 mmol, 4 equiv), and 1.0 mL of CH_3CN were placed in a Schlenk flask. The mixture was degassed by three evacuation/nitrogen fill cycles and heated at 80°C overnight. Tetrahedron **Co-3•BF$_4$** was precipitated from the crude solution by addition of diethyl ether, this suspension was

centrifuged and the supernatant CH_3CN/Et_2O was decanted; this process was repeated with Et_2O and the excess solvent was removed by a gentle N_2 flow. Clean **Co-3•BF$_4$** cage was recovered as a dark orange solid (7.2 mg, yield 92%). ^{1}H NMR [Peaks corresponding to the main species, the *T–symmetric* isomer] (400 MHz, CD_3CN, 298 K): δ = 240.5, 85.9, 73.6, 51.3, 16.4, –2.1, –27.7. ESI-MS (CH_3CN): *m/z* = 356.7 [**Co-3**$(BF_4)]^{+7}$, 430.6 [**Co-3**$(BF_4)_2]^{+6}$, 534.1 [**Co-3**$(BF_4)_3]^{+5}$, 689.3 [**Co-3**$(BF_4)_4]^{+4}$, 948.3 [**Co-3**$(BF_4)_5]^{+3}$, 1465.5 [**Co-3**$(BF_4)_6]^{+2}$. Elemental analysis (%) calcd for $C_{144}H_{108}B_8Co_4F_{32}N_{24}$•$2CH_3CN$: C 55.78, H 3.61, N 11.43; found: C 56.12, H 3.72, N 11.38.

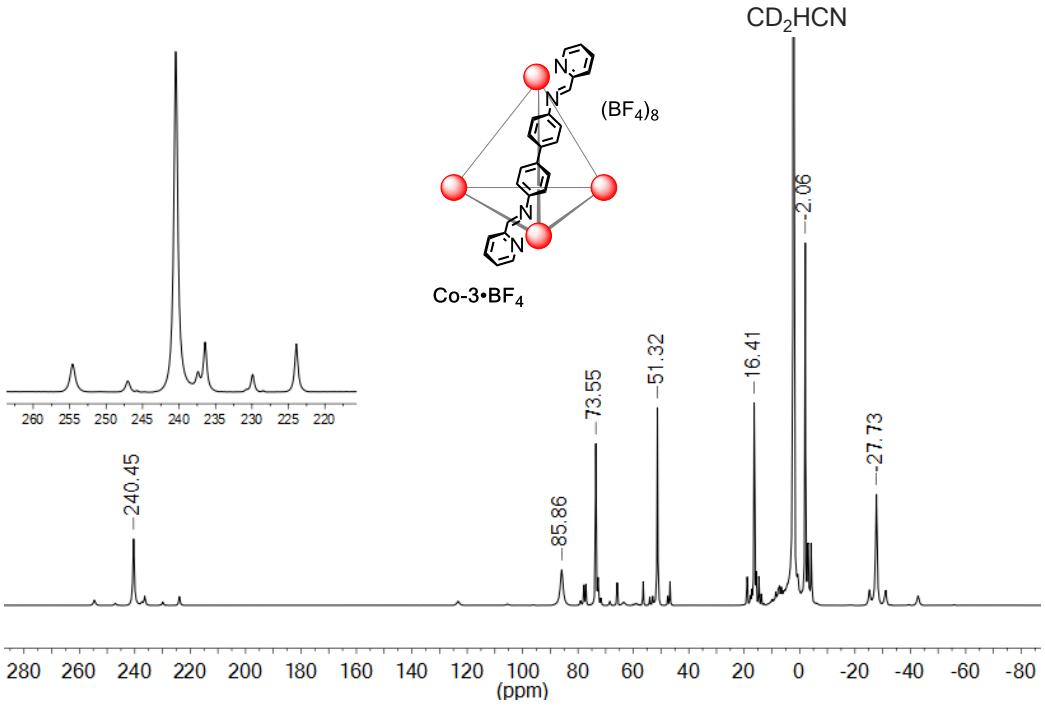

Figure S9. Wide sweep ^{1}H NMR spectrum (400 MHz, CD_3CN, 298 K) of **Co–3•BF$_4$**. Deconvolution of the imine region can be observed as indication of the presence of different diasteromers (*T*, C_3, S_4); major peaks in the spectrum correspond to the *T* isomer that is estimated to account for *ca.* 72% of the total distribution.

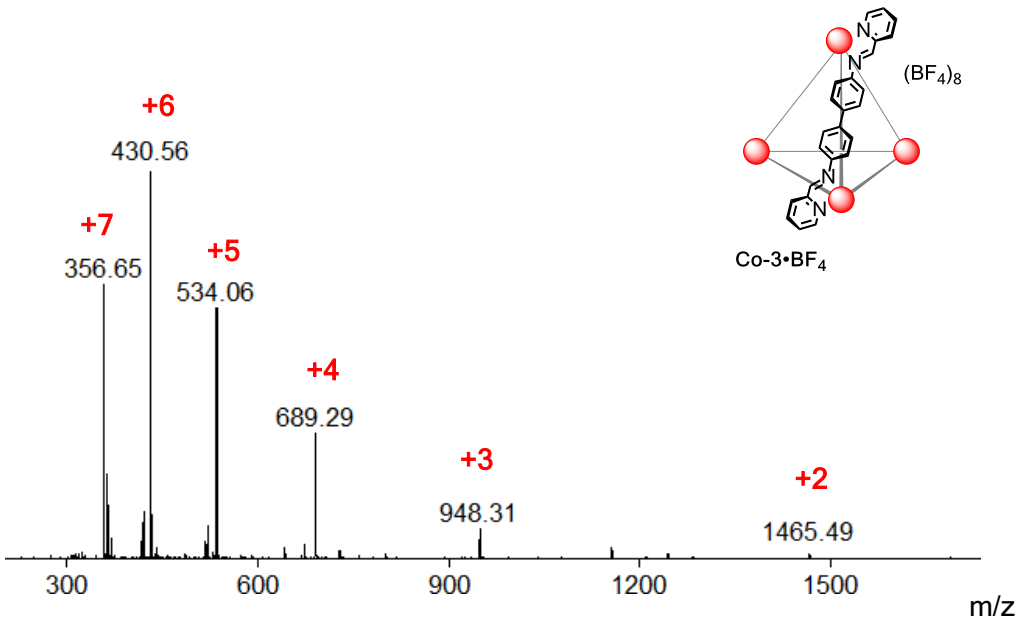

Figure S10. ESI-MS spectrum of **Co–3•BF_4** (CH_3CN).

Then, **Co-3•BF_4** cage was dissolved in CH_3CN and tetrabutylammonium sulfate (TBA_2SO_4) solution 50wt % in H_2O (12 equivalents per cage) was added leading to precipitation of a dark orange solid that was inferred to contain cage **Co-3•SO_4**; the mixture was centrifuged and the supernatant was decanted; this process was repeated with CH_3CN and the excess solvent was removed with N_2. Although this dark orange solid could be dissolved in pure water, it rapidly decomposed as evidenced by cloudiness of the red solution and precipitation of dianiline **C** within the first 10 minutes after dissolution.

*2.4 Synthesis of acetonitrile-soluble **Co–4•OTf** and its disassembly as **Co–4•SO₄** in water*

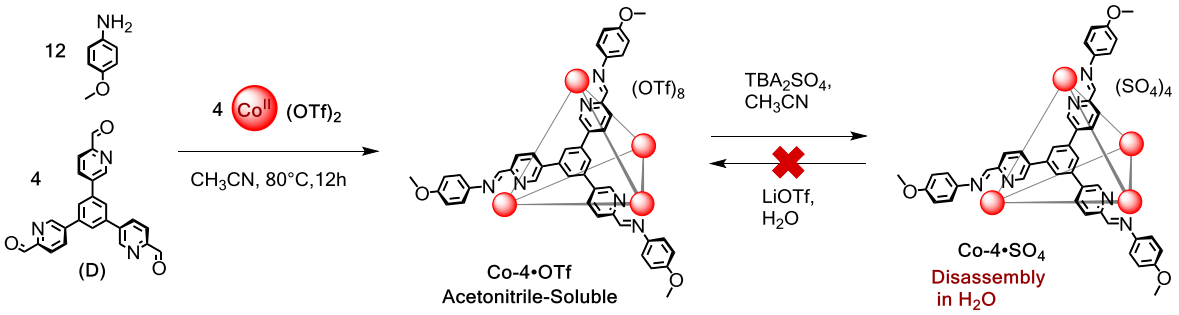

Subcomponent **D** (4.0 mg, 0.010 mmol, 4 equiv), 4-methoxyaniline (3.7 mg, 0.031 mmol, 12 equiv), cobalt(II) triflate dihydrate (4.0 mg, 0.010 mmol, 4 equiv), and 1.0 mL of CH_3CN were placed in a Schlenk flask. The mixture was degassed by three evacuation/nitrogen fill cycles and heated at 80°C overnight. Tetrahedron **Co-4•OTf** was precipitated from the crude solution by addition of diethyl ether, this suspension was centrifuged and the supernatant CH_3CN/Et_2O was decanted; this process was repeated with Et_2O. Clean **Co-4•OTf** cage was recovered as a dark orange solid (6.88 mg, yield 87%). ^{1}H NMR (400 MHz, CD_3CN, 298 K): δ = 246.4, 75.8, 71.1, 10.6, 8.0, 0.9, –12.1, –21.6. ESI-MS (CH_3CN): *m/z* = 460.4 [**Co-4**(OTf)]$^{+7}$, 561.8 [**Co-4**$(OTf)_2$]$^{+6}$, 703.7 [**Co-4**$(OTf)_3$]$^{+5}$, 917.6 [**Co-4**$(OTf)_4$]$^{+4}$, 1273.3 [**Co-4**$(OTf)_5$]$^{+3}$. Elemental analysis (%) calcd for $C_{188}H_{144}Co_4F_{24}N_{24}O_{36}S_8$•$H_2O$: C 52.52, H 3.47, N 7.82; found: C 52.62, H 3.55, N 7.88.

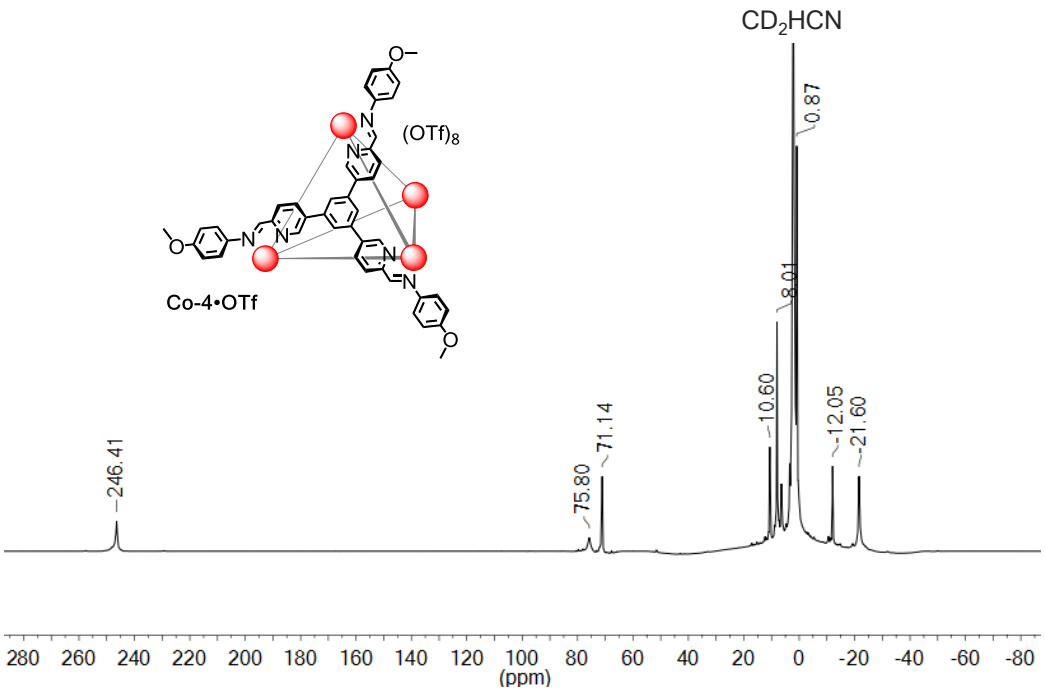

Figure S11. Wide sweep ^{1}H NMR spectrum (400 MHz, CD_3CN, 298 K) of **Co–4•OTf**.

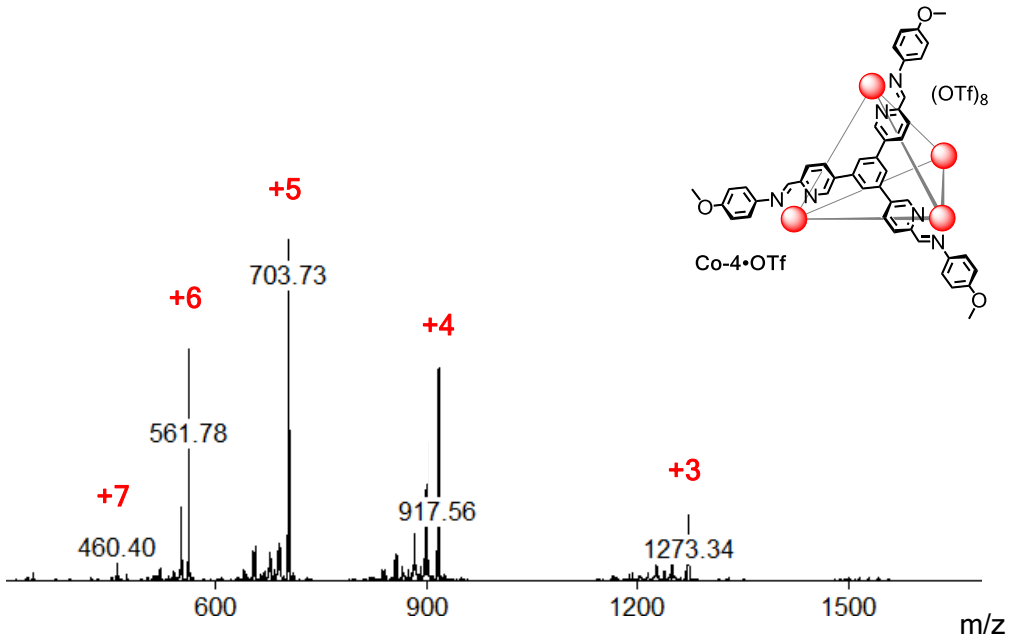

Figure S12. ESI-MS spectrum of **Co–4•OTf** (CH_3CN).

Then, **Co-4•OTf** capsule was dissolved in CH_3CN and tetrabutylammonium sulfate (TBA_2SO_4) solution 50wt % in H_2O (12 equivalents per cage) was added leading to precipitation of a dark orange solid that was inferred to contain cage **Co-4•SO_4**; the mixture was centrifuged and the supernatant was decanted; this process was repeated with CH_3CN and the excess solvent was removed with N_2. Although the dark orange solid could be dissolved after immediate addition of pure water, it rapidly decomposed as evidenced by cloudiness of the orange solution and precipitation of aldehyde **D** within the first 10 minutes after dissolution.

*2.5 Synthesis of acetonitrile-soluble **Co–5•OTf** and its disassembly as **Co–5•SO_4** in water*

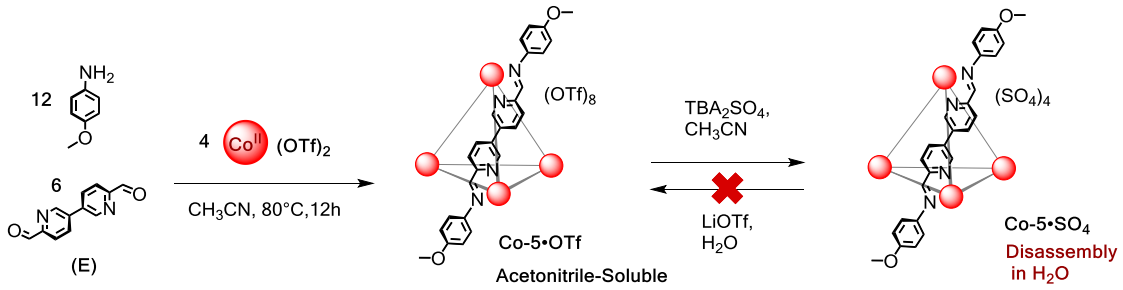

Capsule **Co-5•OTf** was prepared following our previously reported method.1 Subcomponent **E** (4.0 mg, 0.019 mmol, 6 equiv), 2-formylpyridine (3.6 µL, 0.039 mmol, 12 equiv), cobalt(II) triflate dihydrate (4.6 mg, 0.013 mmol, 4 equiv), and 1.0 mL of CH_3CN were placed in a Schlenk flask. The mixture was degassed by three evacuation/nitrogen fill cycles and heated at 80°C overnight. Clean **Co-5•OTf** cage was recovered as a dark orange solid by addition of diethyl ether (9.9 mg, yield 86%). The NMR and ESI-MS data fully correspond to those previously obtained. ESI-MS (CH_3CN): *m/z* = 512.8 [**Co-5**$(OTf)_2]^{+6}$, 643.7 [**Co-5**$(OTf)_3]^{+5}$, 842.0 [**Co-5**$(OTf)_4]^{+4}$, 1172.3 [**Co-5**$(OTf)_5]^{+3}$.

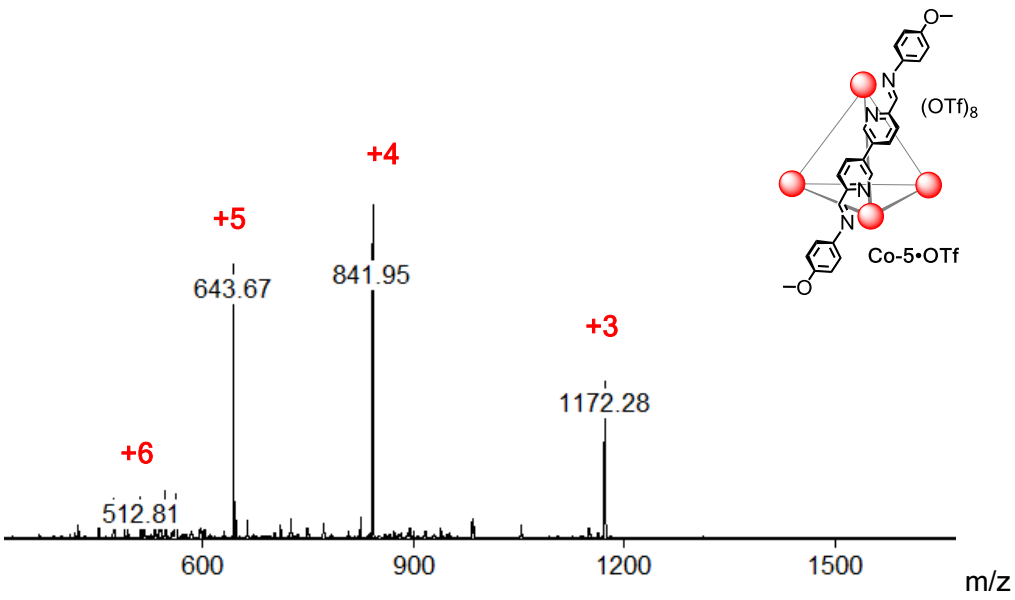

Figure S13. ESI-MS spectrum of **Co–5•OTf** (CH_3CN).

Next, **Co-5•OTf** capsule was dissolved in CH_3CN and tetrabutylammonium sulfate (TBA_2SO_4) solution 50wt % in H_2O (12 equivalents per cage) was added leading to precipitation of a dark orange solid that was inferred to contain cage **Co-5•SO_4**; the mixture was centrifuged and the supernatant was decanted; this process was repeated with CH_3CN and the excess solvent was removed with N_2. Although the dark orange solid could be dissolved after immediate addition of pure water, it rapidly decomposed as evidenced by cloudiness of the red solution and precipitation of aldehyde **E** within the first 10 minutes after dissolution.

3. Synthesis of water-soluble nickel(II)–based capsules and their anion-exchange sequences

The direct self-assembly of the nickel(II)-based sulfate tetrahedral **Ni-2** to **Ni-4** cages was possible through combination of subcomponents **B–D** with $NiSO_4$. Conversely, all attempts to generate the corresponding water-soluble cube from direct assembly of porphyrin **A** with $NiSO_4$ were unsuccessful in the following mixtures of solvents: 1:1 CH_3CN/H_2O, 1:1 DMF/H_2O, or in pure DMF; however, the water-soluble target capsule was obtained via anion exchange with sulfate salts.

*3.1 Synthesis of the water-soluble **Ni–1•SO$_4$** cube and its reversible conversion into the acetonitrile-soluble **Ni–1•OTf** cube*

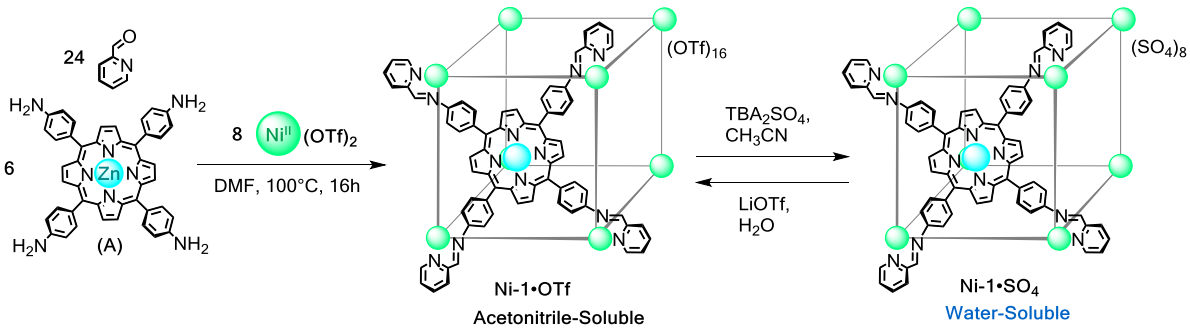

Subcomponent **A** (10.0 mg, 0.014 mmol, 6 equiv), 2-formylpyridine (5.2 µL, 0.054 mmol, 24 equiv), nickel(II) triflate (6.8 mg, 0.019 mmol, 8 equiv), and 2.0 mL of DMF were placed in a Schlenk flask. The mixture was degassed by three evacuation/nitrogen fill cycles and heated at 100°C overnight. Addition of diethyl ether to the crude solution induced precipitation of a dark purple solid that was inferred to contain cube **Ni-1•OTf**, the mixture was centrifuged and the supernatant DMF/Et_2O was decanted; this process was repeated two times with Et_2O. Clean **Ni-1•OTf** cube was recovered as a purple solid (17.9 mg, yield 84%). Next, **Ni-1•OTf** cage was dissolved in CH_3CN and tetrabutylammonium sulfate (TBA_2SO_4) solution 50wt % in H_2O (24 equivalents per cage) was added leading to

precipitation of a purple solid, the mixture was centrifuged and the supernatant was decanted; this process was repeated with CH_3CN:H_2O (9:1) and with CH_3CN for the last time. Cube **Ni-1•SO_4** was obtained as a dark red to crimson solid (13.2 mg, yield 89%). ESI-MS (5:1 H_2O/CH_3CN): *m/z* = 636.0 [**Ni-1**$(OTf)_4]^{+12}$, 707.3 [**Ni-1**$(OTf)_5]^{+11}$, 792.9 [**Ni-1**$(OTf)_6]^{+10}$, 897.8 [**Ni-1**$(OTf)_7]^{+9}$, 1028.5 [**Ni-1**$(OTf)_8]^{+8}$, 1196.8 [**Ni-1**$(OTf)_9]^{+7}$, 1421.0 [**Ni-1**$(OTf)_{10}]^{+6}$, 1735.0 [**Ni-1**$(OTf)_{11}]^{+5}$. Elemental analysis (%) calcd for $C_{408}H_{264}N_{72}Ni_8O_{32}S_8Zn_6$•$4H_2O$•$2CH_3CN$: C 62.17, H 3.52, N 13.02; found: C 62.24, H 3.56, N 13.00.

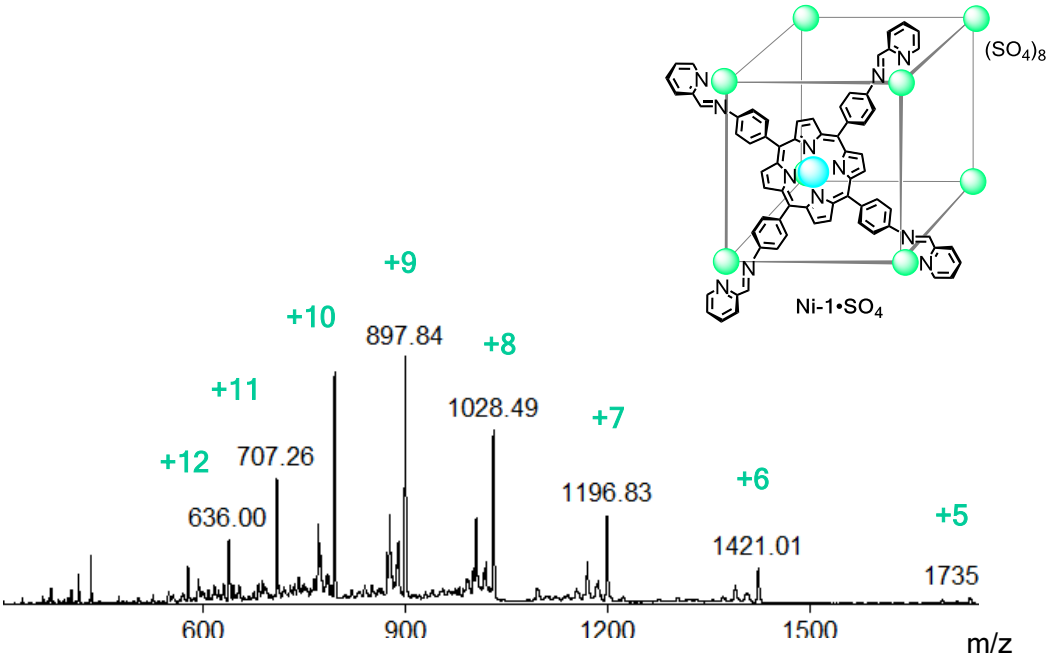

Figure S14. ESI-MS spectrum of **Ni–1•SO_4** (5:1 H_2O/CH_3CN).

Addition of 24 equivalents of LiOTf (1.5 equiv per sulfate) to a H_2O solution of **Ni-1•SO_4** (5.0 mg in 500 μL) induced precipitation of a purple solid in quantitative yield (5.67 mg, yield 94%); the mixture was centrifuged and the supernatant H_2O was decanted; this process was repeated two times with H_2O. ESI-MS recorded in CH_3CN confirmed that this solid corresponded to the former **Ni-1•OTf** complex (Figure S15); spectroscopic details as

follows: ESI-MS (CH_3CN): *m/z* = 524.0 [**Ni-1**$(OTf)_2]^{+14}$, 573.7 [**Ni-1**$(OTf)_3]^{+13}$, 636.0 [**Ni-1**$(OTf)_4]^{+12}$, 707.4 [**Ni-1**$(OTf)_5]^{+11}$, 792.8 [**Ni-1**$(OTf)_6]^{+10}$, 898.0 [**Ni-1**$(OTf)_7]^{+9}$, 1029.0 [**Ni-1**$(OTf)_8]^{+8}$, 1197.0 [**Ni-1**$(OTf)_9]^{+7}$, 1421.4 [**Ni-1**$(OTf)_{10}]^{+6}$. Elemental analysis (%) calcd for $C_{424}H_{264}F_{48}N_{72}Ni_8O_{48}S_{16}Zn_6$•$9.5H_2O$: C 53.09, H 2.97, N 10.51; found: C 53.12, H 2.94, N 10.32. Notably, X-ray quality crystals were obtained from this solution corroborating the molecular structure of the **Ni-1** framework and further confirming the reversibility of this process to regenerate the original **Ni-1•OTf** complex (see X-ray crystallography section, *vide infra*).

Subsequently, further addition of TBA_2SO_4 to an acetonitrile solution of this freshly regenerated **Ni-1•OTf** induced a precipitation of the water-soluble **Ni-1•SO_4**. The complete **Ni-1•OTf→Ni-1•SO_4→Ni-1•OTf** anion exchange cycle was carried out multiple times, with 88-94% recovery by weight per cycle.

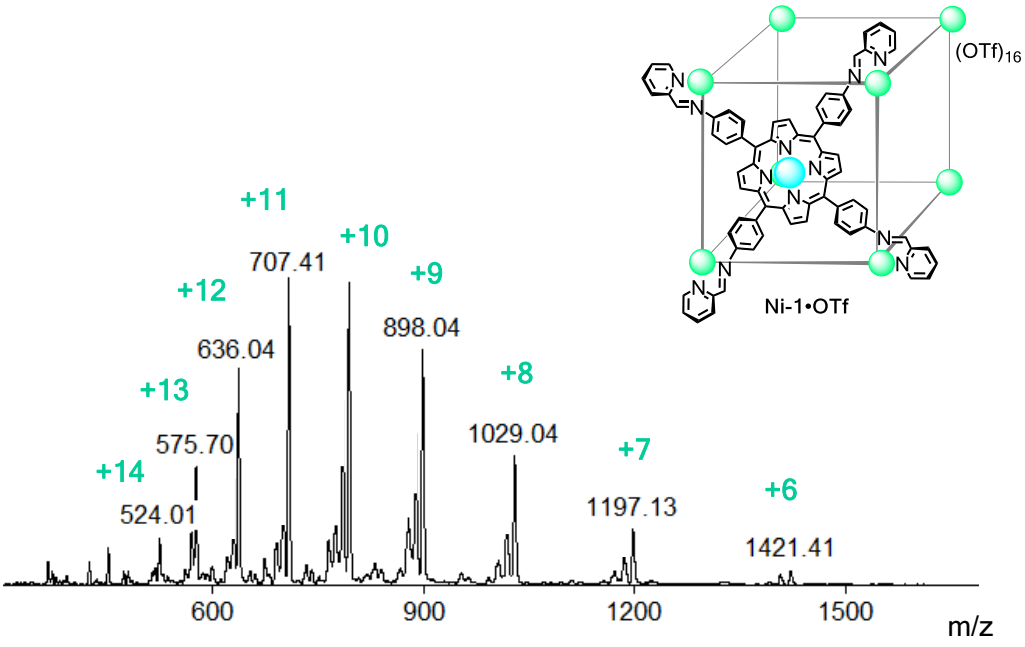

Figure S15. ESI-MS spectrum of **Ni–1•OTf** (CH_3CN) obtained upon reversible anion exchange from **Ni–1•SO_4**.

*3.2 Synthesis of the water-soluble tetrahedron **Ni–2•SO₄** and its reversible conversion into the acetonitrile-soluble **Ni–2•OTf** cage.*

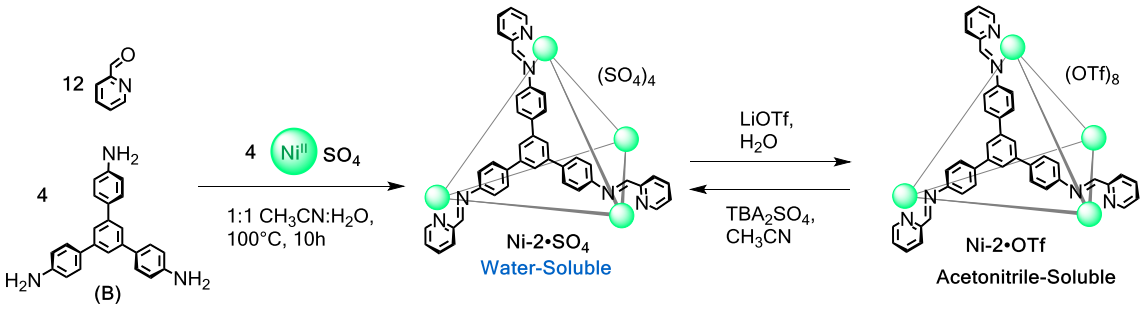

Subcomponent **B** (5.0 mg, 0.014 mmol, 4 equiv), 2-formylpyridine (4.0 μL, 0.043 mmol, 12 equiv), nickel(II) sulfate hexahydrate (3.7 mg, 0.014 mmol, 4 equiv), and 1.5 mL of 1:1 CH_3CN/H_2O solution were placed in a Schlenk flask. The mixture was degassed by three evacuation/nitrogen fill cycles and heated at 100°C overnight giving a dark orange solution. Afterward, the crude solution was cooled down to room temperature and excess of cold acetonitrile was added leading to precipitation of an orange solid. The mixture was centrifuged and the supernatant CH_3CN/H_2O was decanted, this process was repeated with CH_3CN:H_2O (9:1), then with CH_3CN, and the excess solvent was removed under N_2 flow. Clean **Ni–2•SO₄** was recovered as a pale orange solid (9.4 mg, yield 86%). ESI-MS (H_2O): *m/z* = 338.5 $[\mathbf{Ni\text{-}2}]^{+8}$, 393.4 $[\mathbf{Ni\text{-}2}(CHO_2)]^{+7}$, 467.2 $[\mathbf{Ni\text{-}2}(SO_4)]^{+6}$, 573.4 $[\mathbf{Ni\text{-}2}(SO_4)(NO_3)]^{+5}$, 734.3 $[\mathbf{Ni\text{-}2}(SO_4)(HSO_4)(CHO_2)]^{+4}$. Elemental analysis (%) calcd for $C_{168}H_{120}N_{24}Ni_4O_{16}S_4•H_2O•CH_3CN$: C 64.76, H 4.00, N 11.11; found: C 64.96, H 3.95, N 11.09.

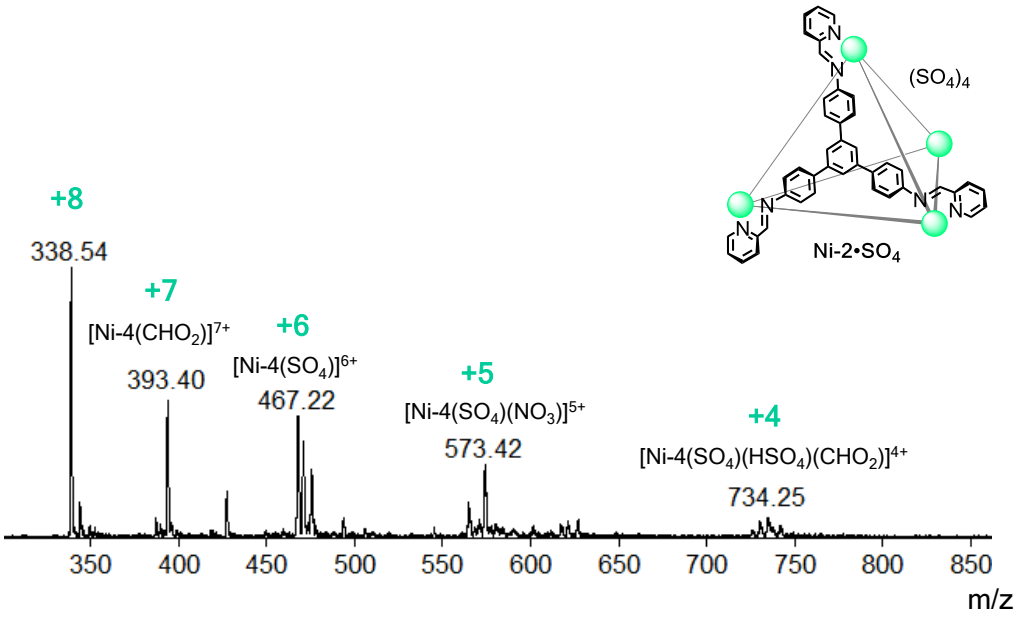

Figure S16. ESI-MS spectrum of **Ni–2•SO_4** (H_2O).

Addition of 12 equivalents of LiOTf (1.5 equiv per sulfate) to an aqueous solution of **Ni-2•SO_4** (5.5 mg in 500 μL) induced precipitation of a pale yellow solid, the mixture was centrifuged and the solvent decanted yielding cage **Ni-2•OTf** in almost quantitative yield (6.41 mg, yield 93%). ESI-MS analyses in CH_3CN confirmed that this solid corresponded to **Ni-2•OTf** complex (Figures S17); spectroscopic details as follows: ESI-MS (CH_3CN): *m/z* = 338.7 [**Ni-2**]$^{+8}$, 408.2 [**Ni-2**(OTf)]$^{+7}$, 501.2 [**Ni-2**$(OTf)_2$]$^{+6}$, 631.8 [**Ni-2**$(OTf)_3$]$^{+5}$, 826.3 [**Ni-2**$(OTf)_4$]$^{+4}$, 1151.7 [**Ni-2**$(OTf)_5$]$^{+3}$. Elemental analysis (%) calcd for $C_{176}H_{120}F_{24}N_{24}Ni_4O_{24}S_8$•$2H_2O$: C 53.68, H 3.17, N 8.54; found: C 53.78, H 3.28, N 8.80.

Addition of TBA_2SO_4 to an acetonitrile solution of this **Ni-2•OTf** induced precipitation of the former water-soluble **Ni-2•SO_4**. The complete **Ni-2•SO_4**→**Ni-2•OTf**→**Ni-2•SO_4** anion exchange cycle was carried out multiple times, with 87-93% recovery by weight per cycle.

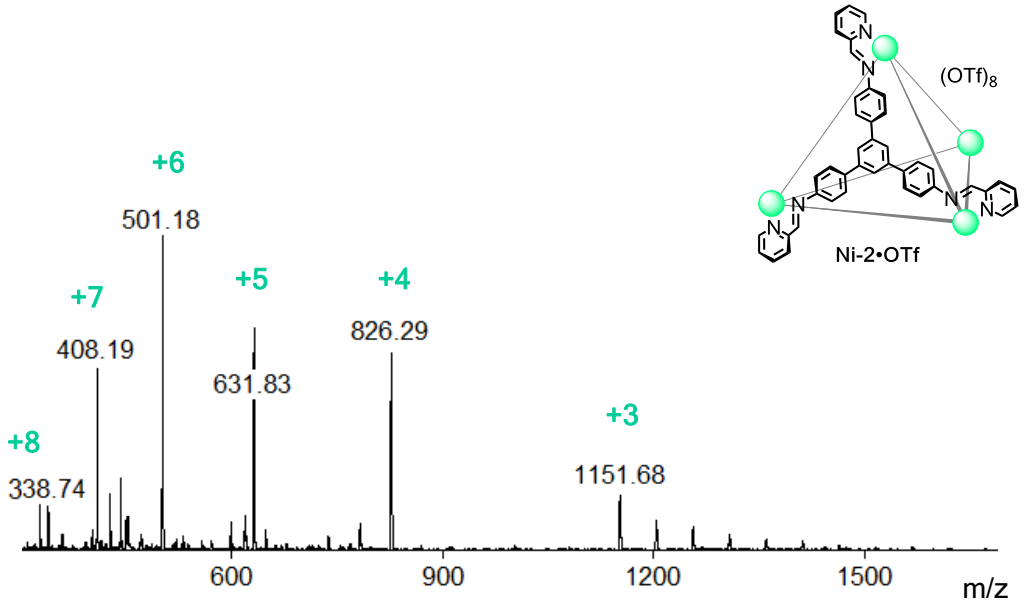

Figure S17. ESI-MS spectrum of **Ni–2•OTf** (CH_3CN) obtained upon reversible anion exchange from **Ni–2•SO_4**.

*3.3 Synthesis of the water-soluble tetrahedron **Ni–3•SO_4** and its reversible conversion into the acetonitrile-soluble **Ni–3•OTf** cage.*

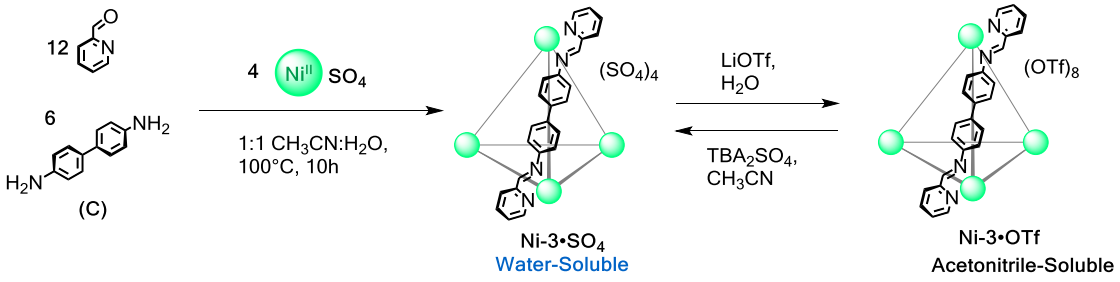

Subcomponent **C** (3.2 mg, 0.017 mmol, 6 equiv), 2-formylpyridine (3.3 μL, 0.043 mmol, 12 equiv), nickel(II) sulfate hexahydrate (2.8 mg, 0.011 mmol, 4 equiv), and 1.5 mL of 1:1 CH_3CN/H_2O solution were placed in a Schlenk flask. The mixture was degassed by three evacuation/nitrogen fill cycles and heated at 100°C overnight giving a dark yellow solution.

Afterward, the crude solution was cooled down to room temperature and excess cold acetonitrile was added until a yellow solid precipitated out from the solution. The mixture was centrifuged and the supernatant CH_3CN/H_2O was decanted, this process was repeated with $CH_3CN:H_2O$ (9:1), then with CH_3CN, and the excess solvent was removed under N_2 flow. Cage **Ni–3•SO$_4$** was recovered as a pale yellow solid (7.1 mg, yield 88%). ESI-MS (H_2O): *m/z* = 301.1 [**Ni-3**]$^{+8}$, 417.4 [**Ni-3**(SO_4)]$^{+6}$, 650.4, [**Ni-3**$(SO_4)_2$]$^{+4}$. Elemental analysis (%) calcd for $C_{144}H_{108}N_{24}Ni_4O_{16}S_4$•$2CH_3CN$: C 61.82, H 4.00, N 12.66; found: C 61.98, H 4.10, N 12.76.

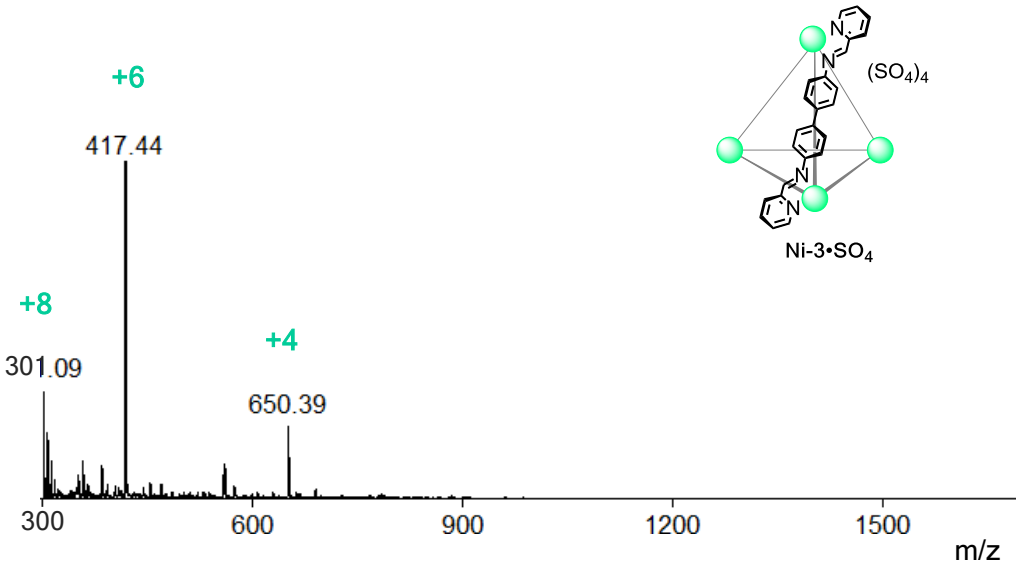

Figure S18. ESI-MS spectrum of **Ni–3•SO$_4$** (H_2O).

Addition of 12 equivalents of LiOTf (1.5 equiv per sulfate) to an aqueous solution of **Ni-3•SO$_4$** (6.5 mg in 500 μL) induced precipitation of a pale yellow solid, the mixture was centrifuged and the solvent decanted yielding cage **Ni-3•OTf** in quantitative yield (7.8 mg, yield 93%). ESI-MS analyses in CH_3CN confirmed that this solid corresponded to the **Ni-3•OTf** complex (Figure S19); spectroscopic details as follows: ESI-MS (CH_3CN): *m/z* = 365.3 [**Ni-3**(OTf)]$^{+7}$, 451.0 [**Ni-3**$(OTf)_2$]$^{+6}$, 571.0 [**Ni-3**$(OTf)_3$]$^{+5}$, 751.1 [**Ni-3**$(OTf)_4$]$^{+4}$, 1051.2 [**Ni-3**$(OTf)_5$]$^{+3}$, 1651.6 [**Ni-3**$(OTf)_6$]$^{+2}$. Elemental analysis (%) calcd for

$C_{152}H_{108}F_{24}N_{24}Ni_4O_{24}S_8$•$2H_2O$: C 50.18, H 3.10, N 9.24; found: C 50.49, H 3.28, N 9.42. Noteworthy, X-ray quality crystals were obtained from this solution corroborating the tetrahedral structure of the **Ni-3** framework and further confirming the reversibility of this process to regenerate the original **Ni-3•SO_4** complex (see X-ray crystallography section, *vide infra*).

Addition of TBA_2SO_4 to an acetonitrile solution of this **Ni-3•OTf** induced precipitation of the former water-soluble **Ni-3•SO_4**. The complete **Ni-3•SO_4→Ni-3•OTf→Ni-3•SO_4** anion exchange cycle was carried out multiple times, with 87-93% recovery by weight per cycle.

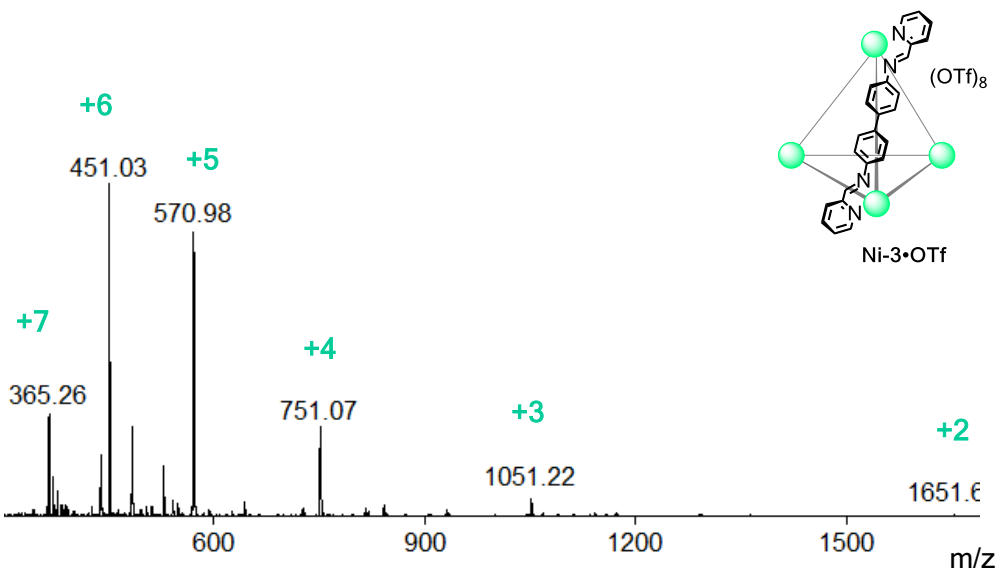

Figure S19. ESI-MS spectrum of **Ni–3•OTf** (CH_3CN) obtained upon reversible anion exchange from **Ni–3•SO_4**.

*3.4 Synthesis of the water-soluble tetrahedron **Ni–4•SO₄** and its reversible conversion into the acetonitrile-soluble **Ni–4•OTf** cage*

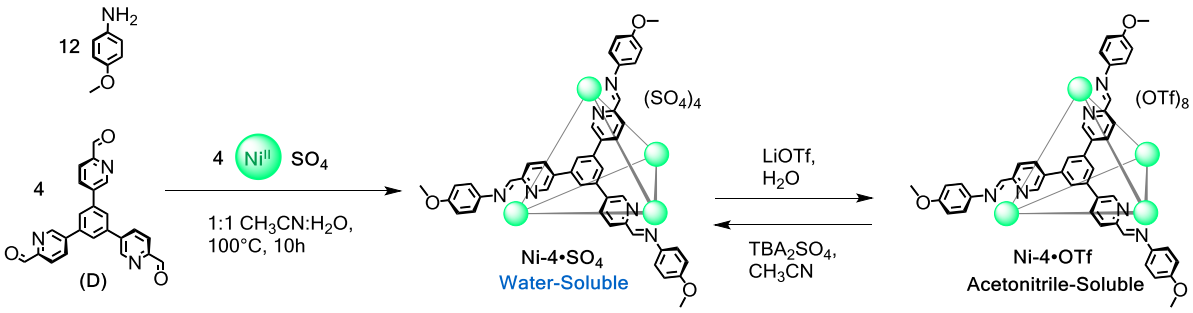

Subcomponent **D** (4.0 mg, 0.010 mmol, 4 equiv), 4-methoxyaniline (3.7 mg, 0.031 mmol, 12 equiv), nickel(II) sulfate hexahydrate (2.7 mg, 0.010 mmol, 4 equiv), and 1.5 mL of 1:1 CH_3CN/H_2O solution were placed in a Schlenk flask. The mixture was degassed by three evacuation/nitrogen fill cycles and heated at 100°C overnight giving a dark yellow solution. Afterward, the crude solution was cooled down to room temperature and excess of cold acetonitrile was added until a yellow solid precipitated out from the solution. The mixture was centrifuged and the supernatant CH_3CN/H_2O was decanted, this process was repeated with CH_3CN:H_2O (9:1), then with CH_3CN, and the excess of solvent was removed under N_2 flow. Cage **Ni–4•SO₄** was recovered as a pale yellow solid (7.4 mg, yield 86%). ESI-MS (H_2O): *m/z* = 459.9 [**Ni-4**(OTf)]$^{+7}$, 525.1 [**Ni-4**$(CHO_2)_2$]$^{+6}$, 543.9 [**Ni-4**(CHO_2)(OTf)]$^{+6}$, 560.7 [**Ni-4**$(OTf)_2$]$^{+6}$, 661.5 [**Ni-4**$(CHO_2)_2$(OTf)]$^{+5}$, 671.9 [**Ni-4**$(HSO_4)_3$]$^{+5}$, 682.2 [**Ni-4**$(HSO_4)_2$(OTf)]$^{+5}$, 851.3 [**Ni-4**$(CHO_2)_2(HSO_4)$(OTf)]$^{+4}$, 864.7 [**Ni-4**$(CHO_2)_2(OTf)_2$]$^{+4}$. Elemental analysis (%) calcd for $C_{180}H_{144}N_{24}Ni_4O_{28}S_4$•$CH_3CN$•$H_2O$: C 62.22, H 4.27, N 9.97; found: C 62.59, H 4.32, N 9.92.

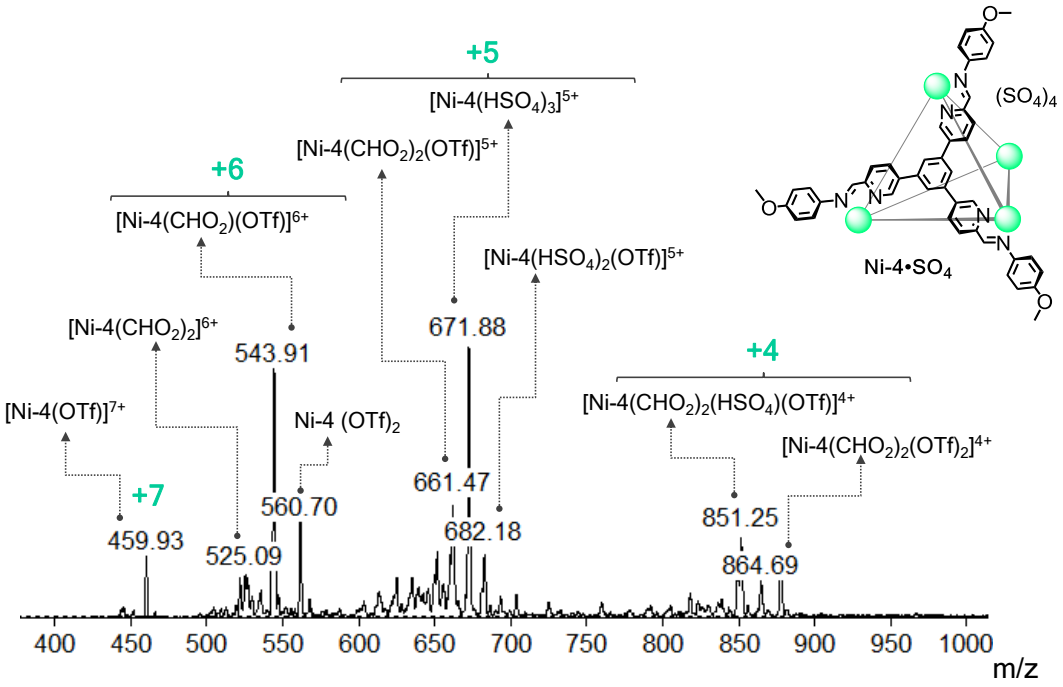

Figure S20. ESI-MS spectrum of **Ni–4•SO_4** in H_2O evidencing the **Ni–4** framework in solution. Anion exchange under ESI-MS conditions is observed.

Addition of 12 equivalents of LiOTf (1.5 equiv per sulfate) to an aqueous solution of **Ni-4•SO_4** (4.0 mg in 500 μL) induced precipitation of a pale yellow solid, the mixture was centrifuged and the solvent decanted yielding cage **Ni-4•OTf** in almost quantitative yield (4.4 mg, yield 90%). ESI-MS analyses in CH_3CN confirmed that this solid corresponded to the **Ni-4•OTf** complex (Figure S21); spectroscopic details as follows: ESI-MS (CH_3CN): *m/z* = 459.6 [**Ni-4**(OTf)]$^{+7}$, 560.8 [**Ni-4**$(OTf)_2$]$^{+6}$, 702.8 [**Ni-4**$(OTf)_3$]$^{+5}$, 916.1 [**Ni-4**$(OTf)_4$]$^{+4}$, 1271.3 [**Ni-4**$(OTf)_5$]$^{+3}$. Elemental analysis (%) calcd for $C_{188}H_{144}F_{24}N_{24}Ni_4O_{36}S_8$•$3H_2O$: C 52.31, H 3.50, N 7.79; found: C 52.44, H 3.58, N 7.84.

Addition of TBA_2SO_4 to an acetonitrile solution of this **Ni-4•OTf** induced precipitation of the former water-soluble **Ni-4•SO_4**. The complete **Ni-4•SO_4**→**Ni-4•OTf**→**Ni-4•SO_4** anion exchange cycle was carried out multiple times, with 87-93% recovery by weight per cycle.

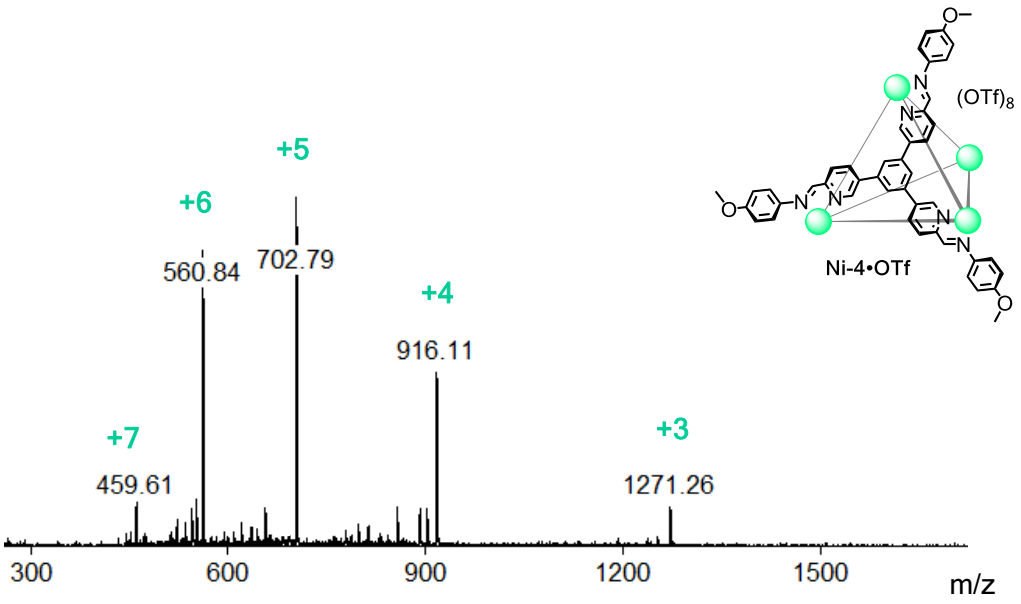

Figure S21. ESI-MS spectrum of **Ni–4•OTf** (CH_3CN) obtained upon reversible anion exchange from **Ni–4•SO_4**.

*3.5 Attempted reaction to prepare a water-soluble **Ni–5•SO_4** tetrahedron*

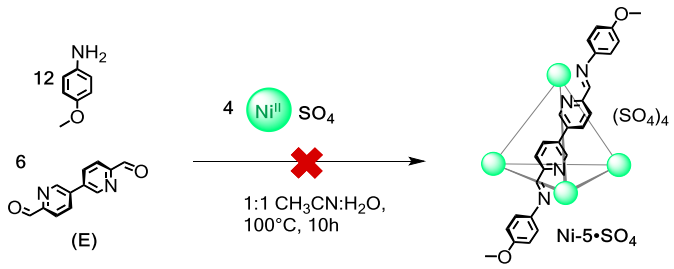

Reactions between subcomponent **E** and $NiSO_4$ were attempted using diverse temperature and solvent conditions in order to prepare cage **Ni-5•SO_4**, all reactions remained unsuccessful and only led to insoluble materials.

We have previously reported that reactions of aldehyde **E** with nickel(II) salts containing BF_4^-, NTf_2^-, ClO_4^-, or NO_3^- did not yield tetrahedral structure **Ni-5**. As previously

observed, **E** reacts with $Ni(OTf)_2$ to form a mixture of assemblies.[12] When treated with TBA_2SO_4 in MeCN, this mixture gave species that were initially soluble in water, but which decomposed by precipitation within minutes.

3.6 Selected binding experiments using water-soluble Ni^{II}-based capsules with fluorinated guests

The ^1H NMR spectra of complexes containing octahedrally coordinated Ni^{II} produced little insight due to the long relaxation times arising from the orbitally non-degenerate ground state of these complexes.[12] Given that we have gained knowledge into the outcome of the self-assembly reactions and anion exchange sequences solely through ESI-MS and X-ray crystallography, we carried out selected encapsulation experiments using these Ni^{II}-based capsules with some common fluorinated aromatics as guests including fluorobenzene, 1,3,5-trifluorobenzene, and hexafluorobenzene; the binding of each prospective guest was followed by ^{19}F NMR. These host-guest experiments only intended to serve as further proof of the capsular nature of the Ni^{II}-based complexes and a full investigation into the host-guest properties of these capsules is beyond the scope of this work.

No encapsulation of prospective fluorinated guests or triflate anion in CD_3CN was inferred to have taken place when the triflate versions of the capsules were used. Only one signal was observed in the ^{19}F NMR spectra, the signals for the fluorinated aromatics were identical to those in the absence of host. On the other hand, host occupation was inferred to occur in D_2O using sulfate derivatives of nickel(II)-capsules; shifting or broadening of the guest peaks were observed.

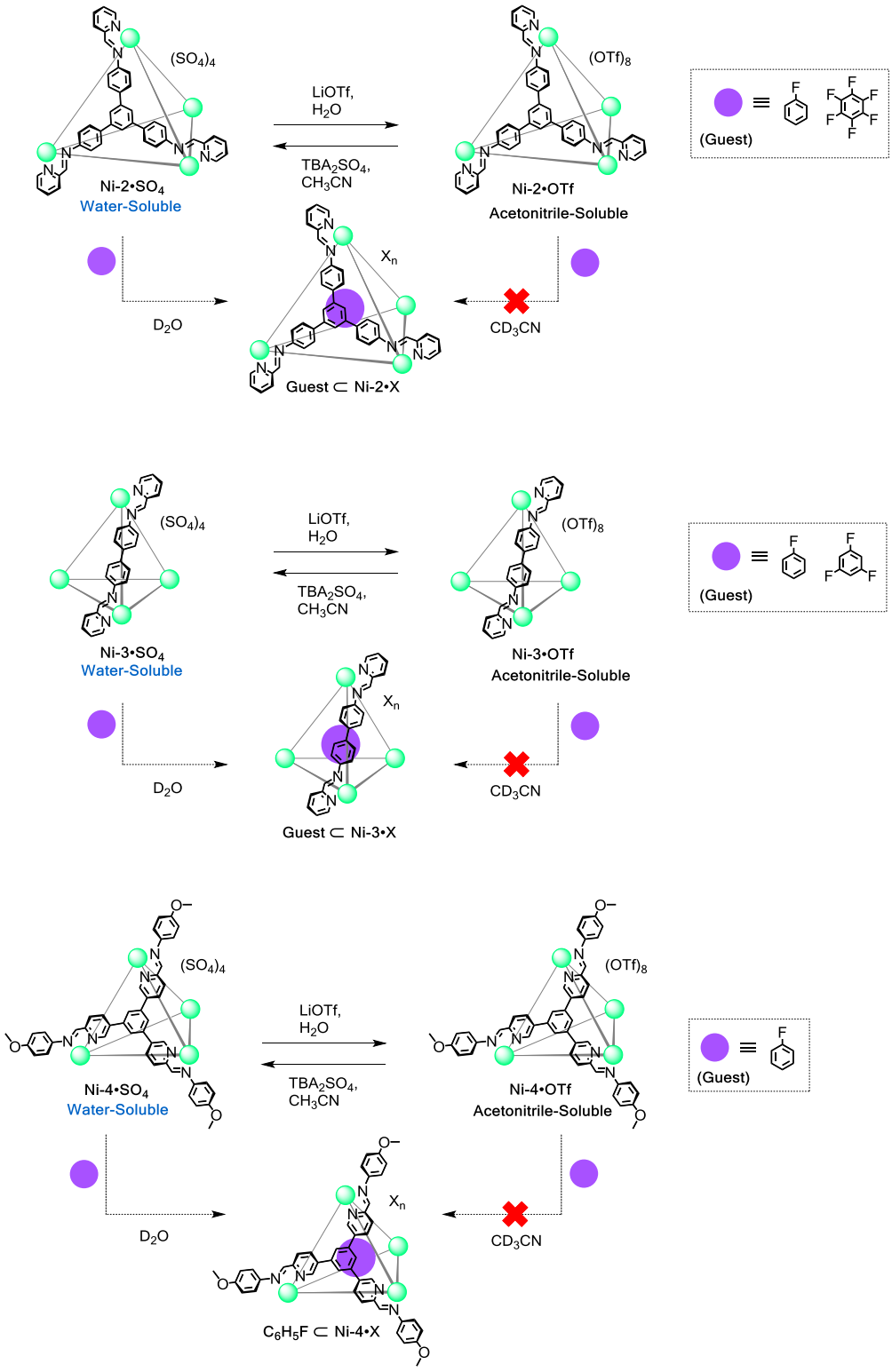

Figure S22. Reaction systems for investigating the Host-Guest interaction between cages **Ni–2•X** to **Ni–4•X** (X = OTf^-, SO_4^{2-}) and fluorinated aromatic guests in water and acetonitrile.

Solutions of **Ni-n•SO$_4$** (n = 2, 3, 4) capsules (200–300 μM) in D_2O were transferred to an NMR tube and the prospective fluorinated guest was added in excess due to their low solubility and miscibility in water (~10–15 equivalents per cage). The mixture was sonicated for 10 minutes and then stored at room temperature; the spectra were recorded periodically until the host-guest complex equilibrated as shown by the ^{19}F NMR spectra; generally, equilibration times were short (t < 8 h).

Initially, the ^{19}F NMR spectra revealed the presence of two peaks corresponding to the free and encapsulated fluorinated molecule. The peaks for the free fluorinated molecules progressively vanished likely due to separation and evaporation from the aqueous solution given their very poor solubility in water; Figures S23 and S24 exemplify such observations. As a result, only the peak of the encapsulated guest (host-guest complex) persisted in the ^{19}F NMR spectra over the time. The free and bound guests were referenced to C_6F_6 (as an external standard in a capillary tube at δ = –164.9 ppm). Likewise, the assignment of the free and bound guest was further aided using ^{19}F NMR spectra of samples containing only the free guest in D_2O and C_6F_6 as an external standard in a capillary tube.

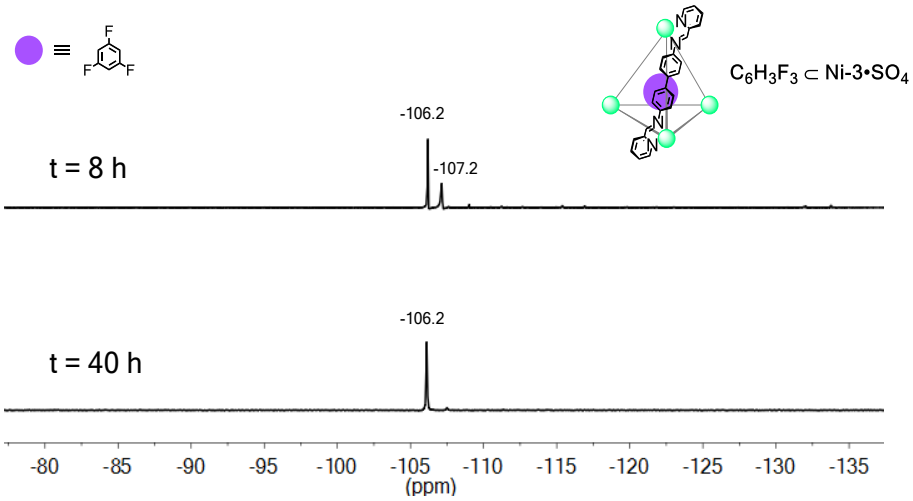

Figure S23. ^{19}F NMR spectra (376 MHz, D_2O, 298 K) of the $C_6H_3F_3$⊂**Ni–3•SO$_4$** Host-Guest complex showing signals for the free and encapsulated guest (*top*), and the disappearance of the resonance for the free molecule over the time (*bottom*).

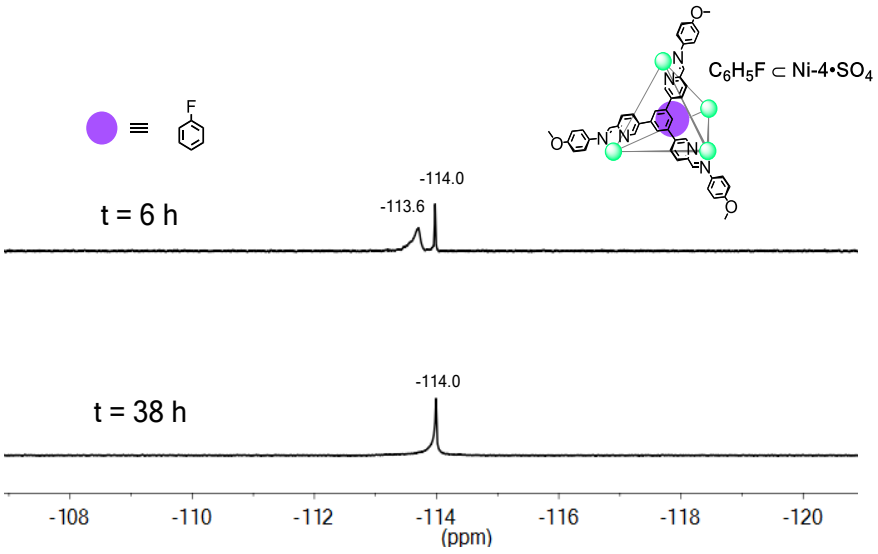

Figure S24. ^{19}F NMR spectra (376 MHz, D_2O, 298 K) of the C_6H_5F⊂**Ni–4•SO$_4$** Host-Guest complex showing signals for the free and encapsulated guest (*top*), and disappearance of the free guest peak over the time (*bottom*).

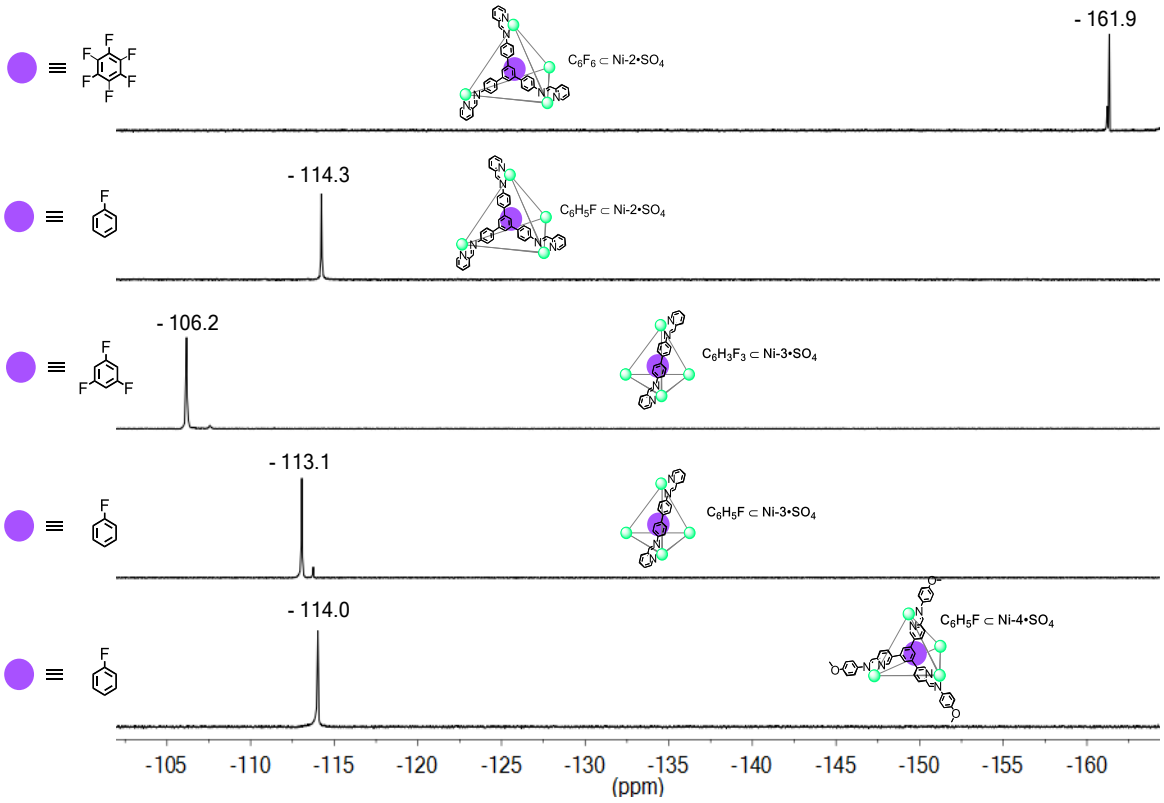

Figure S25. ^{19}F NMR spectra (376 MHz, D_2O, 298 K) of the equilibrated Host-Guest complexes derived from cages **Ni–2•SO$_4$**, **Ni–3•SO$_4$**, and **Ni–4•SO$_4$** showing signals for the encapsulated guest.

4. Attempted preparations of water-soluble Zn^{II}– and Cd^{II}–based capsules

Reactions of subcomponents **A** and **D** with 2-formylpyridine and anisidine respectively, yielded the corresponding acetonitrile-soluble capsules (as triflate salts) when combined with Zn^{II} and Cd^{II}. These capsules precipitated upon addition of TBA_2SO_4 in acetonitrile suggesting the exchange of triflate for sulfate. Addition of water to these solids enabled their immediate dissolution; however, the resulting solutions became cloudy just after a few seconds leading to mostly insoluble material within the first three minutes after dissolution in the case of frameworks **Zn-4•SO_4** and **Cd-4•SO_4** formed by aldehyde **D**.

Although the cubic structures **Zn-1•SO_4** and **Cd-1•SO_4** also failed to survive in aqueous solution, it was possible to record initial NMR spectra and monitor the disassembly process in aqueous solution.

Dissolution of cubic structures **Zn-1•SO_4** and **Cd-1•SO_4** in D_2O brought about cloudiness of the red brick to dark brown solutions and the eventual appearance of insoluble blue solid (free porphyrin **A**). While it was possible to observe peaks of low-intensity corresponding to cube **Zn-1** within the first hour, the **Cd-1** framework was almost completely hydrolysed after 20 minutes strongly indicating its lower stability.

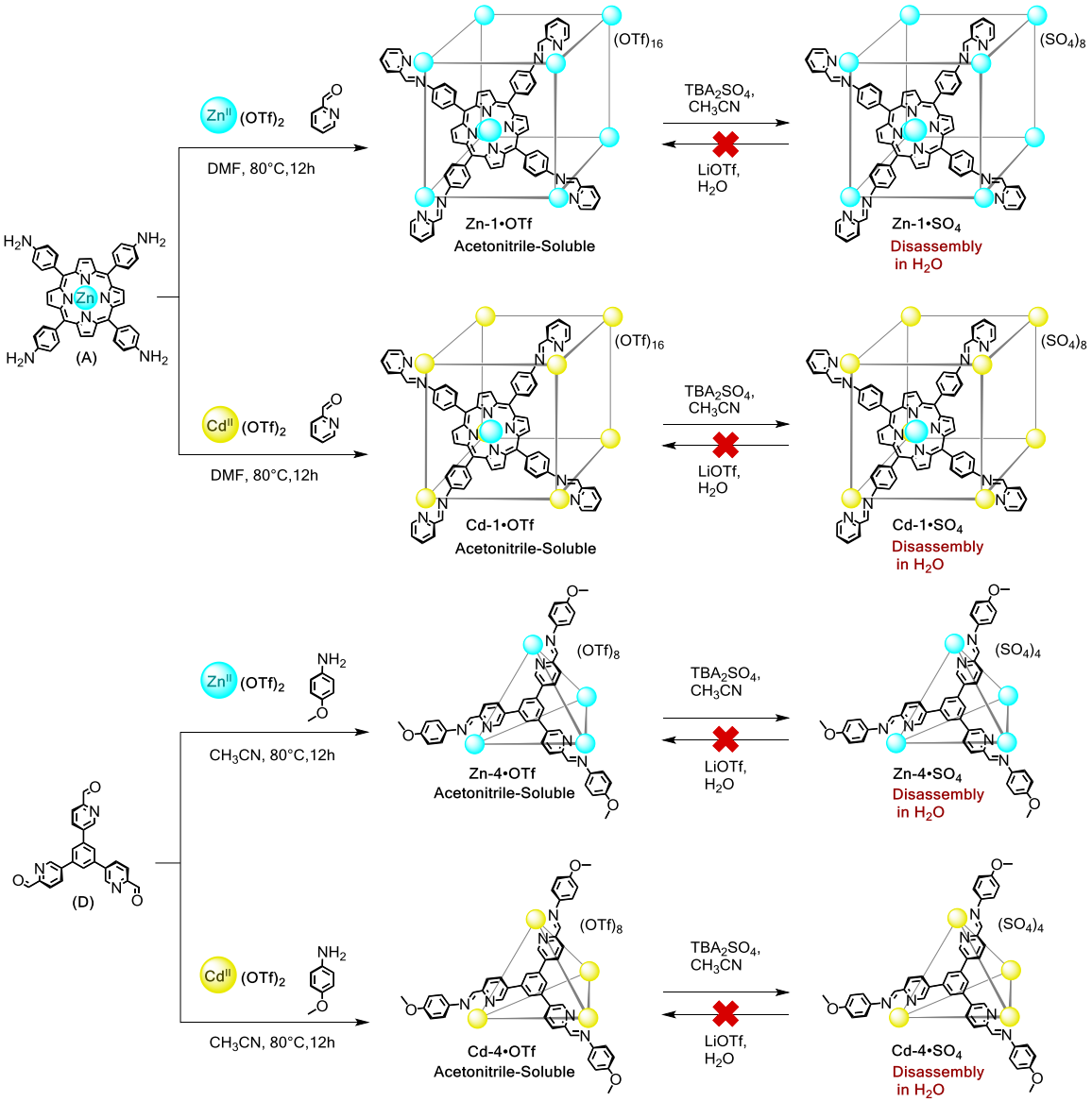

Figure S26. Selected self-assembly reactions tested to investigate the dissolution and stability in water of Zn^{II}– and Cd^{II}–based capsules. All reactions, either via direct assembly with sulfate salts or via anion exchange, remained unsuccessful for the formation of stable cages.

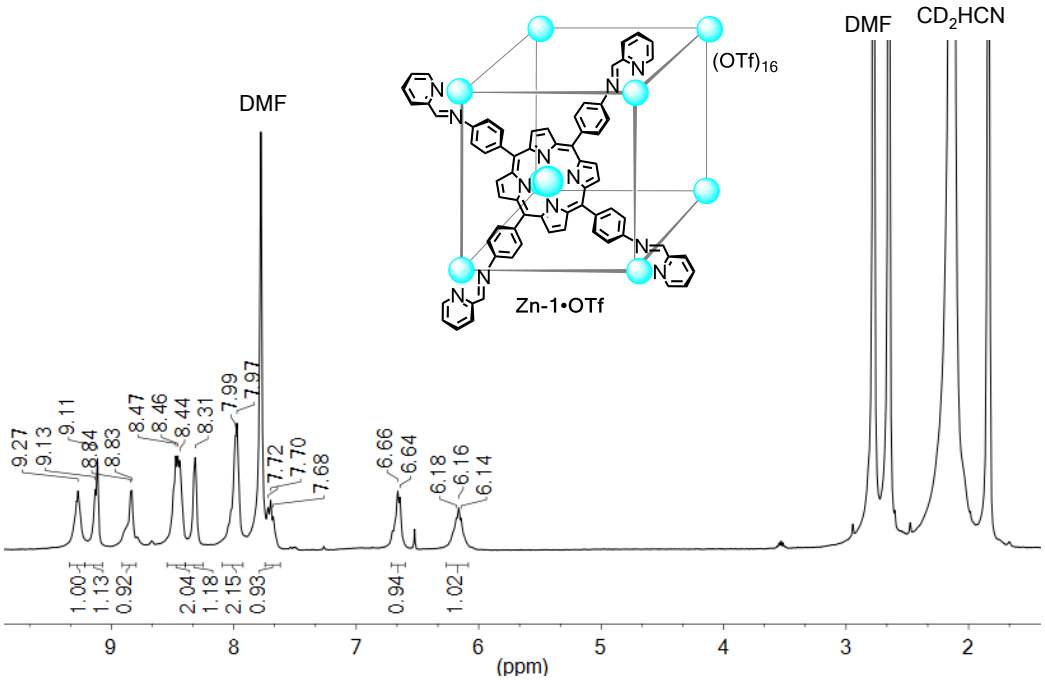

Figure S27. ^{1}H NMR spectrum (400 MHz, CD_3CN, 298 K) of **Zn–1•OTf**.

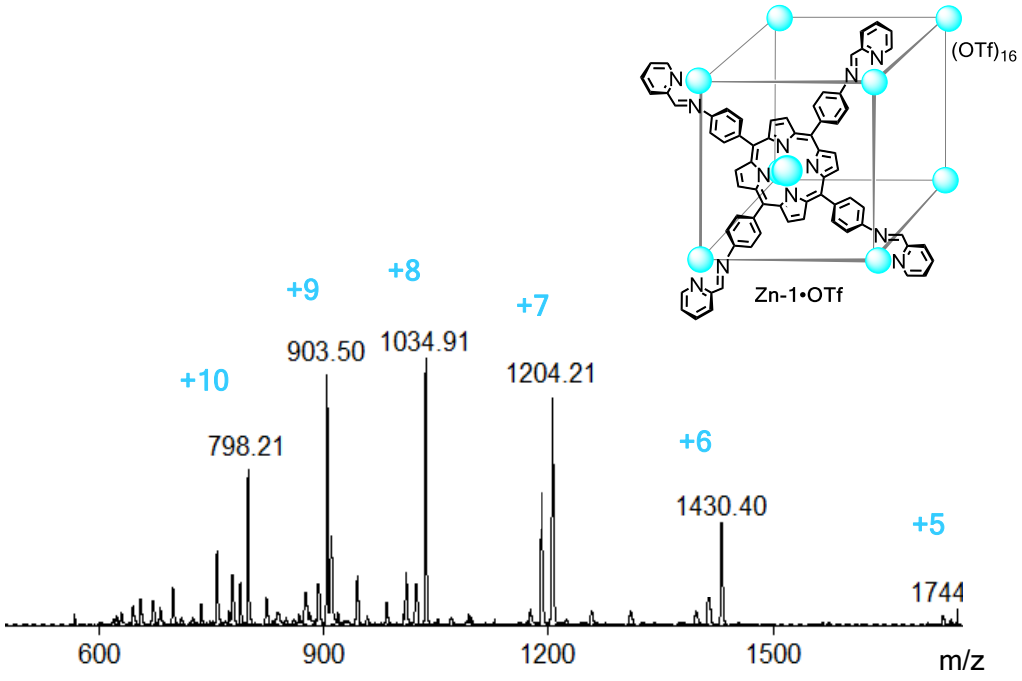

Figure S28. ESI-MS spectrum (CH_3CN) of **Zn–1•OTf**.

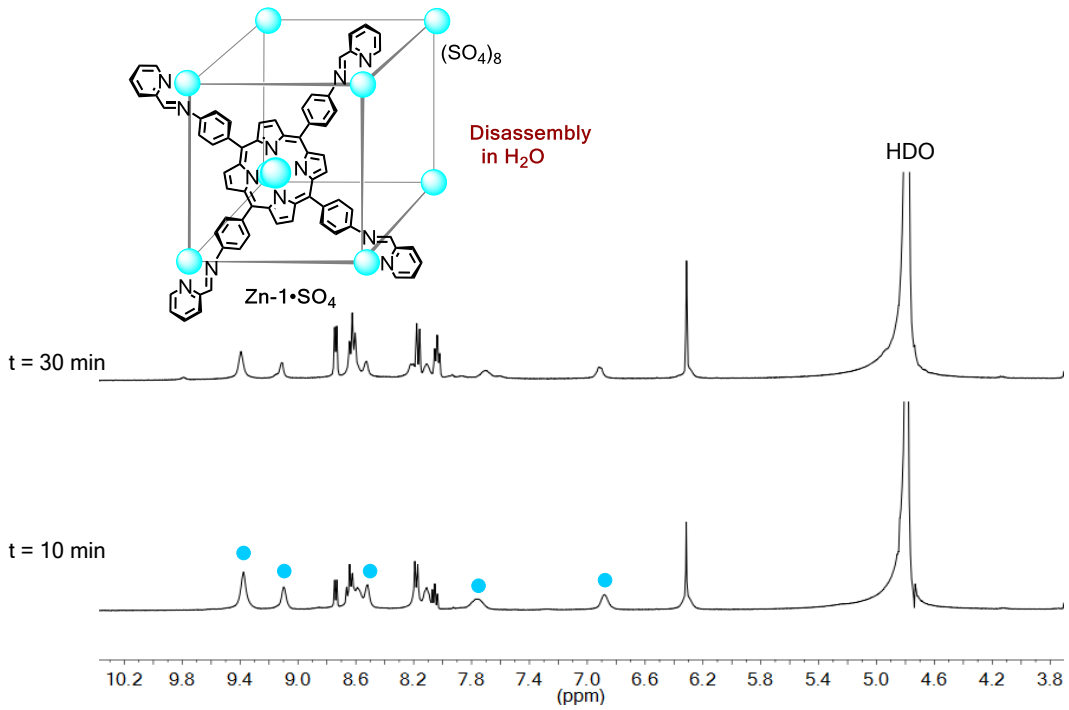

Figure S29. ^{1}H NMR spectra (400 MHz, D_2O, 298 K) of **Zn–1•SO$_4$** showing the progressive vanishing of the cube peaks over the time; blue circles denote cage peaks.

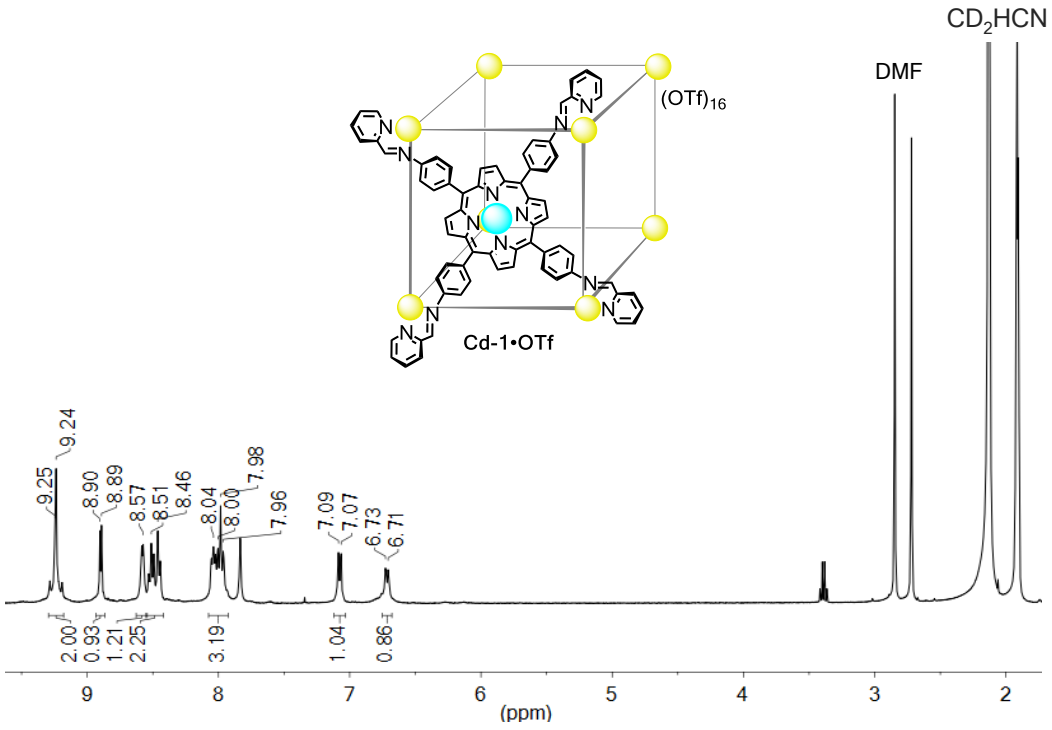

Figure S30. ^{1}H NMR spectrum (400 MHz, CD_3CN, 298 K) of **Cd–1•OTf**.

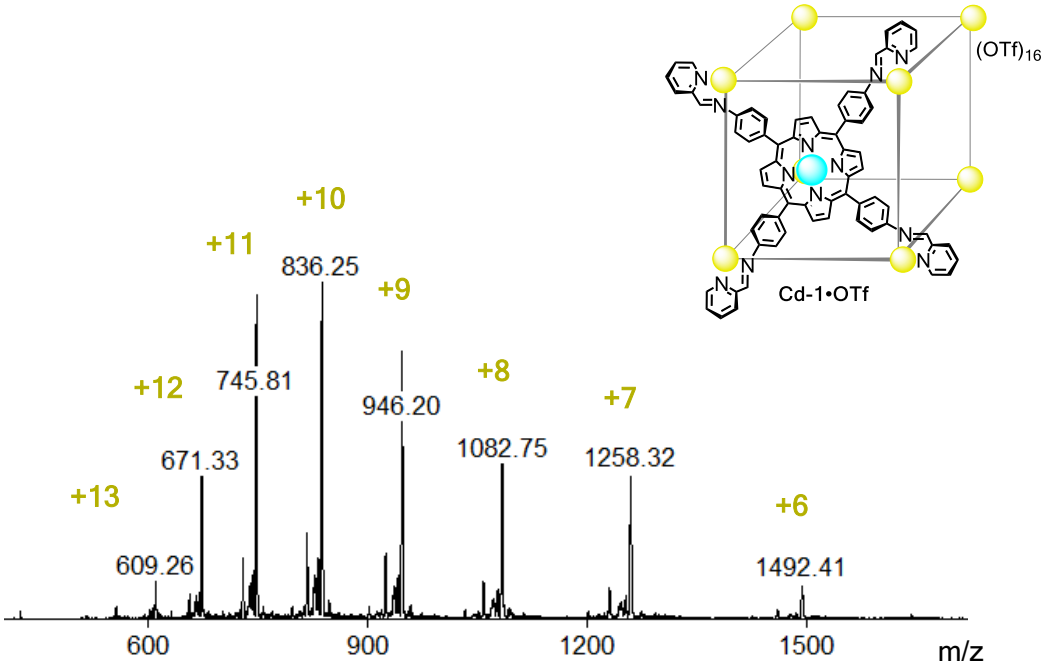

Figure S31. ESI-MS spectrum (CH_3CN) of **Cd–1•OTf**.

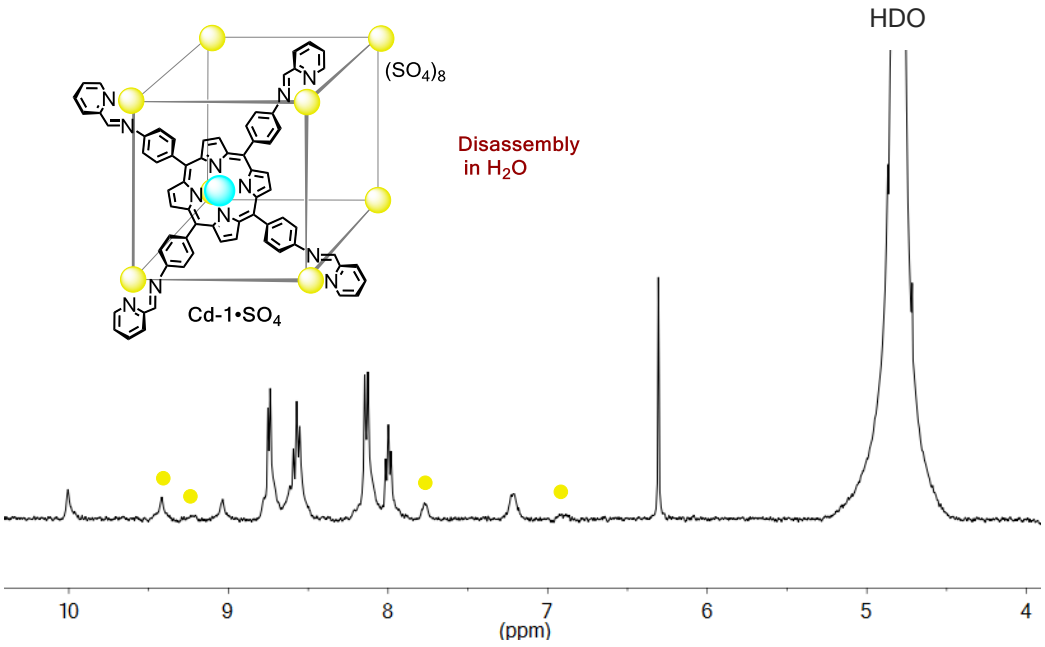

Figure S32. ^{1}H NMR spectra (400 MHz, D_2O, 298 K, recorded 15 min after dissolution) of **Cd–1•SO_4** evidencing rapid disassembly in solution; yellow circles denote cage peaks.

5. Chelating amines for the synthesis of water-soluble Zn^{II}– and Cd^{II}–based architectures

The C_2-symmetric subcomponents **E–H** were combined with chelating amines TREN or TRPN for the direct self-assembly reactions with $ZnSO_4$ or $CdSO_4$ yielding a collection of water soluble self-assembled structures. Two sets of conditions for the same aldehyde-based subcomponent were used, Zn^{II}/TREN or Cd^{II}/TRPN, leading to the synthesis of helicates **Zn–6•SO$_4$** to **Zn–9•SO$_4$** and tetrahedra **Cd–11•SO$_4$** to **Cd–14•SO$_4$**, respectively. Conversely, reactions of the C_3-symmetric subcomponent **D** using both sets of conditions exclusively afforded tetrahedra, cages **Zn–10•SO$_4$** and **Cd–15•SO$_4$**. Similar to the Co^{II}– and Ni^{II}–based structures presented, these assemblies are robust enough to undergo anion metathesis with LiOTf and generate the corresponding acetonitrile-soluble derivatives. Crystallization of helical structures **Zn–7** and **Zn–8** as well as tetrahedra **Cd–12** and **Cd–14** from their acetonitrile solutions clearly attests to this quality; Figures S68, S69 and S78 also illustrate the dissolution in acetonitrile of these assemblies as triflate derivatives.

Although all ESI-MS spectra (obtained in pure H_2O) showed charged states consistent with the $Zn^{II}_2L_3$, $Cd^{II}_4L_6$, $Zn^{II}_4L_4$, and $Cd^{II}_4L_4$ formulations of the target frameworks, some peaks resulted from anion exchange under ESI-MS conditions. Hence, peaks with SO_4^{2-}, HSO_4^-, Cl^-, NTF_2^-, CHO_2^-, BF_4^- counter anions were observed due to their residual and persistent presence in the equipment or to washing with formic acid (Figures S36, S40, S44, S49, S53, S57, S62, S67, S74 and S77).

*5.1 Reactions of aldehyde **E** to form helicate **Zn–6•SO$_4$** or tetrahedron **Cd–11•SO$_4$***

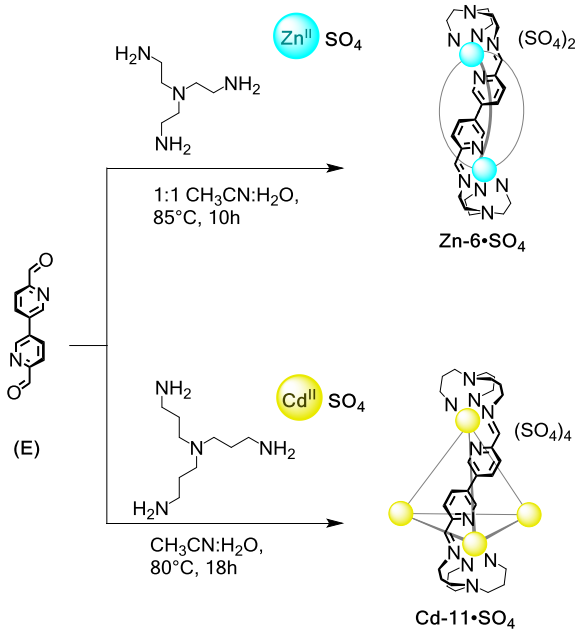

Subcomponent **E** (10.0 mg, 0.047 mmol, 3 equiv), tris(2-aminoethyl)amine (TREN) (4.8 μL, 0.031 mmol, 2 equiv), zinc(II) sulfate heptahydrate (2.7 mg, 0.031 mmol, 2 equiv), and 1.0 mL of 1:1 CH_3CN/H_2O were placed in a Schlenk flask. The mixture was degassed by three evacuation/nitrogen fill cycles, sonicated for 15 minutes and heated at 85°C overnight yielding a yellow solution with a small amount of fine dark yellow solid. The fine yellow solid was removed by filtration using a small column with celite, and excess of CH_3CN was added to the bright yellow liquor giving a yellow suspension. The suspension was centrifuged and the supernatant CH_3CN/H_2O was decanted. To remove the excess of unreacted aldehyde **E** and TREN, the solid was washed with CH_2Cl_2, centrifuged and the supernatant decanted; this process was carried out a second time with Et_2O, and a two times with CH_3CN. Finally, the excess of solvents was removed by a gentle flow of N_2 gas yielding helicate **Zn-6•SO$_4$** as a microcrystalline beige solid (15.9 mg, yield 88%). ^{1}H NMR (400 MHz, D_2O, 298 K): δ = 8.92 (s, 6H, imine-H*a*), 8.14 (dd, $^3J_{1H–1H}$ = 7.9, 2.0 Hz, 6H, Py-H*b*), 8.09 (d, $^3J_{1H–1H}$ = 7.9 Hz, 6H, Py-H*c*), 6.05 (d, $^3J_{1H–1H}$ = 1.9 Hz, 6H, Py-H*d*), 4.11 (dd, $^2J_{1H–1H}$ = 12.2, $^3J_{1H–1H}$ = 12.0 Hz, 6H, TREN-H*e*), 3.84 (dd, $^2J_{1H–1H}$ = 12.4, $^3J_{1H–1H}$ = 3.2 Hz, 6H, TREN-H*e*), 3.31 (dd, $^2J_{1H–1H}$ = 13.6, $^3J_{1H–1H}$ = 3.6 Hz, 6H, TREN-H*f*), 3.12

(ddd, $^{2}J_{1H–1H}$ = 13.6, $^{3}J_{1H–1H}$ = 13.4, 3.5 Hz, 6H, TREN-H*f*). ^{13}C NMR (100 MHz, D_2O, 298 K): δ = 163.7, 148.6, 148.5, 139.9, 138.2, 129.0, 56.5, 54.1. DOSY Diffusion coefficient = 2.98 × 10^{-10} m^2/s. ESI-MS (H_2O): *m/z* = 237.7 [**Zn-6**]$^{+4}$, 349.4 [**Zn-6**(HSO_4)]$^{+3}$, 524.1 [**Zn-6**(SO_4)]$^{+2}$. Elemental analysis (%) calcd for $C_{48}H_{48}N_{14}O_8S_2Zn_2$•$H_2O$: C 49.62, H 4.34, N 16.88; found: C 49.28, H 4.36, N 16.72.

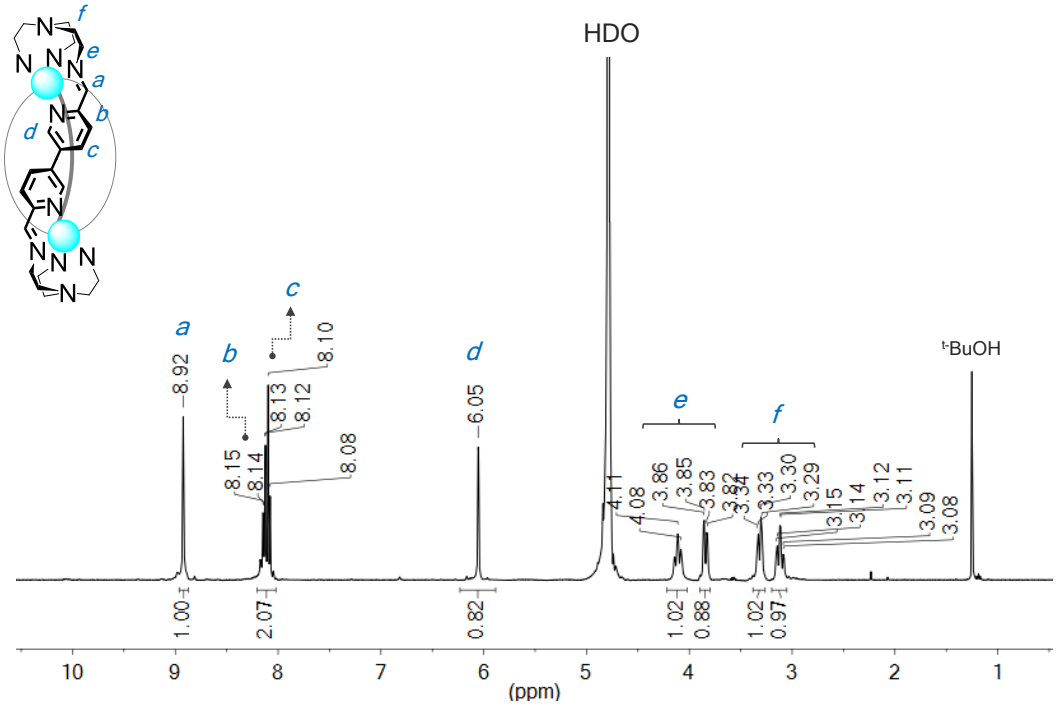

Figure S33. ^{1}H NMR spectrum (400 MHz, D_2O, 298 K) of helicate **Zn–6•SO_4**.

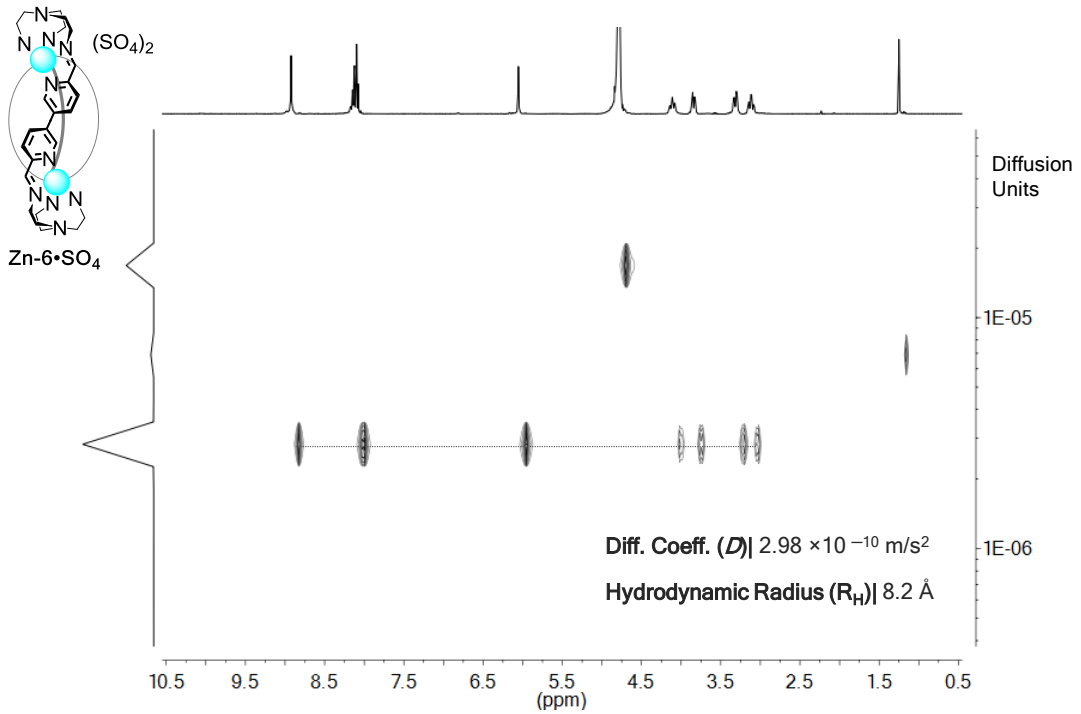

Figure S34. ^{1}H DOSY NMR spectrum (400 MHz, D_2O, 298 K) of helicate **Zn–6•SO$_4$**.

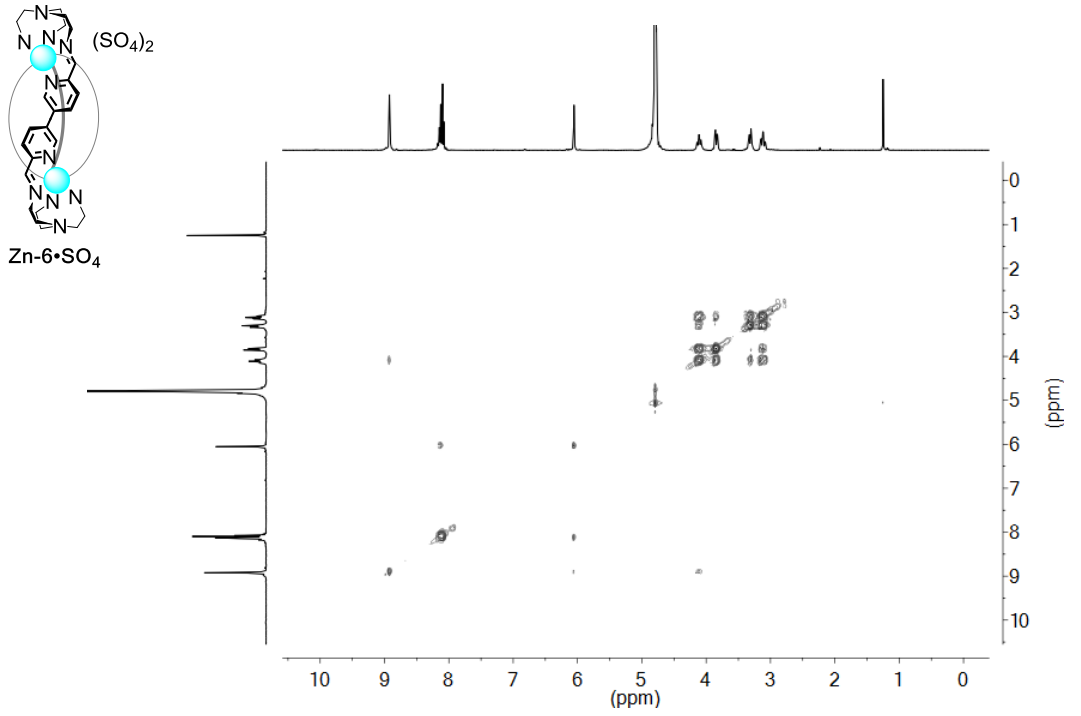

Figure S35. ^{1}H–^{1}H COSY NMR spectrum (400 MHz, D_2O, 298 K) of helicate **Zn–6•SO$_4$**.

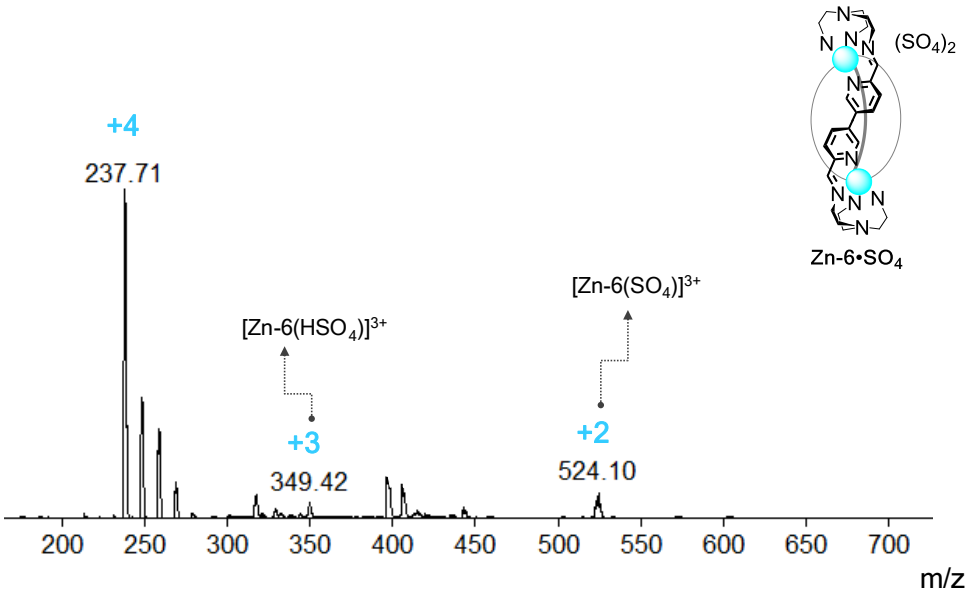

Figure S36. ESI-MS spectrum of helicate **Zn–6•SO$_4$** recorded in H_2O.

Subcomponent **E** (5.0 mg, 0.024 mmol, 6 equiv), tris(3-aminopropyl)amine (TRPN) (3.1 µL, 0.016 mmol, 4 equiv), cadmium(II) sulfate (3.2 mg, 0.018 mmol, 4 equiv), and 1.0 mL of 1:1 CH_3CN/H_2O were placed in a Schlenk flask. The mixture was degassed by three evacuation/nitrogen fill cycles, sonicated for 15 minutes and heated at 80°C overnight yielding a yellow solution with a small amount of fine dark yellow solid. This yellow solid was removed by filtration using a small column with celite, and excess of CH_3CN was added to the bright yellow liquor giving a yellow suspension. The suspension was centrifuged and the supernatant CH_3CN/H_2O was decanted. To remove the excess of unreacted aldehyde **E** and TRPN, the solid was washed with CH_2Cl_2, centrifuged and the supernatant decanted; this process was carried out a second time with Et_2O, and a two times with CH_3CN. Finally, the excess of solvents was removed by a gentle flow of N_2 gas yielding cage **Cd-11•SO$_4$** as a microcrystalline light yellow solid (8.5 mg, yield 82%). ^{1}H NMR (400 MHz, D_2O, 298 K): δ = 9.02 (s, $^3J_{1H–113Cd}$ = 21.4 Hz, 12H, imine-H*a*), 8.19 (d, $^3J_{1H–1H}$ = 7.6 Hz, 12H, Py-H*b*), 8.01 (d, $^3J_{1H–1H}$ = 7.9 Hz, 12H, Py-H*c*), 7.32 (s, 12H, Py-H*d*), 3.98 (d, $^2J_{1H–1H}$ = 10.6 Hz, 12H, TRPN-H*e*), 3.40 (m, 24H, TRPN-H*e*, H*f*), 2.35 (m, 12H, TRPN-H*f*), 2.23 (m, 12H, TRPN-H*g*), 1.94 (d, $^2J_{1H–1H}$ = 13.9 Hz, 12H, TRPN-H*g*). ^{13}C NMR (100 MHz, D_2O, 298 K): δ = 161.4, 147.9, 147.5, 140.3, 137.9, 129.1, 61.9, 58.5,

26.0. DOSY Diffusion coefficient = 2.13 × 10^{-10} m^2/s. ESI-MS (H_2O): *m/z* = 282.8 [**Cd-11**]$^{+8}$, 328.4 [**Cd-11**(Cl)]$^{+7}$, 392.7 [**Cd-11**(SO_4)]$^{+6}$, 474.0 [**Cd-11**($Cl)_3$]$^{+5}$, 613.1 [**Cd-11**($SO_4)_2$]$^{+4}$, 822.4 [**Cd-11**($CHO_2)_3(Cl)_2$]$^{+3}$, 1274.5 [**Cd-11**($SO_4)_3$]$^{+2}$. Elemental analysis (%) calcd for $C_{108}H_{120}Cd_4N_{28}O_{16}S_4$•$3.5H_2O$•$CH_3CN$: C 48.07, H 4.77, N 14.78; found: C 48.18, H 4.76, N 14.72.

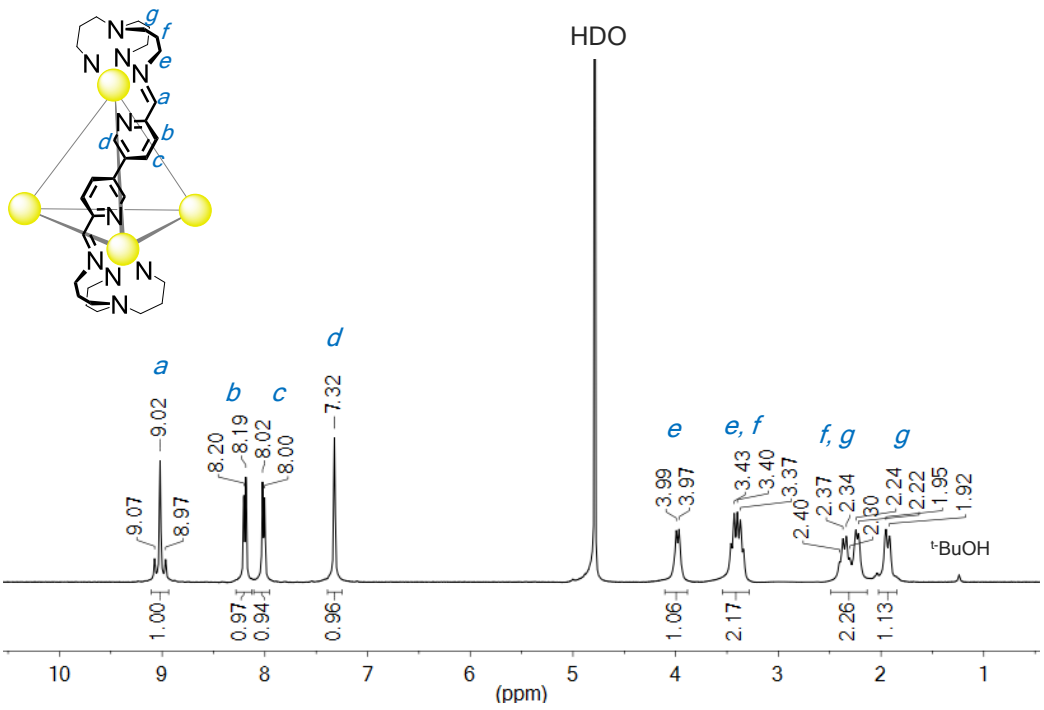

Figure S37. ^{1}H NMR spectrum (400 MHz, D_2O, 298 K) of tetrahedron **Cd–11•SO_4**.

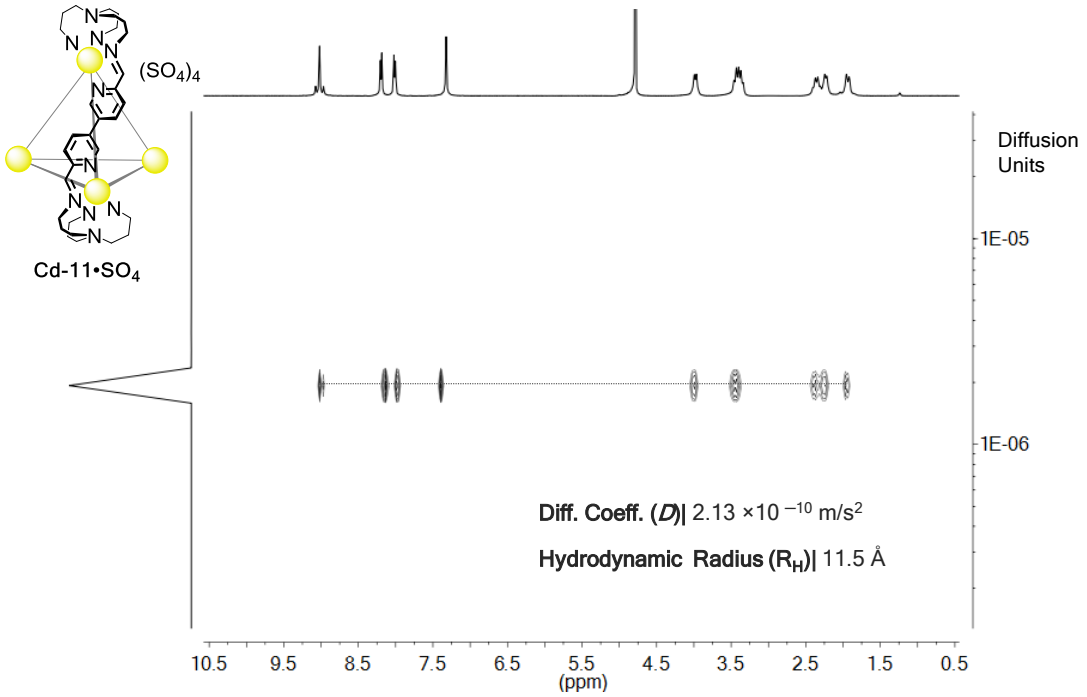

Figure S38. ^{1}H DOSY NMR spectrum (400 MHz, D_2O, 298 K) of tetrahedron **Cd–11•SO$_4$**.

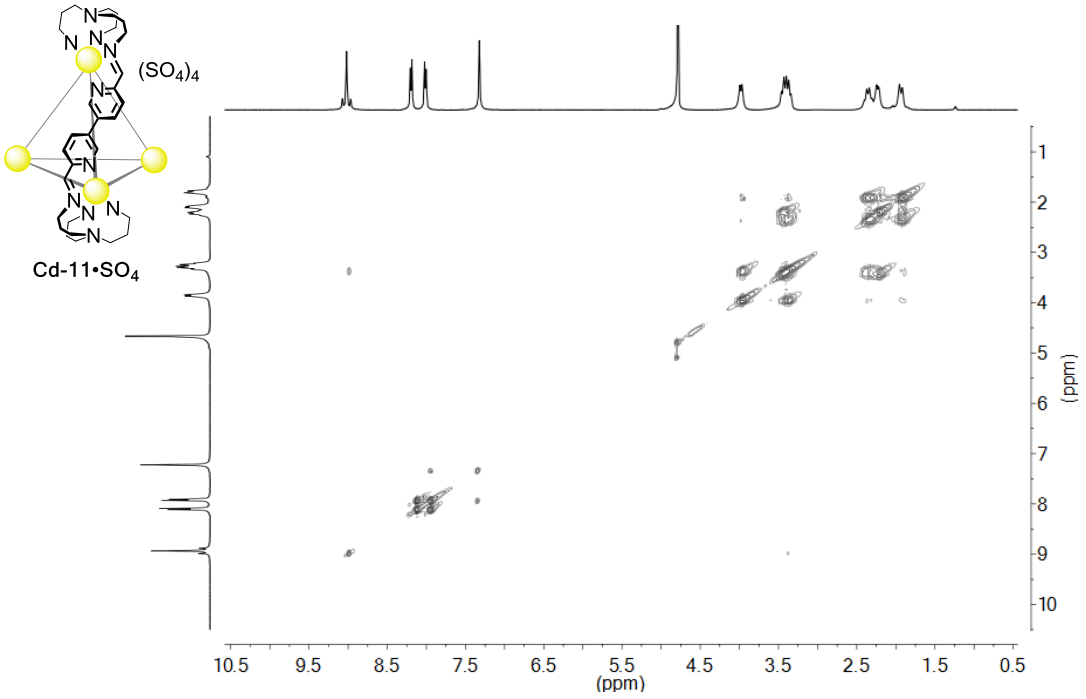

Figure S39. ^{1}H–^{1}H COSY NMR spectrum (400 MHz, D_2O, 298 K) of tetrahedron **Cd–11•SO$_4$**.

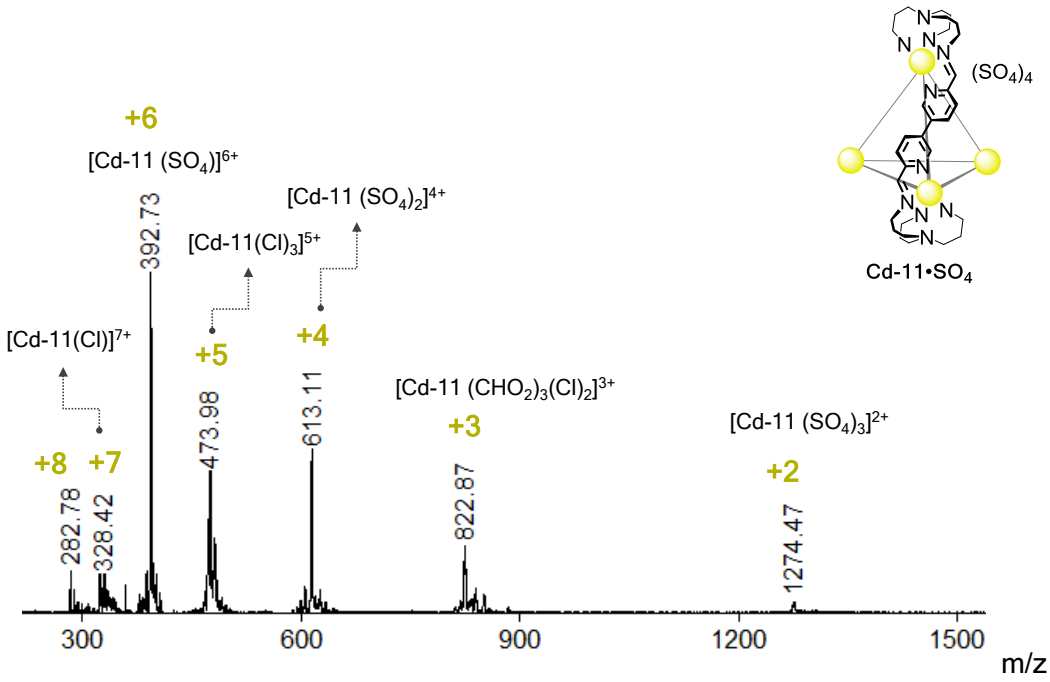

Figure S40. ESI-MS spectrum of tetrahedron **Cd–11•SO_4** recorded in H_2O.

*5.2 Reactions of aldehyde **F** to form helicate **Zn–7•SO_4** or tetrahedron **Cd–12•SO_4***

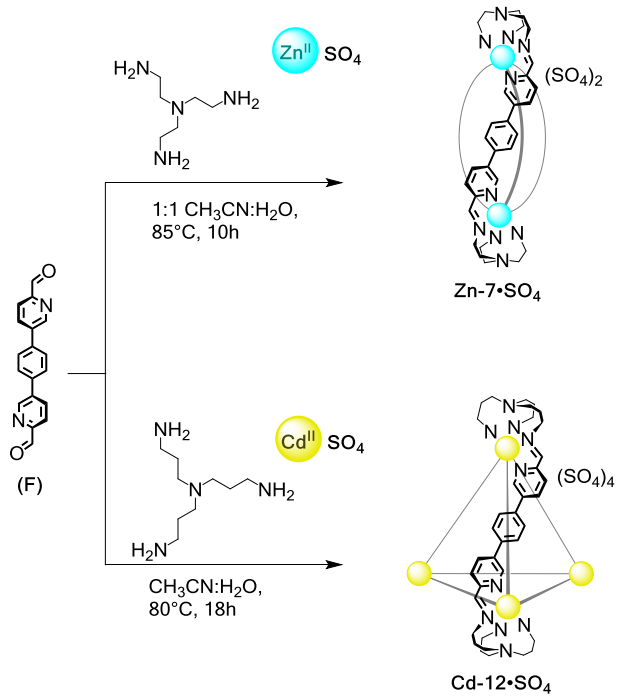

Subcomponent **F** (8.2 mg, 0.028 mmol, 3 equiv), tris(2-aminoethyl)amine (TREN) (2.9 μL, 0.019 mmol, 2 equiv), zinc(II) sulfate heptahydrate (5.4 mg, 0.019 mmol, 2 equiv), and 1.0 mL of 1:1 CH_3CN/H_2O were placed in a Schlenk flask. The mixture was degassed by three evacuation/nitrogen fill cycles, sonicated for 15 minutes and heated at 85°C overnight yielding a yellow solution with some yellow insoluble material. The insoluble material was removed by filtration through celite, and excess CH_3CN was added to the bright yellow liquor leading to precipitation of a light yellow solid. The mixture was centrifuged and the supernatant CH_3CN/H_2O was decanted. To remove excess unreacted aldehyde **F** and TREN, the solid was washed with CH_2Cl_2, centrifuged and the supernatant decanted; this process was carried out a second time with Et_2O, and two times with CH_3CN. Finally, the excess of solvents was removed by a gentle flow of N_2 gas yielding helicate **Zn-7•SO$_4$** as a microcrystalline beige solid (11.7 mg, yield 90%). ^{1}H NMR (400 MHz, D_2O, 298 K): δ = 8.91 (s, 6H, imine-H*a*), 8.63 (d, $^3J_{1H–1H}$ = 8.0 Hz, 6H, Py-H*b*), 8.19 (d, $^3J_{1H–1H}$ = 8.1 Hz, 6H, Py-H*c*), 7.25 (s, 12H, Ar-H*h*), 6.53 (s, 6H, Py-H*d*), 4.10 (dd, $^2J_{1H–1H}$ = 12.6, $^3J_{1H–1H}$ = 12.2 Hz, 6H, TREN-H*e*), 3.81 (d, $^2J_{1H–1H}$ = 12.4 Hz, 6H, TREN-H*e*), 3.32 (d, $^2J_{1H–1H}$ = 11.9 Hz, 6H, TREN-H*f*), 3.11 (dd, $^2J_{1H–1H}$ = 12.1, $^3J_{1H–1H}$ = 12.0 Hz, 6H, TREN-H*f*). ^{13}C NMR (100 MHz, D_2O, 298 K): δ = 163.5, 147.2, 147.0, 138.1, 135.7, 129.6, 128.1, 57.1, 54.3. DOSY Diffusion coefficient = 2.70 × 10^{-10} m^2/s. ESI-MS (H_2O): *m/z* = 294.7 [**Zn-7**]$^{+4}$, 408.2 [**Zn-7**(CHO_2)]$^{+3}$, 425.6 [**Zn-7**(HSO_4)]$^{+3}$, 635.1 [**Zn-7**$(CHO_2)_2$]$^{+2}$, 661.2 [**Zn-7**$(CHO_2)_2$]$^{+2}$, 687.3 [**Zn-7**$(HSO_4)_2$]$^{+2}$. Elemental analysis (%) calcd for $C_{60}H_{60}N_{14}O_8S_2Zn_2$•$2.5H_2O$: C 53.57, H 4.87, N 14.58; found: C 53.86, H 4.91, N 14.72.

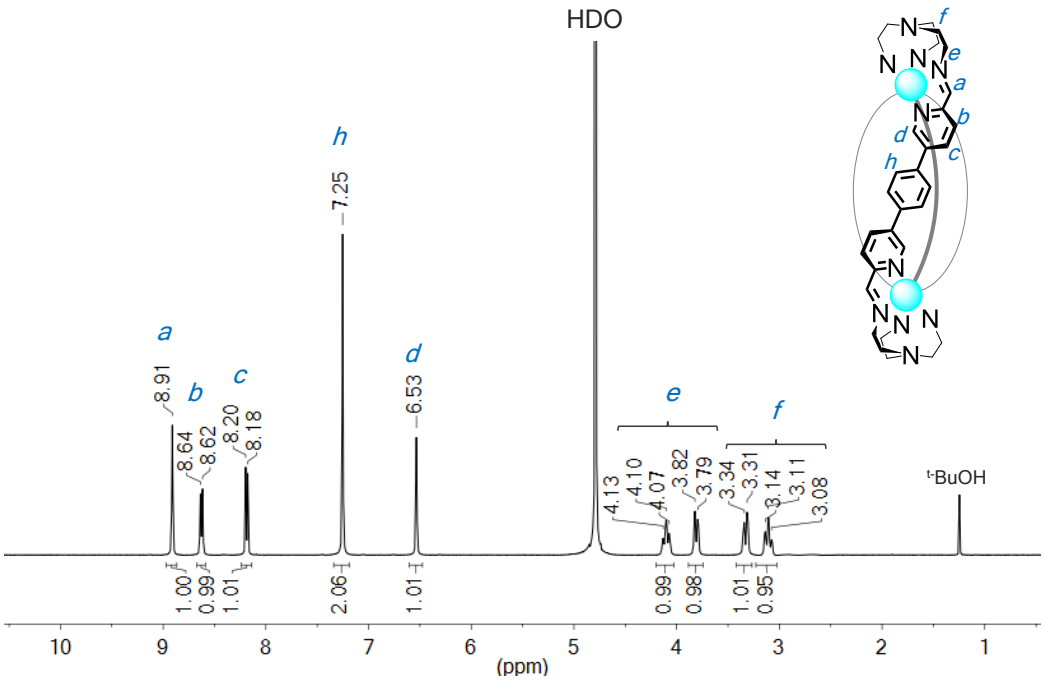

Figure S41. ^{1}H NMR spectrum (400 MHz, D_2O, 298 K) of helicate **Zn–7•SO$_4$**.

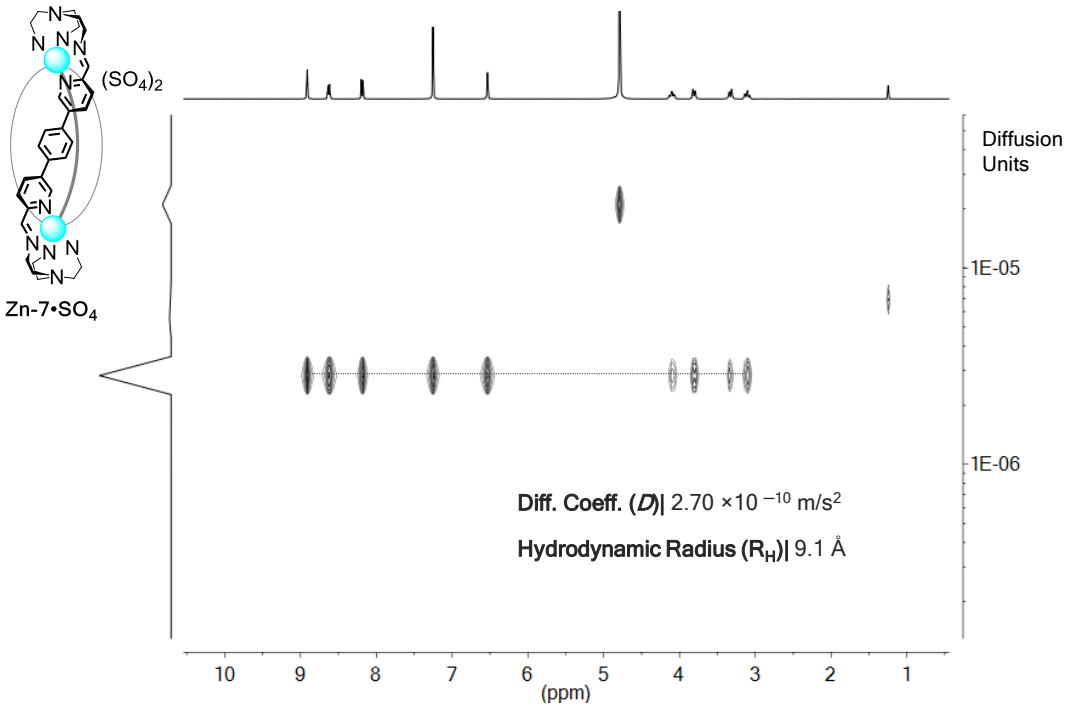

Figure S42. ^{1}H DOSY NMR spectrum (400 MHz, D_2O, 298 K) of helicate **Zn–7•SO$_4$**.

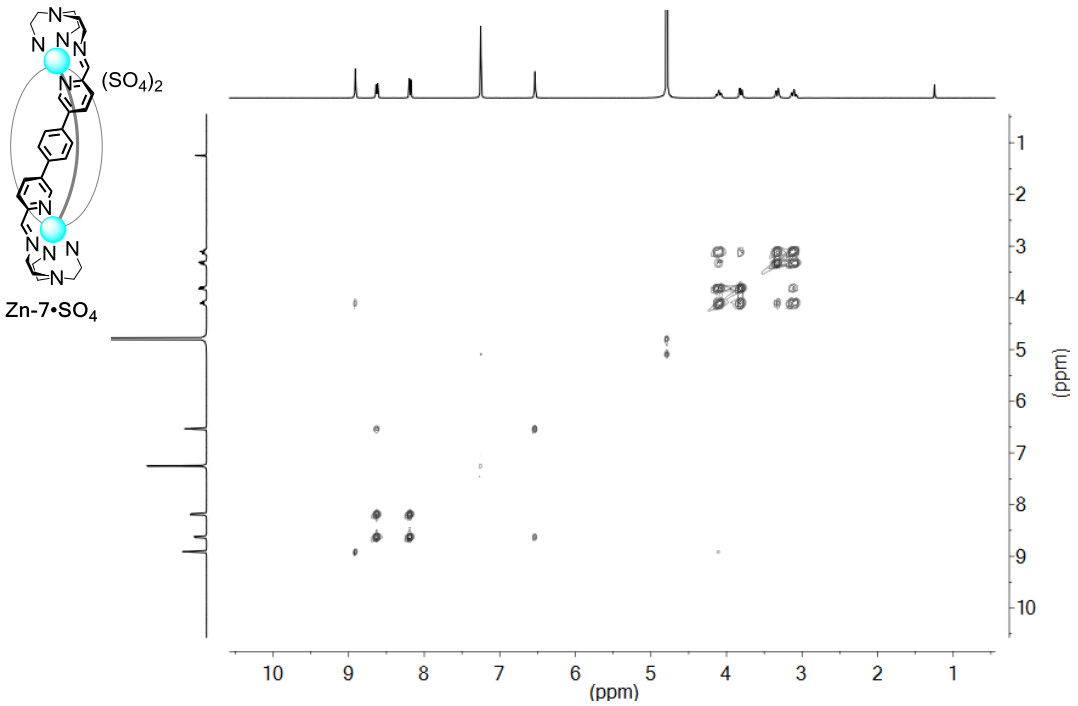

Figure S43. $^{1}H–^{1}H$ COSY NMR spectrum (400 MHz, D_2O, 298 K) of helicate **Zn–7•SO$_4$**.

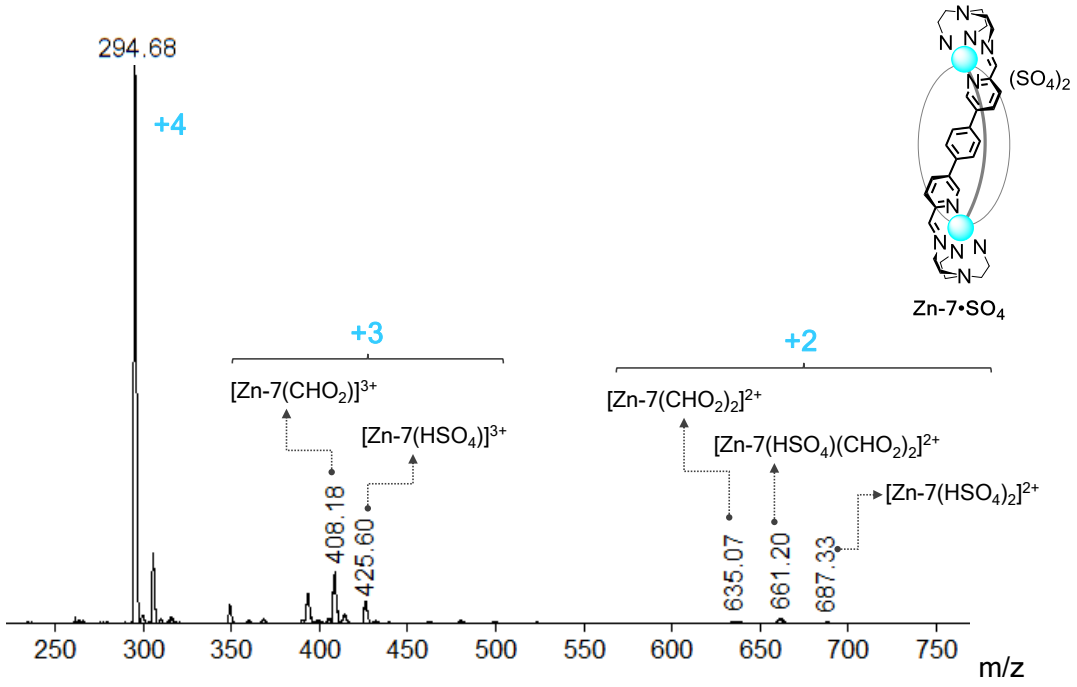

Figure S44. ESI-MS spectrum of helicate **Zn–7•SO$_4$** recorded in H_2O.

The products of the reactions between aldehyde **F** and $CdSO_4$ aimed to prepare tetrahedron **Cd-12•SO$_4$** were dependent on the concentration. It was observed that higher concentration of subcomponents yielded a mixture of two species, the target Cd_4L_6 capsule and a Cd_2L_3 helicate. While the self-assembly reaction using aldehyde **F** with a concentration of 17.4 mM (5.0 mg in 1000 µL of solvent) yielded a water-soluble mixture of helicate/tetrahedron, reaction at a concentration of 5.7 mM (5.0 mg in 3000 µL of solvent) assured the formation of the target tetrahedron **Cd-12•SO$_4$** as the pure product in good yield (Figure S45).

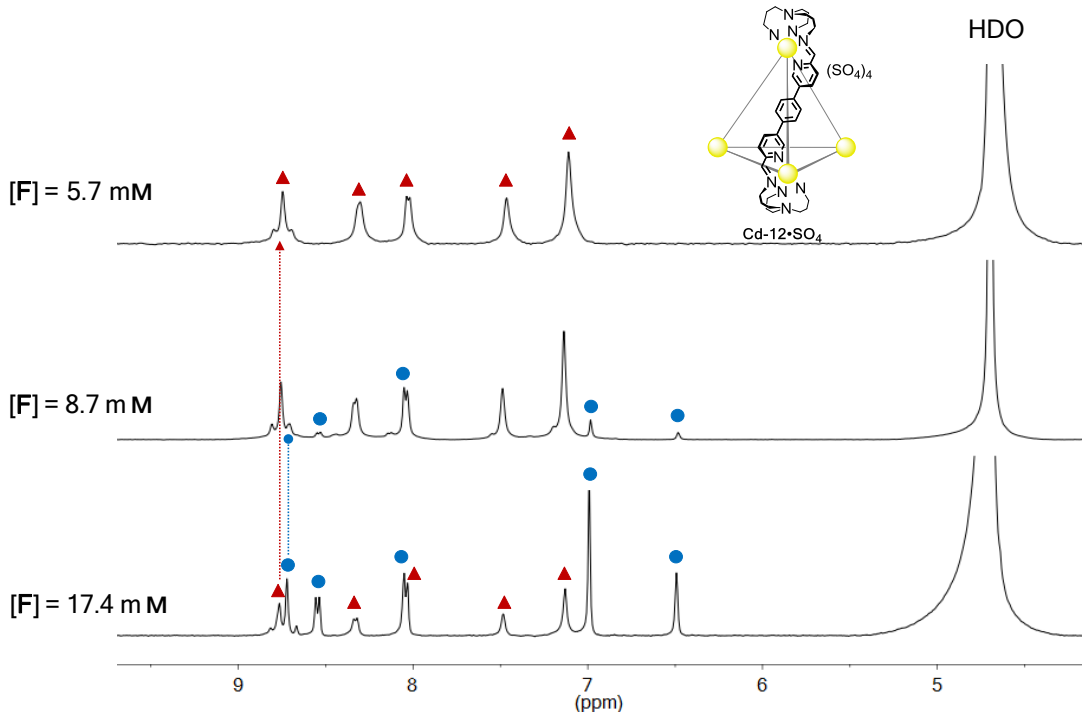

Figure S45. Aromatic region of the ^{1}H NMR spectra (400 MHz, D_2O, 298 K) of products obtained from three different self-assembly reactions of aldehyde **F** with $CdSO_4$ and TRPN at varied concentrations; such variations may yield either a mixture of helicate/tetrahedron or only tetrahedron **Cd–12•SO$_4$** as products. Blue circles (●) denote helicate peaks and red triangles (▲) the tetrahedron signals.

Details of the preparation of pure tetrahedron are given as follows: Subcomponent **F** (5.0 mg, 0.017 mmol, 6 equiv), tris(3-aminopropyl)amine (TRPN) (2.1 µL, 0.012 mmol, 4 equiv), cadmium(II) sulfate (2.4 mg, 0.012 mmol, 4 equiv), and 3.0 mL of 1:1 CH_3CN/H_2O

were placed in a Schlenk flask. The mixture was degassed by three evacuation/nitrogen fill cycles, sonicated for 15 minutes and heated at 80°C overnight yielding a yellow solution with a small amount of beige insoluble material. This solid was removed by filtration through celite, and excess CH_3CN was added to the bright yellow liquor leading to precipitation of a light yellow solid. The mixture was centrifuged and the supernatant CH_3CN/H_2O was decanted. To remove the excess of unreacted aldehyde **F** and TRPN, the solid was washed with CH_2Cl_2, centrifuged and the supernatant decanted; this process was carried out a second time with Et_2O, and a two times with CH_3CN. Finally, the excess of solvents was removed by a gentle flow of N_2 gas yielding cage **Cd-12•SO$_4$** as a microcrystalline light yellow solid (7.1 mg, yield 80%). ^{1}H NMR (400 MHz, D_2O, 298 K): δ = 8.98 (s, $^3J_{1H–113Cd}$ = 21.0 Hz, 12H, imine-H*a*), 8.56 (d, $^3J_{1H–1H}$ = 8.1 Hz, 12H, Py-H*b*), 8.27 (d, $^3J_{1H–1H}$ = 8.0 Hz, 12H, Py-H*c*), 7.70 (s, 12H, Py-H*d*), 7.36 (s, 24H, Ar-H*h*), 4.04 (d, $^2J_{1H–1H}$ = 10.8 Hz, 12H, TRPN-H*e*), 3.64 (m, 24H, TRPN-H*e*, H*f*), 2.50 (m, 12H, TRPN-H*f*), 2.37 (m, 12H, TRPN-H*g*), 2.06 (d, $^2J_{1H–1H}$ = 13.9 Hz, 12H, TRPN-H*g*). ^{13}C NMR (100 MHz, D_2O, 298 K): δ = 162.0, 147.4, 147.0, 140.6, 138.8, 136.7, 129.0, 128.3, 62.3, 58.9, 26.2. DOSY Diffusion coefficient = 1.82 × 10^{-10} m^2/s. ESI-MS (H_2O): *m/z* = 339.5 [**Cd-12**]$^{+8}$, 394.3 [**Cd-12**(CHO_2)]$^{+7}$, 468.0 [**Cd-12**(SO_4)]$^{+6}$, 476.4 [**Cd-12**$(CHO_2)(HSO_4)$]$^{+6}$, 571.4 [**Cd-12**$(CHO_2)(SO_4)$]$^{+5}$, 580.9 [**Cd-12**$(HSO_4)(SO_4)$]$^{+5}$ 725.7 [**Cd-12**$(SO_4)_2$]$^{+4}$, 737.2 [**Cd-12**$(CHO_2)(HSO_4)(SO_4)$]$^{+4}$. Elemental analysis (%) calcd for $C_{144}H_{144}Cd_4N_{28}O_{16}S_4$•$4.5H_2O$: C 54.36, H 4.85, N 12.33; found: C 54.28, H 4.76, N 12.25.

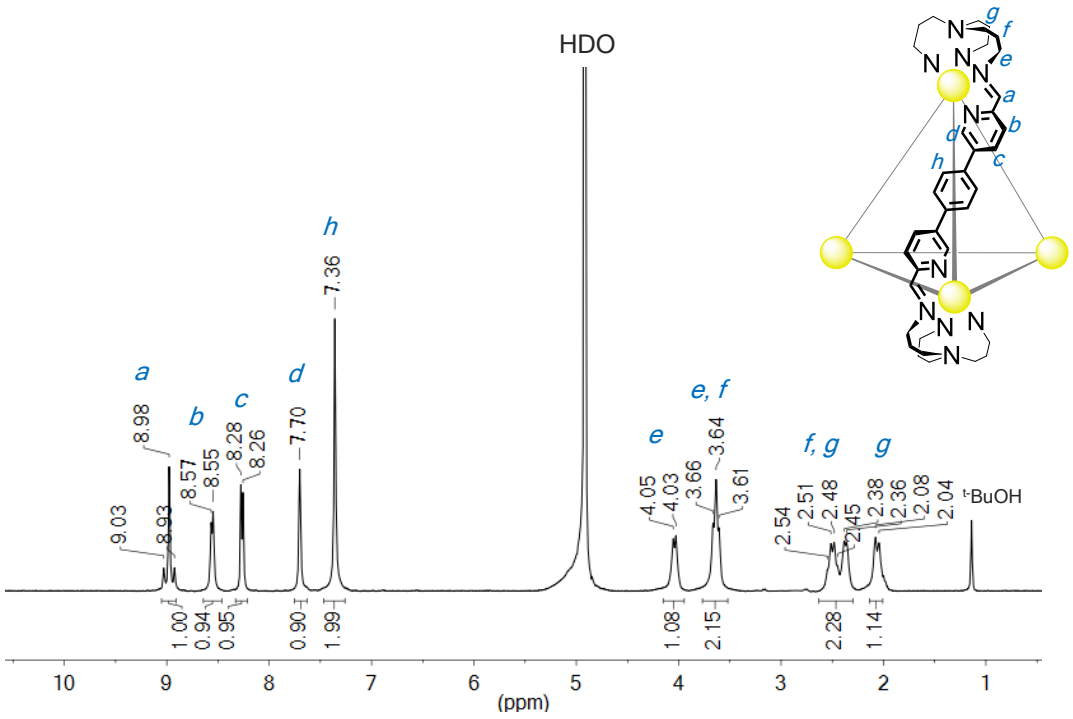

Figure S46. ^{1}H NMR spectrum (400 MHz, D_2O, 298 K) of tetrahedron **Cd–12•SO$_4$**.

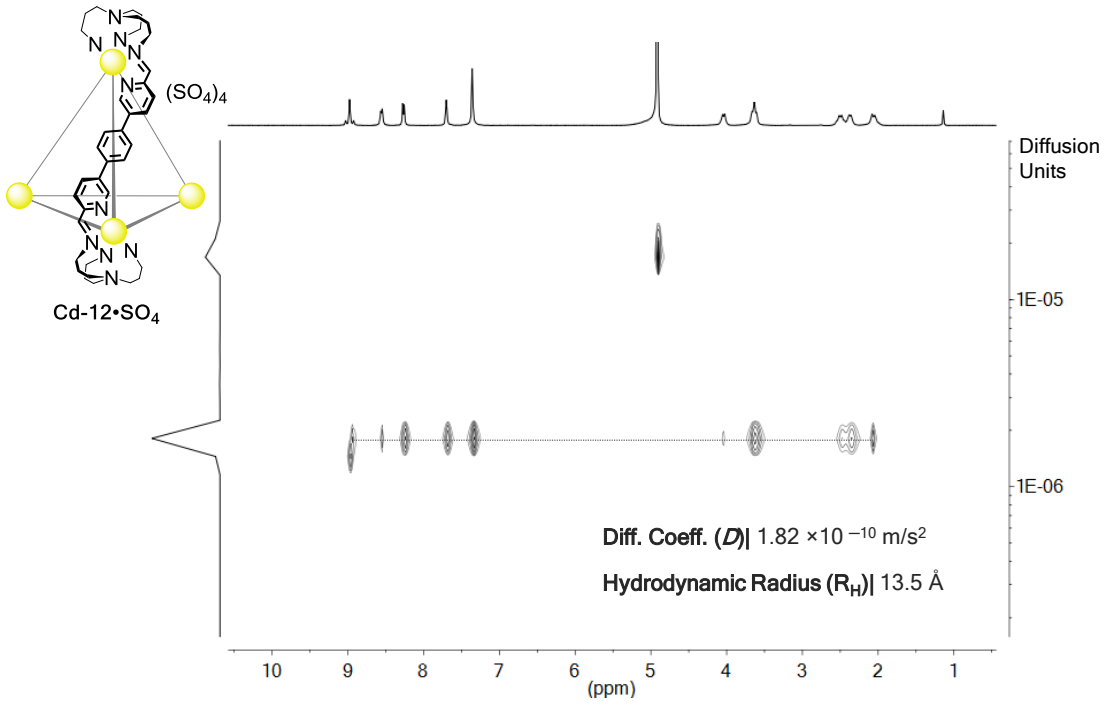

Figure S47. ^{1}H DOSY NMR spectrum (400 MHz, D_2O, 298 K) of tetrahedron **Cd–12•SO$_4$**.

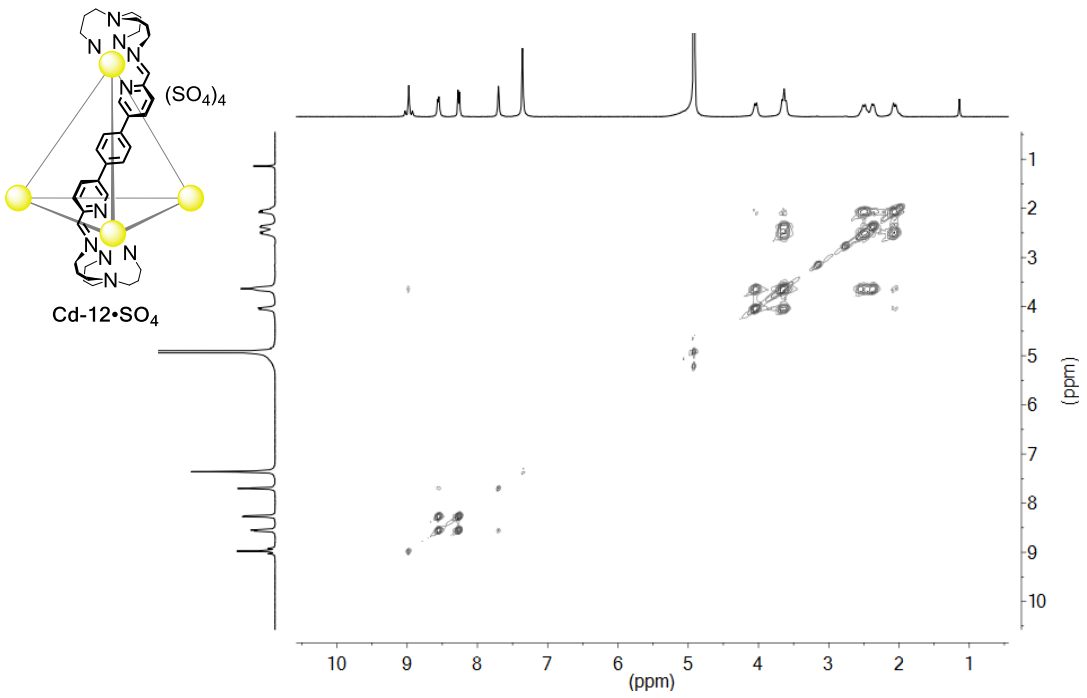

Figure S48. $^{1}H–^{1}H$ COSY NMR spectrum (400 MHz, D_2O, 298 K) of tetrahedron **Cd–12•SO_4**.

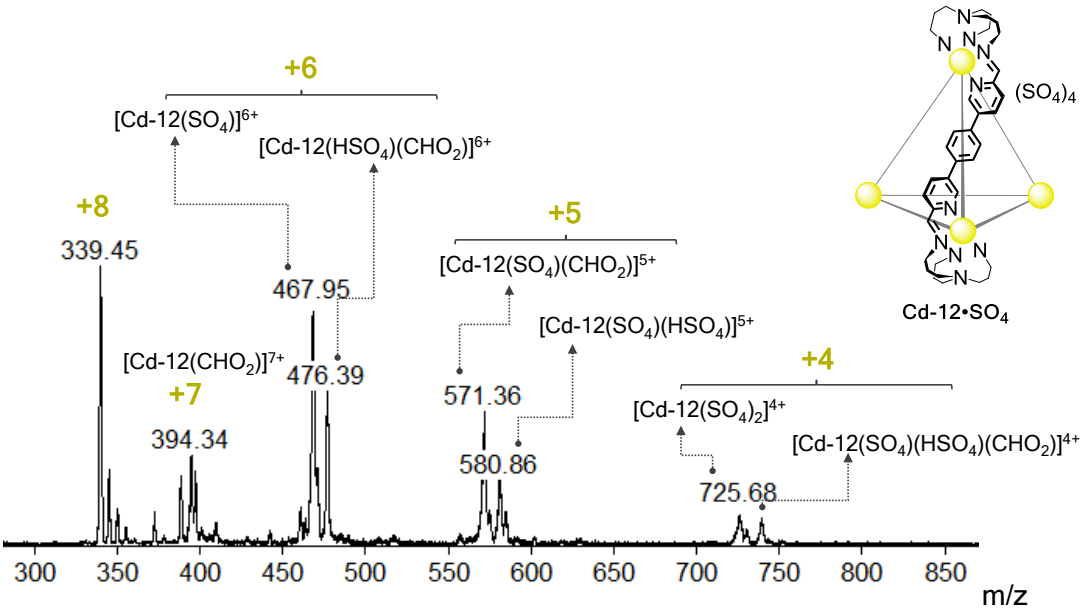

Figure S49. ESI-MS spectrum of tetrahedron **Cd–12•SO_4** recorded in H_2O.

*5.3 Reactions of aldehyde **G** to form helicate **Zn–8•SO$_4$** or tetrahedron **Cd–13•SO$_4$***

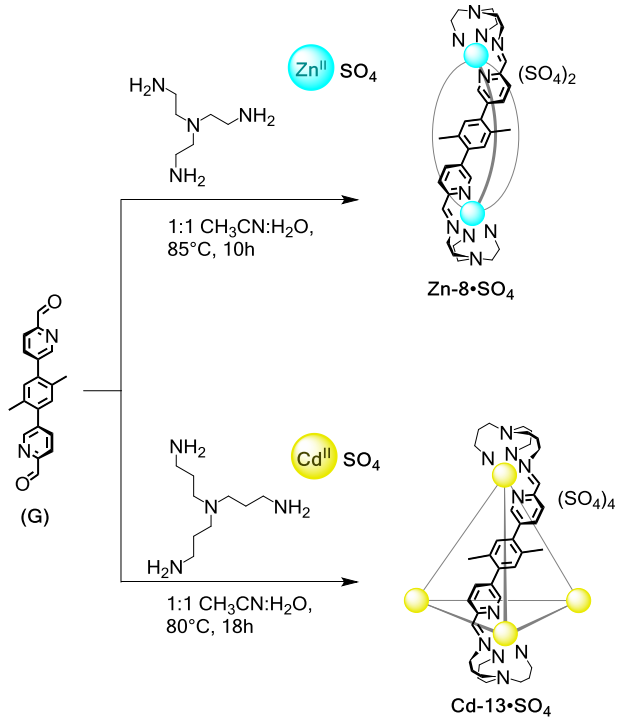

Subcomponent **G** (7.5 mg, 0.024 mmol, 3 equiv), tris(2-aminoethyl)amine (TREN) (2.4 µL, 0.016 mmol, 2 equiv), zinc(II) sulfate heptahydrate (4.5 mg, 0.016 mmol, 2 equiv), and 1.5 mL of 1:1 CH_3CN/H_2O were placed in a Schlenk flask. The mixture was degassed by three evacuation/nitrogen fill cycles, sonicated for 15 minutes and heated at 85°C overnight yielding a yellow solution with a minor amount of insoluble material, which was removed by filtration using a small column with celite. Excess of CH_3CN was added to the bright yellow liquor leading to precipitation of a cream-colored solid. The mixture was centrifuged and the supernatant CH_3CN/H_2O was decanted. To remove excess unreacted aldehyde **G** and TREN, the precipitate was washed with CH_2Cl_2, centrifuged and the supernatant decanted; this process was carried out a second time with Et_2O, and two times more with CH_3CN. Finally, the excess of solvents was removed by a gentle flow of N_2 gas yielding helicate **Zn-8•SO$_4$** as a microcrystalline white solid (10.2 mg, yield 88%). ^{1}H NMR (400 MHz, D_2O, 298 K): δ = 8.87 (s, 6H, imine-H*a*), 8.48 (d, $^3J_{1H–1H}$ = 8.0 Hz, 6H, Py-H*b*), 8.19 (d, $^3J_{1H–1H}$ = 7.9 Hz, 6H, Py-H*c*), 7.23 (s, 6H, Ar-H*h*), 7.21 (s, 6H, Py-H*d*), 4.01 (dd, $^2J_{1H–1H}$ = 12.4, $^3J_{1H–1H}$ = 11.8 Hz, 6H, TREN-H*e*), 3.74 (d, $^2J_{1H–1H}$ = 11.2 Hz, 6H, TREN-H*e*), 3.34 (d, $^2J_{1H–1H}$ = 12.9 Hz, 6H, TREN-H*f*), 3.06 (dd, $^2J_{1H–1H}$ = 13.6, $^3J_{1H–1H}$ =

12.9 Hz, 6H, TREN-H*f*), 1.70 (s, 18H, –CH_3-H*i*). ^{13}C NMR (100 MHz, D_2O, 298 K): δ = 163.8, 148.4, 146.4, 141.5, 140.9, 135.9, 134.2, 133.2, 130.2, 57.6, 54.9, 19.0. DOSY Diffusion coefficient = 2.45 × 10^{-10} m^2/s. ESI-MS (H_2O): *m/z* = 316.1 [**Zn-8**]$^{+4}$, 436.4 [**Zn-8**(CHO_2)]$^{+3}$, 453.8 [**Zn-8**(HSO_4)]$^{+3}$, 679.0 [**Zn-8**(SO_4)]$^{+2}$, 729.3 [**Zn-8**(HSO_4)$_2$]$^{+2}$. Elemental analysis (%) calcd for $C_{72}H_{72}N_{14}O_8S_2Zn_2$•$4H_2O$: C 56.58, H 5.28, N 12.83; found: C 56.86, H 5.56, N 12.78.

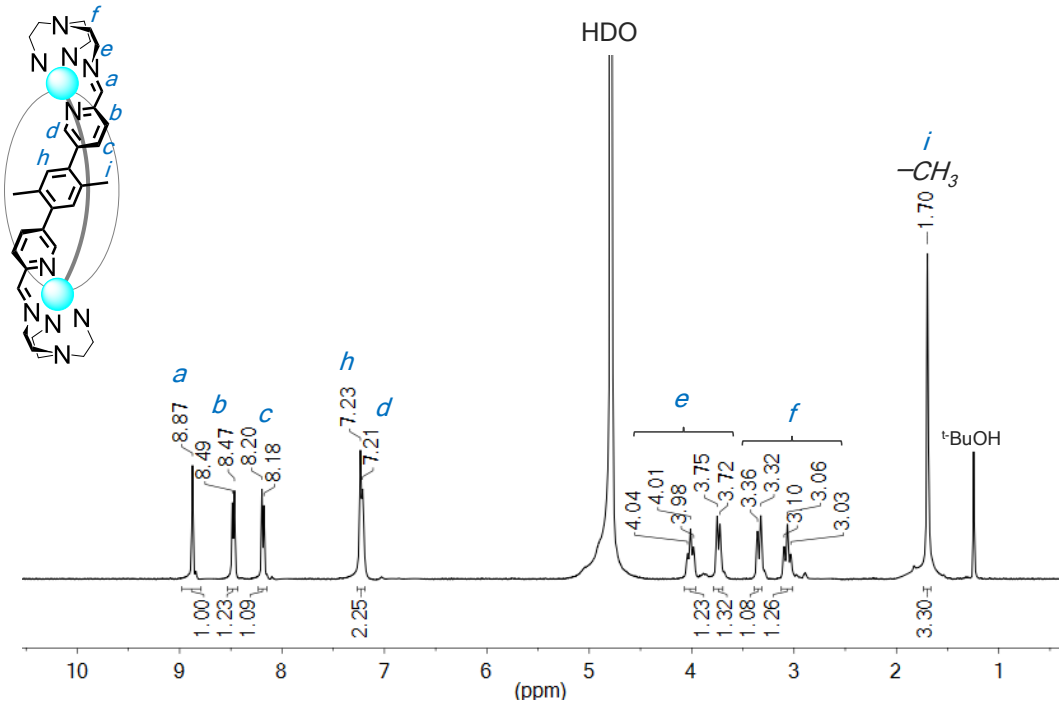

Figure S50. ^{1}H NMR spectrum (400 MHz, D_2O, 298 K) of helicate **Zn–8•SO_4**.

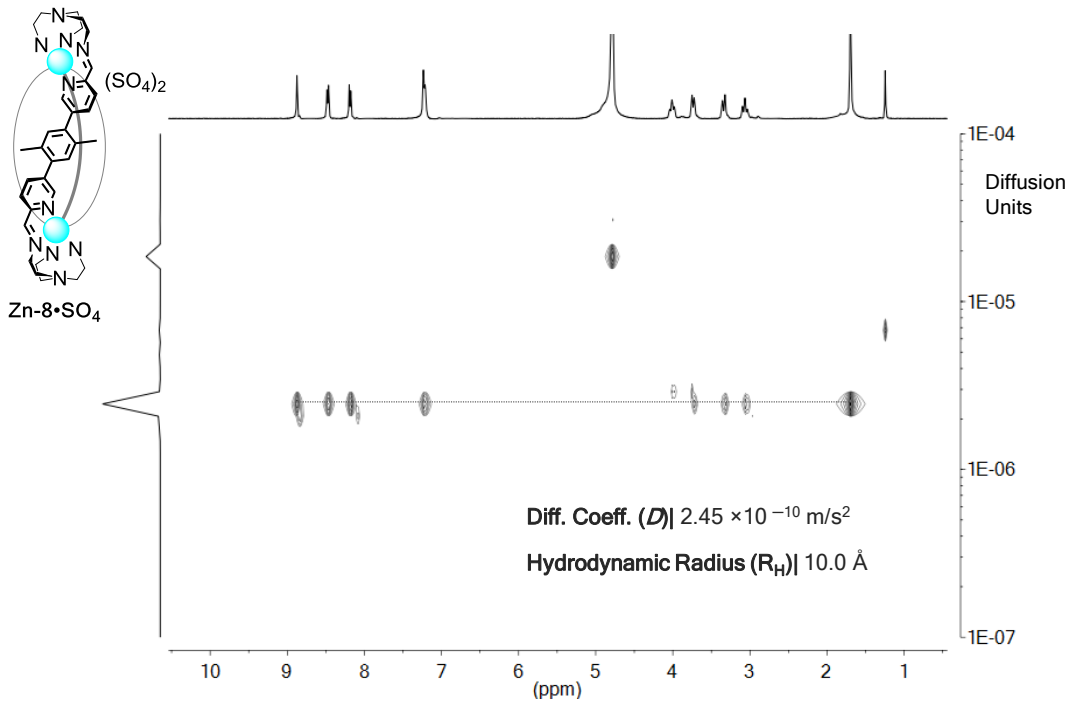

Figure S51. ^{1}H DOSY NMR spectrum (400 MHz, D_2O, 298 K) of helicate **Zn–8•SO$_4$**.

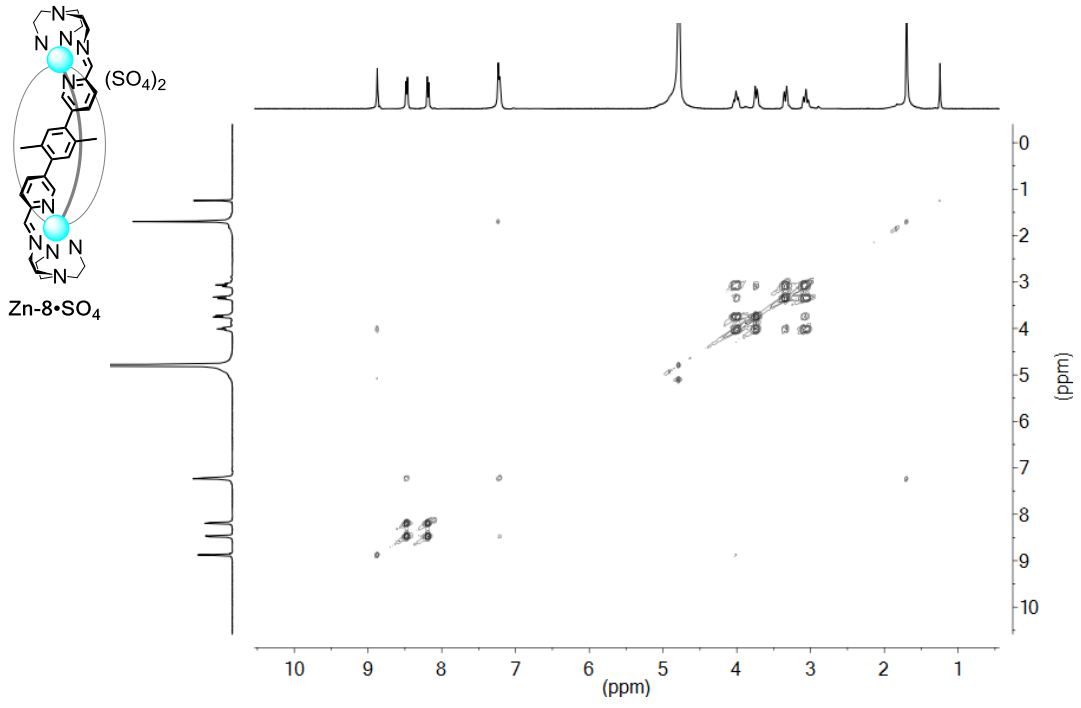

Figure S52. ^{1}H–^{1}H COSY NMR spectrum (400 MHz, D_2O, 298 K) of helicate **Zn–8•SO$_4$**.

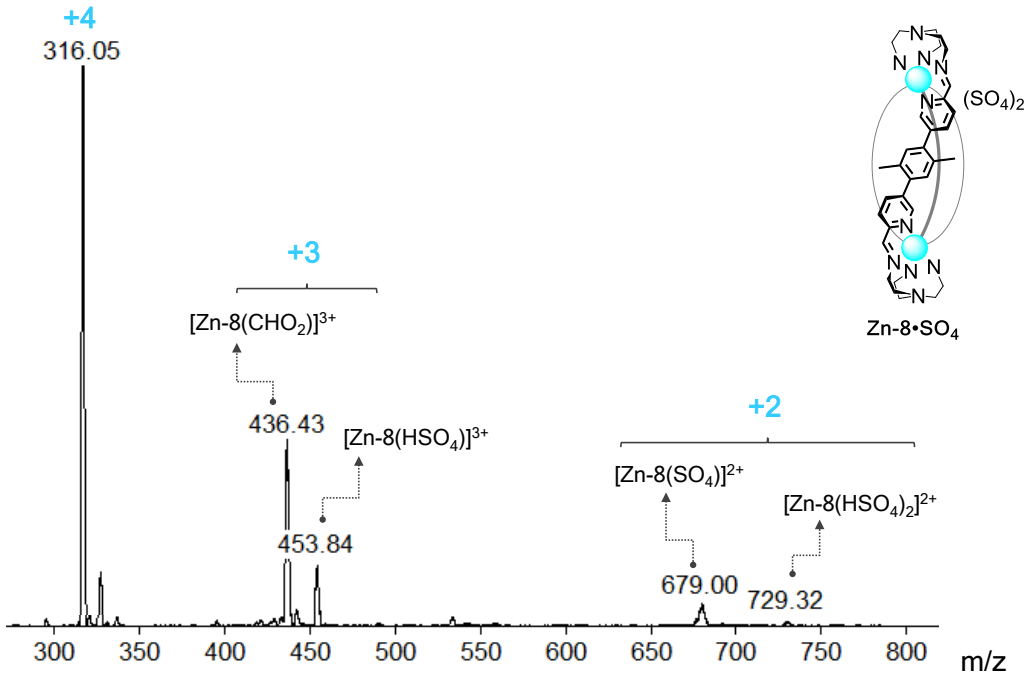

Figure S53. ESI-MS spectrum of helicate **Zn–8•SO_4** recorded in H_2O.

Subcomponent **G** (5.2 mg, 0.016 mmol, 6 equiv), tris(3-aminopropyl)amine (TRPN) (2.1 µL, 0.011 mmol, 4 equiv), cadmium(II) sulfate (2.3 mg, 0.011 mmol, 4 equiv), and 1.5 mL of 1:1 CH_3CN/H_2O were placed in a Schlenk flask. The mixture was degassed by three evacuation/nitrogen fill cycles, sonicated for 15 minutes and heated at 80°C overnight yielding a yellow solution with a small amount of pale yellow insoluble material. This solid was removed by filtration using a small column with celite, and excess of CH_3CN was added to the bright yellow liquor leading to precipitation of a creamy solid. The mixture was centrifuged and the supernatant CH_3CN/H_2O was decanted. To remove the excess of unreacted aldehyde **G** and TRPN, the solid was washed with CH_2Cl_2, centrifuged and the supernatant decanted; this process was carried out a second time with Et_2O, and two times more with CH_3CN. Finally, the excess of solvents was removed by a gentle flow of N_2 gas yielding cage **Cd-13•SO_4** as a microcrystalline white solid (6.3 mg, yield 80%). ^{1}H NMR (400 MHz, D_2O, 298 K): δ = 8.97 (s, $^3J_{1H–113Cd}$ = 20.5 Hz, 12H, imine-H*a*), 8.25 (d, $^3J_{1H–1H}$ = 7.2 Hz, 12H, Py-H*c*), 8.20 (d, $^3J_{1H–1H}$ = 7.6 Hz, 12H, Py-H*b*), 7.42 (s, 12H, Py-H*d*), 7.09

(s, 12H, Ar-H*h*), 4.09 (d, $^{2}J_{1H–1H}$ = 10.0 Hz, 12H, TRPN-H*e*), 3.81–3.61 (m, 24H, TRPN-H*e*, H*f*), 2.54 (m, 12H, TRPN-H*f*), 2.43 (d, $^{2}J_{1H–1H}$ = 10.5 Hz, 12H, TRPN-H*g*), 2.11 (d, $^{2}J_{1H–1H}$ = 13.2 Hz, 12H, TRPN-H*g*), 1.76 (s, 36H, –CH_3-H*i*). ^{13}C NMR (100 MHz, D_2O, 298 K): δ = 161.8, 148.7, 147.0, 141.9, 141.6, 137.2, 133.9, 132.6, 129.1, 62.2, 59.0, 26.2, 19.1. DOSY Diffusion coefficient = 1.79 × 10^{-10} m^2/s. ESI-MS (H_2O): *m/z* = 360.5 [**Cd-13**]$^{+8}$, 420.7 [**Cd-13**(NO_3)]$^{+7}$, 452.1 [**Cd-13**(NTf_2)]$^{+7}$, 496.9 [**Cd-13**(SO_4)]$^{+6}$, 504.6 [**Cd-13**(CHO_2)(HSO_4)]$^{+6}$, 607.9 [**Cd-13**(CHO_2)(NO_3)]$^{+5}$, 769.2 [**Cd-13**(SO_4)$_2$]$^{+4}$. Elemental analysis (%) calcd for $C_{156}H_{156}Cd_4N_{28}O_{16}S_4$•5.5$H_2O$: C 55.83, H 5.02, N 11.69; found: C 55.98, H 5.16, N 11.35.

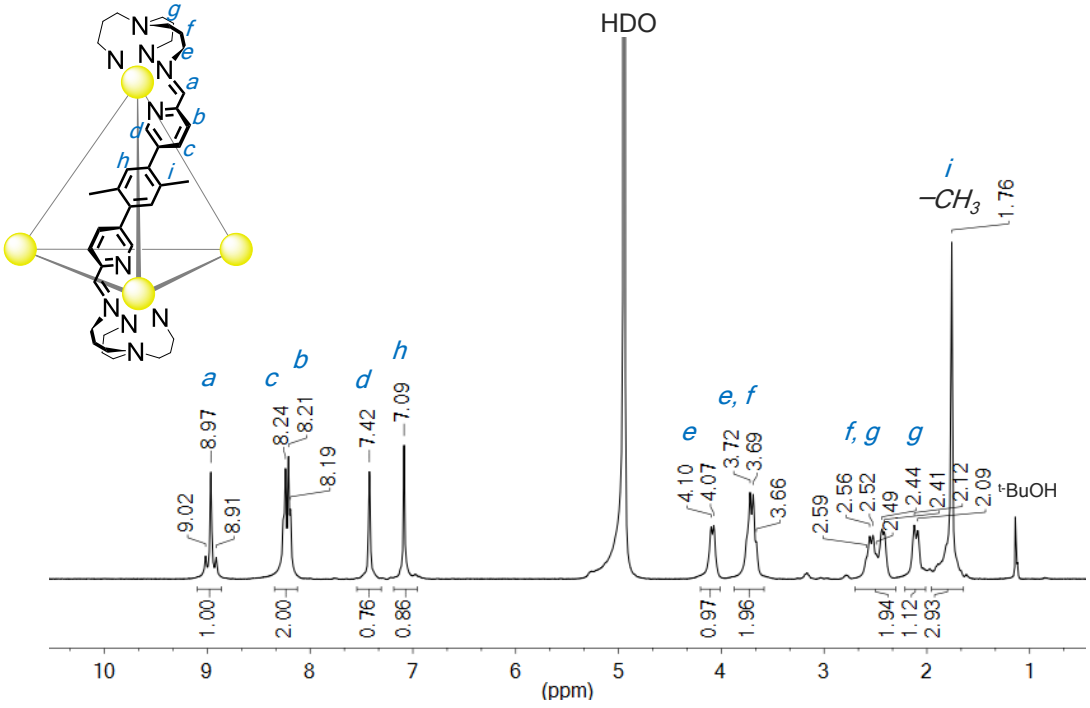

Figure S54. ^{1}H NMR spectrum (400 MHz, D_2O, 298 K) of tetrahedron **Cd–13•SO_4**.

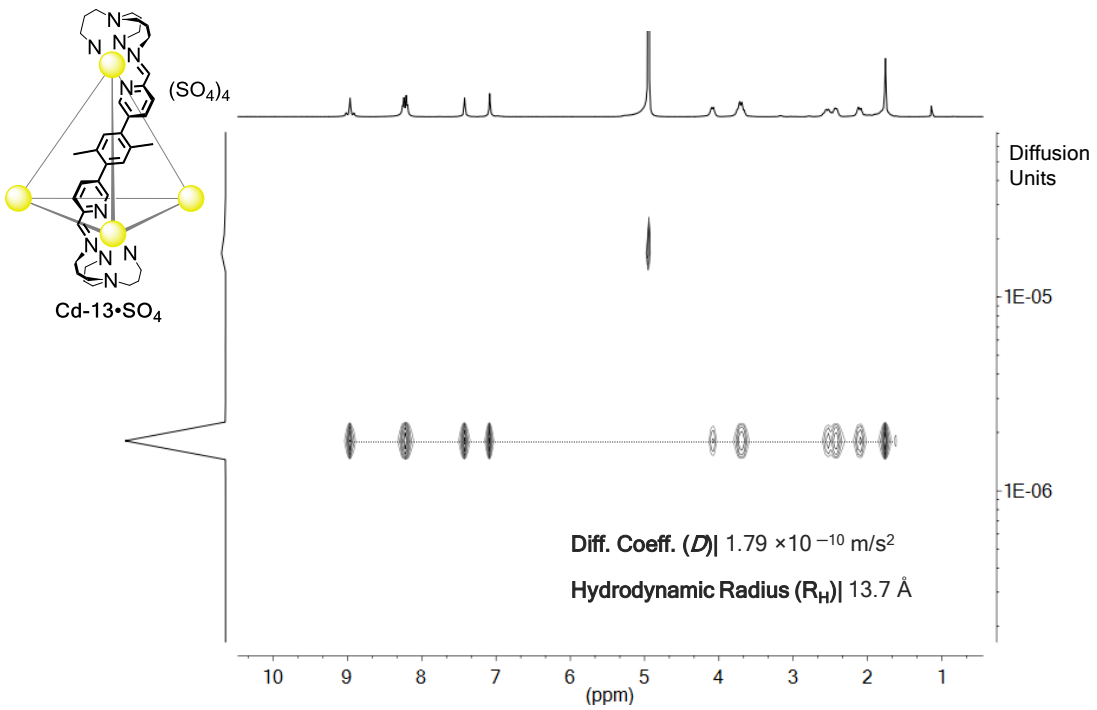

Figure S55. ^{1}H DOSY NMR spectrum (400 MHz, D_2O, 298 K) of tetrahedron **Cd–13•SO$_4$**.

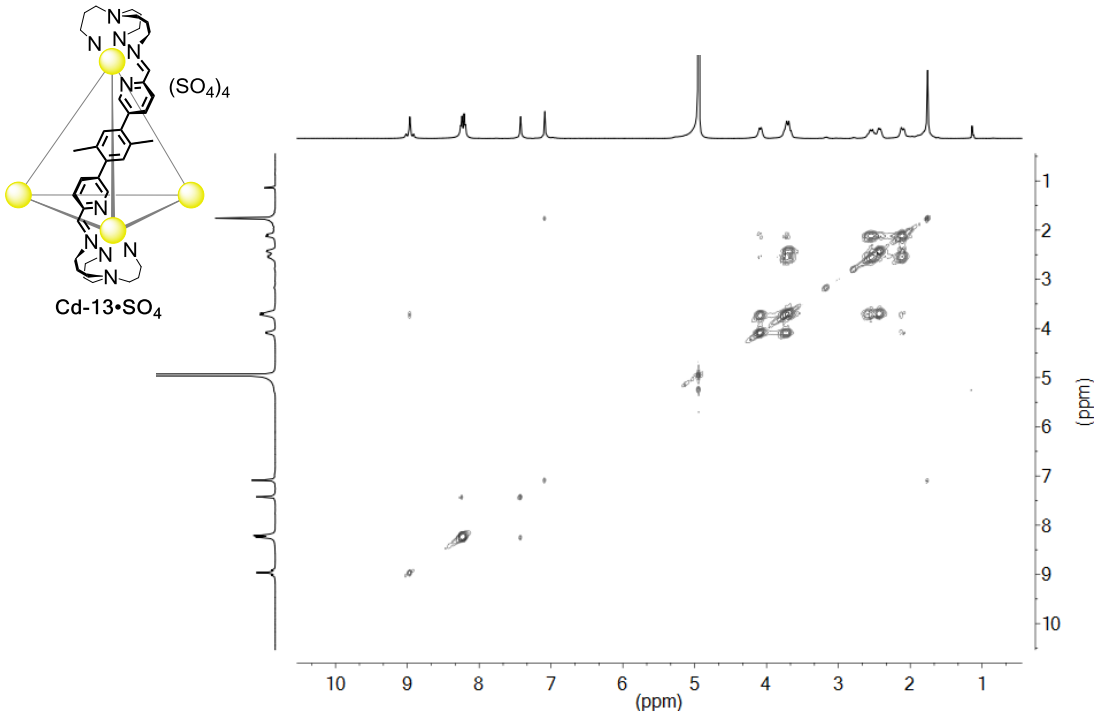

Figure S56. ^{1}H–^{1}H COSY NMR spectrum (400 MHz, D_2O, 298 K) of tetrahedron **Cd–13•SO$_4$**.

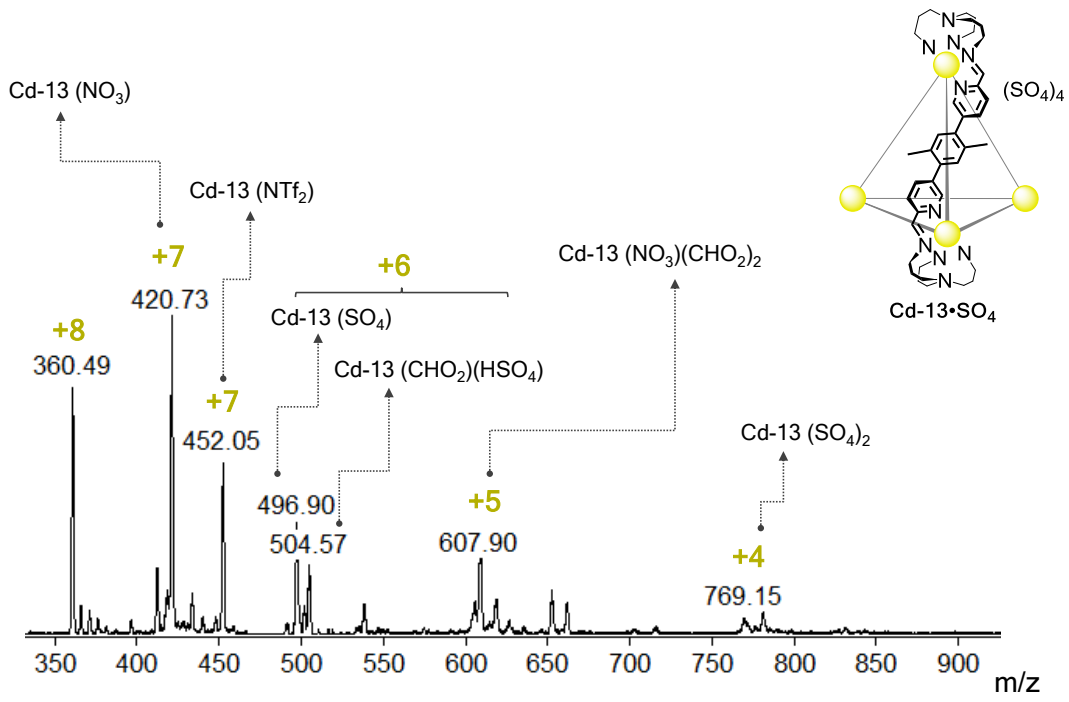

Figure S57. ESI-MS spectrum of tetrahedron **Cd–13•SO_4** recorded in H_2O.

*5.4 Reactions of aldehyde **H** to form helicate **Zn–9•SO_4** or tetrahedron **Cd–14•SO_4***

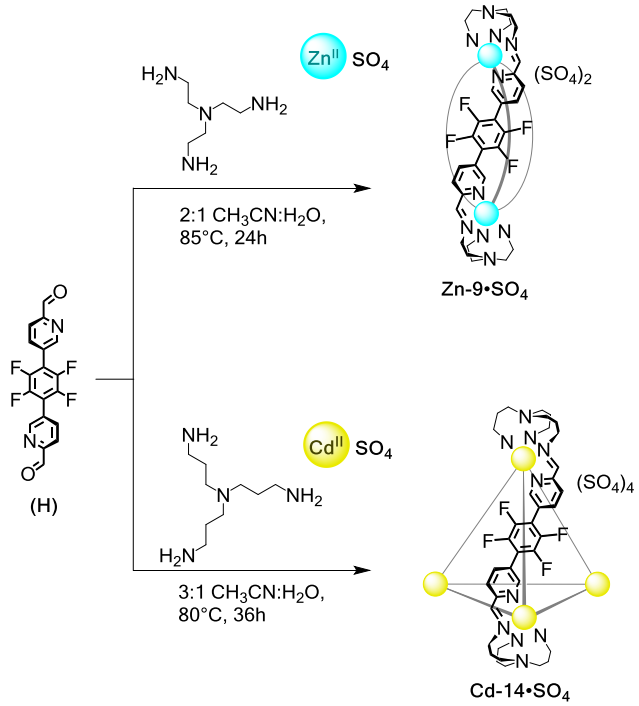

Subcomponent **H** (4.8 mg, 0.013 mmol, 3.6 equiv), tris(2-aminoethyl)amine (TREN) (1.1 μL, 0.007 mmol, 2 equiv), zinc(II) sulfate heptahydrate (2.1 mg, 0.007 mmol, 2 equiv), and 1.5 mL of 2:1 CH_3CN/H_2O were placed in a Schlenk flask. The mixture was degassed by three evacuation/nitrogen fill cycles, sonicated for 20 minutes and heated at 85°C for 24h yielding a yellow suspension. The solid (likely unreacted aldehyde **H** and oligomeric material) was removed by filtration using a small column with celite. Excess of CH_3CN was added to the bright yellow liquor leading to precipitation of yellow solid. The mixture was centrifuged and the supernatant CH_3CN/H_2O was removed. The precipitate was washed with CH_2Cl_2, centrifuged and the supernatant decanted; this process was repeated with Et_2O, and carried out two times with CH_3CN. Finally, the excess of solvents was removed by a gentle flow of N_2 gas yielding helicate **Zn-9•SO$_4$** as a microcrystalline yellow solid (4.5 mg, yield 75%). ^{1}H NMR (400 MHz, D_2O, 298 K): δ = 8.93 (s, 6H, imine-H*a*), 8.56 (d, $^3J_{1H–1H}$ = 8.0 Hz, 6H, Py-H*b*), 8.24 (d, $^3J_{1H–1H}$ = 7.9 Hz, 6H, Py-H*c*), 7.22 (s, 6H, Py-H*d*), 4.09 (dd, $^2J_{1H–1H}$ = 11.2, $^3J_{1H–1H}$ = 10.5 Hz, 6H, TREN-H*e*), 3.80 (d, $^2J_{1H–1H}$ = 11.2 Hz, 6H, TREN-H*e*), 3.34 (d, $^2J_{1H–1H}$ = 13.6 Hz, 6H, TREN-H*f*), 3.09 (dd, $^2J_{1H–1H}$ = 13.4, $^3J_{1H–1H}$ = 12.5 Hz, 6H, TREN-H*f*). ^{13}C NMR (100 MHz, D_2O, 298 K): δ = 165.1, 151.2, 150.3, 143.8, 138.2, 128.0, 122.2, 118.0, 57.9, 54.6. ^{19}F NMR (376 MHz, D_2O, 298 K): δ = –145.3. DOSY Diffusion coefficient = 2.54×10^{-10} m^2/s. ESI-MS (H_2O): *m/z* = 348.8 [**Zn-9**]$^{+4}$, 480.0 [**Zn-9**(CHO_2)]$^{+3}$, 497.4 [**Zn-9**(HSO_4)]$^{+3}$, 745.8 [**Zn-9**(SO_4)]$^{+2}$, 794.9 [**Zn-9**(HSO_4)$_2$]$^{+2}$. Elemental analysis (%) calcd for $C_{60}H_{48}F_{12}N_{14}O_8S_2Zn_2$•3.5$H_2O$•0.5$CH_3CN$: C 45.80, H 3.56, N 12.70; found: C 45.86, H 3.48, N 12.66.

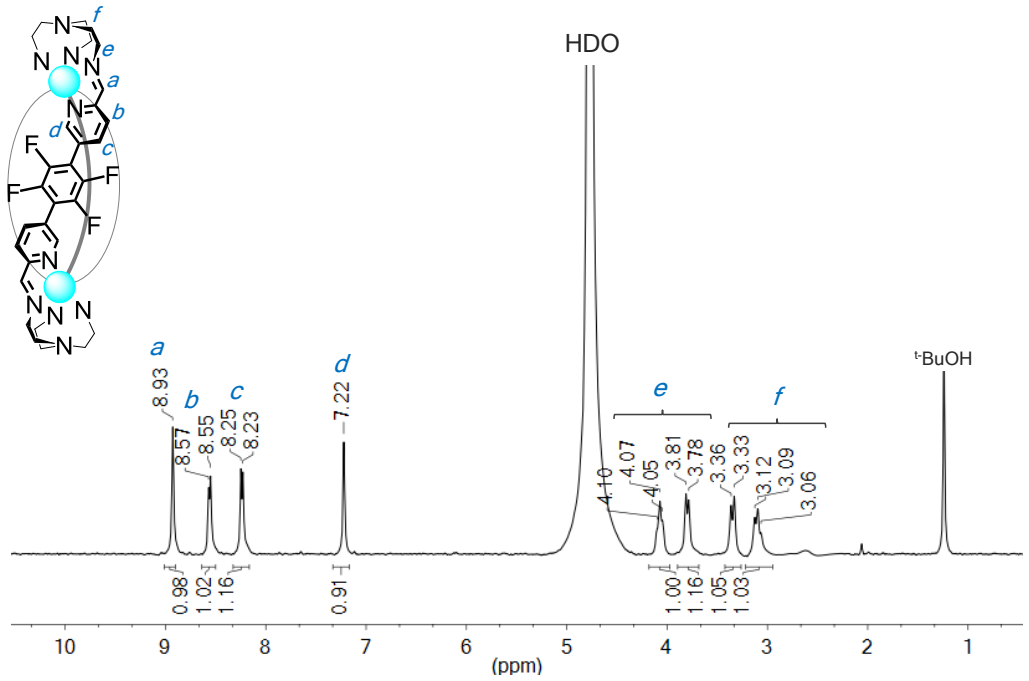

Figure S58. ^{1}H NMR spectrum (400 MHz, D_2O, 298 K) of helicate **Zn–9•SO$_4$**.

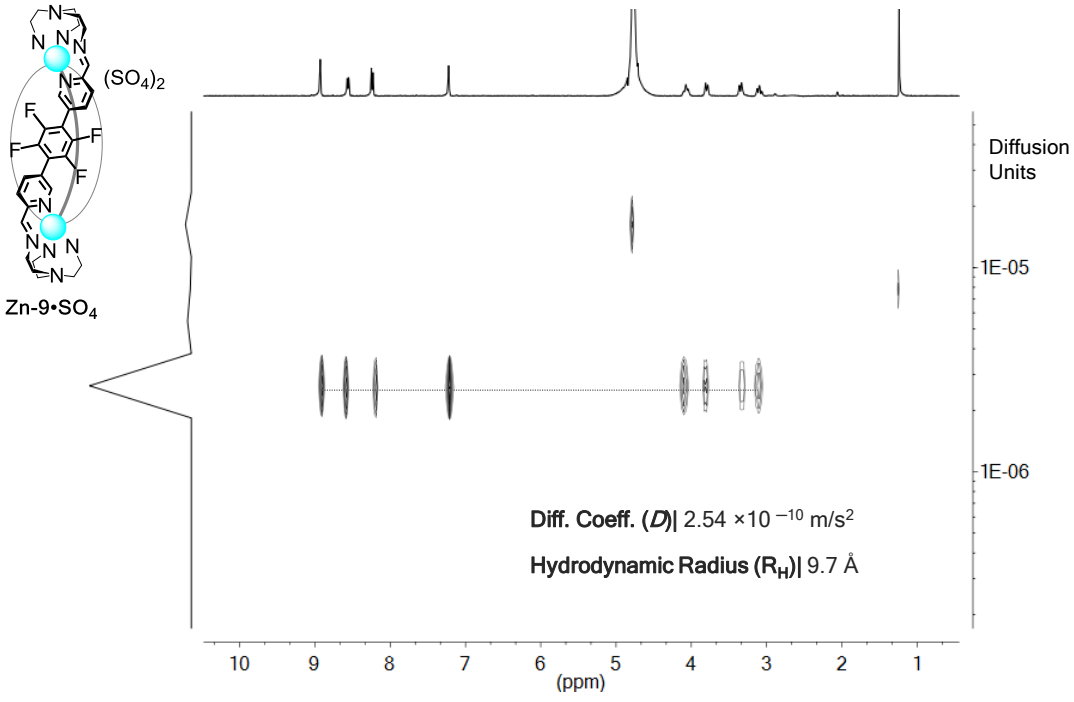

Figure S59. ^{1}H DOSY NMR spectrum (400 MHz, D_2O, 298 K) of helicate **Zn–9•SO$_4$**.

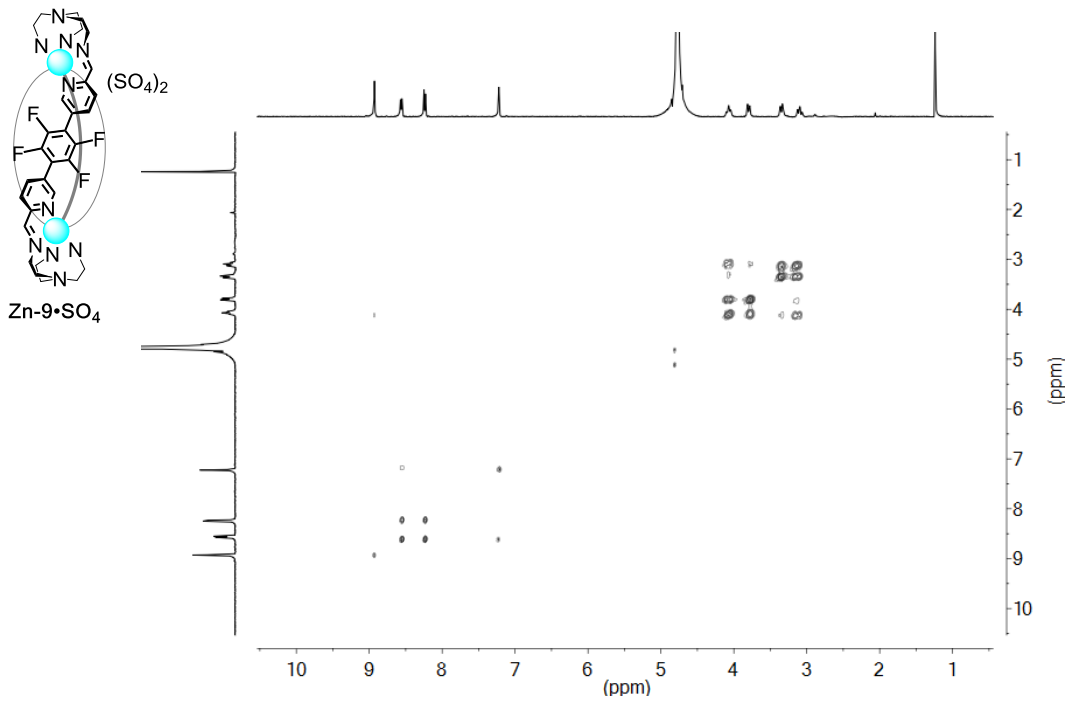

Figure S60. $^{1}H–^{1}H$ COSY NMR spectrum (400 MHz, D_2O, 298 K) of helicate **Zn–9•SO$_4$**.

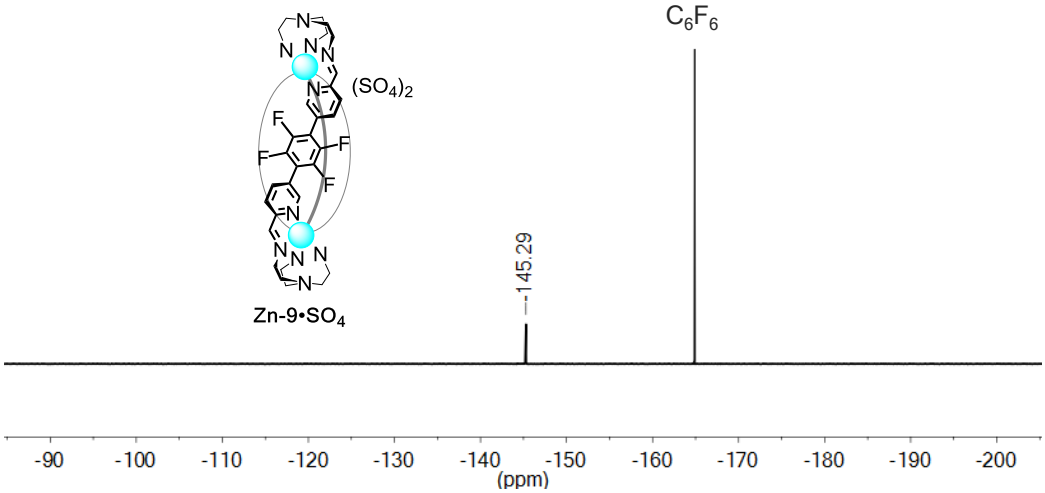

Figure S61. ^{19}F NMR spectrum (376 MHz, D_2O, 298 K) of helicate **Zn–9•SO$_4$**.

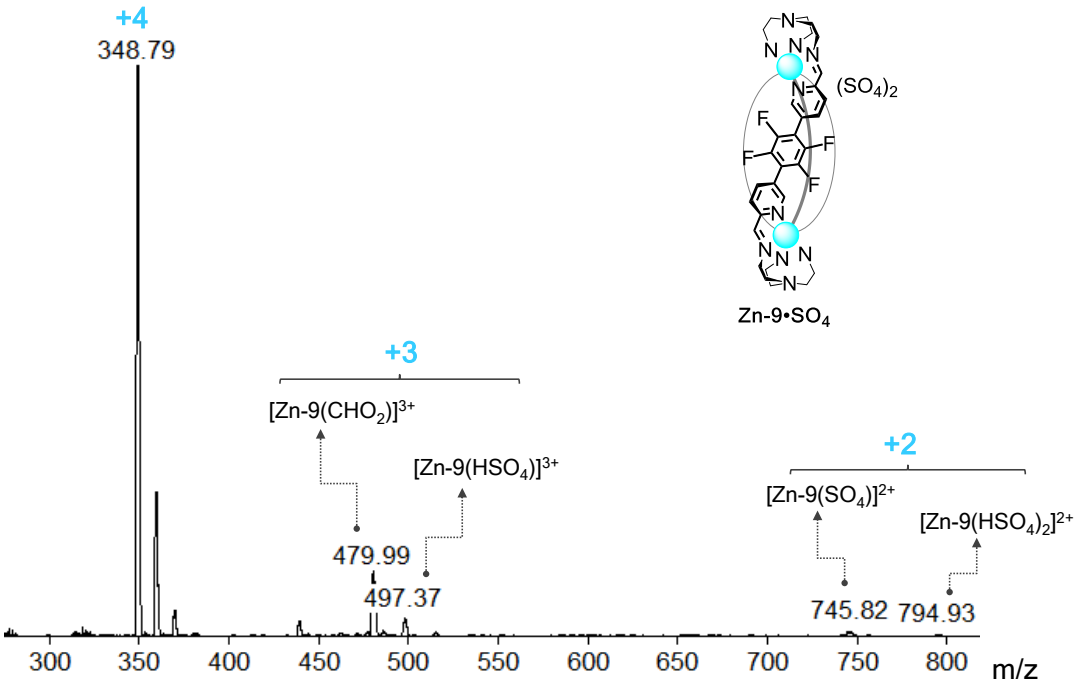

Figure S62. ESI-MS spectrum of helicate **Zn–9•SO$_4$** recorded in H_2O.

Subcomponent **H** (5.4 mg, 0.016 mmol, 7.2 equiv), tris(3-aminopropyl)amine (TRPN) (1.6 µL, 0.008 mmol, 4 equiv), cadmium(II) sulfate (1.7 mg, 0.008 mmol, 4 equiv), and 2.0 mL of 3:1 CH_3CN/H_2O were placed in a Schlenk flask. The mixture was degassed by three evacuation/nitrogen fill cycles, sonicated for 20 minutes and heated at 80°C for 36 h yielding a yellow-mustard suspension. The solid (likely unreacted aldehyde **H** and oligomeric material) was removed by filtration using a small column with celite. Excess of CH_3CN was added to the bright yellow liquor leading to precipitation of yellow solid. The mixture was centrifuged and the supernatant CH_3CN/H_2O was removed. The precipitate was washed with CH_2Cl_2, centrifuged and the supernatant decanted; this process was repeated with Et_2O, and carried out two times with CH_3CN. Finally, the excess of solvents was removed by a gentle flow of N_2 gas yielding cage **Cd-14•SO$_4$** as a microcrystalline yellow solid (5.1 mg, yield 69%). ^{1}H NMR (400 MHz, D_2O, 298 K): δ = 8.93 (s, $^3J_{1H–113Cd}$ = 21.1 Hz, 12H, imine-H*a*), 8.40 (br, 12H, Py-H*c*), 8.19 (d, $^3J_{1H–1H}$ = 7.7 Hz, 12H, Py-H*b*), 7.43 (s, 12H, Py-H*d*), 4.00 (d, $^2J_{1H–1H}$ = 11.9 Hz, 12H, TRPN-H*e*), 3.58 (m, 24H, TRPN-H*e*, H*f*), 2.43 (m, 12H, TRPN-H*f*), 2.32 (d, $^2J_{1H–1H}$ = 10.5 Hz, 12H, TRPN-H*g*), 2.00 (d,

$^{2}J_{1H–1H}$ = 14.2 Hz, 12H, TRPN-H*g*). ^{13}C NMR (100 MHz, D_2O, 298 K): δ = 163.8, 151.7, 151.3, 143.1, 138.6, 128.2, 121.7, 118.1, 63.7, 58.2, 25.9. ^{19}F NMR (376 MHz, D_2O, 298 K): δ = –142.9. DOSY Diffusion coefficient = 1.80 × 10^{-10} m^2/s. ESI-MS (H_2O): *m/z* = 393.3 [**Cd-14**]$^{+8}$, 539.8 [**Cd-14**(CHO_2)]$^{+6}$, 548.6 [**Cd-14**$(CHO_2)(HSO_4)$]$^{+6}$, 658.6 [**Cd-14**$(CHO_2)_2(HSO_4)$]$^{+5}$, 667.1 [**Cd-14**$(CHO_2)_2(HSO_4)$]$^{+5}$, 677.7 [**Cd-14**$(CHO_2)(HSO_4)_2$]$^{+5}$, 845.3 [**Cd-14**$(CHO_2)_3(HSO_4)$]$^{+4}$, 858.3 [**Cd-14**$(CHO_2)_2(HSO_4)_2$]$^{+4}$. Elemental analysis (%) calcd for $C_{144}H_{120}Cd_4F_{24}N_{28}O_{16}S_4$•$8H_2O$: C 47.04, H 3.73, N 10.67; found: C 46.96, H 3.58, N 10.45.

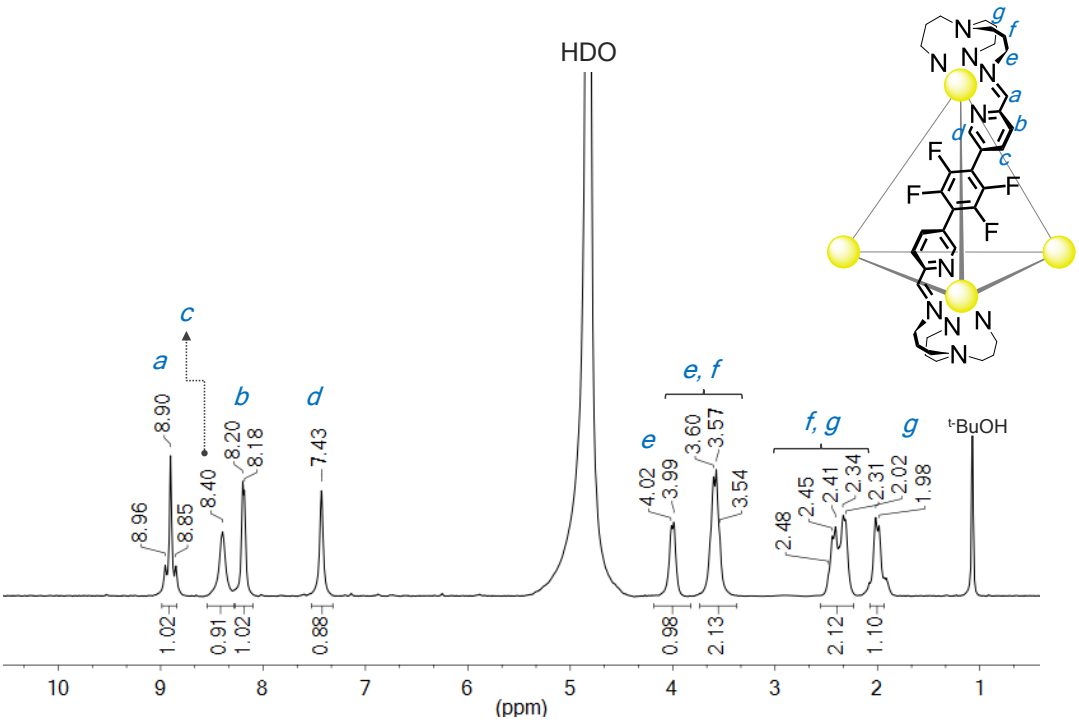

Figure S63. ^{1}H NMR spectrum (400 MHz, D_2O, 298 K) of tetrahedron **Cd–14•SO_4**.

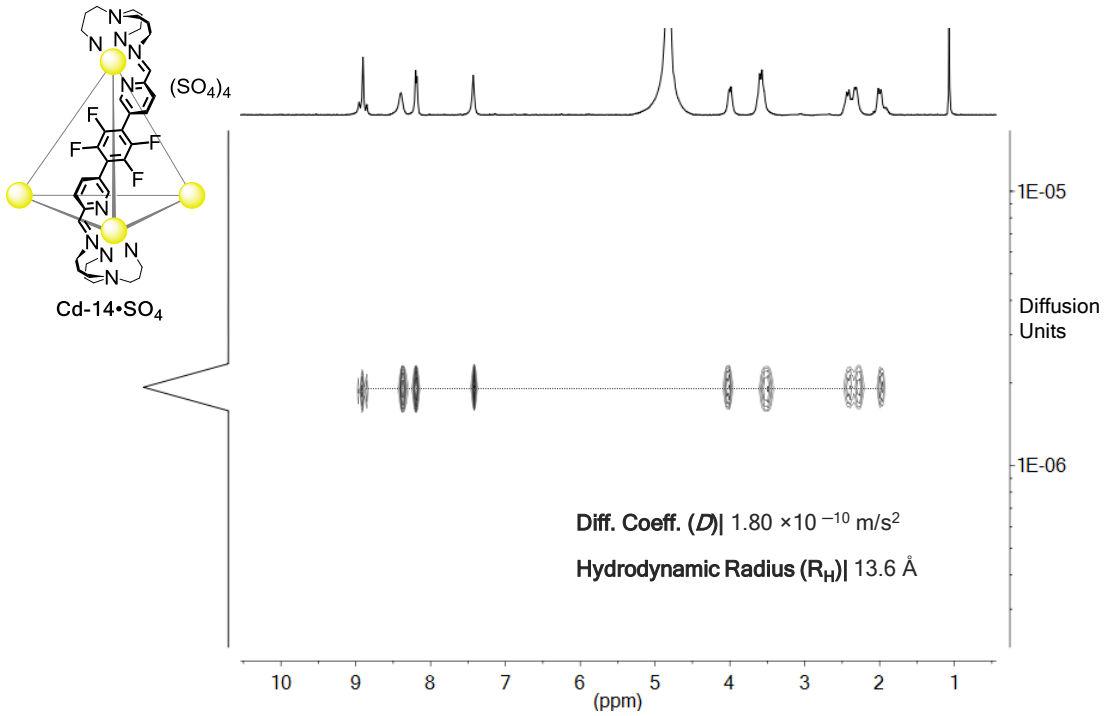

Figure S64. ^{1}H DOSY NMR spectrum (400 MHz, D_2O, 298 K) of tetrahedron **Cd–14•SO$_4$**.

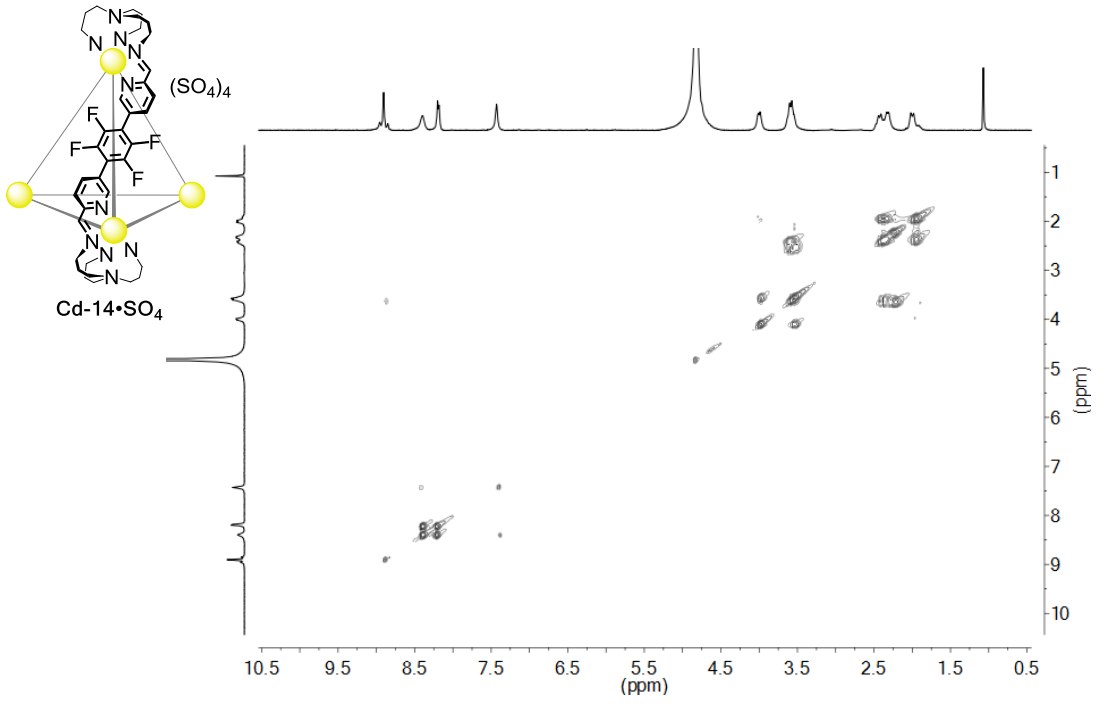

Figure S65. ^{1}H–^{1}H COSY NMR spectrum (400 MHz, D_2O, 298 K) of tetrahedron **Cd–14•SO$_4$**.

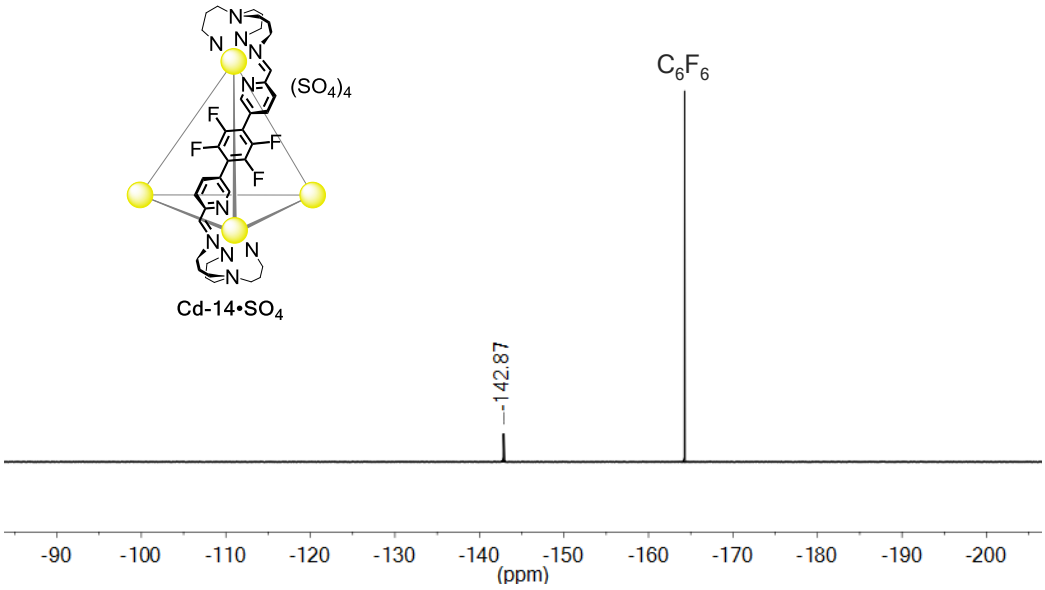

Figure S66. ^{19}F NMR spectrum (376 MHz, D_2O, 298 K) of tetrahedron **Cd–14•SO$_4$**.

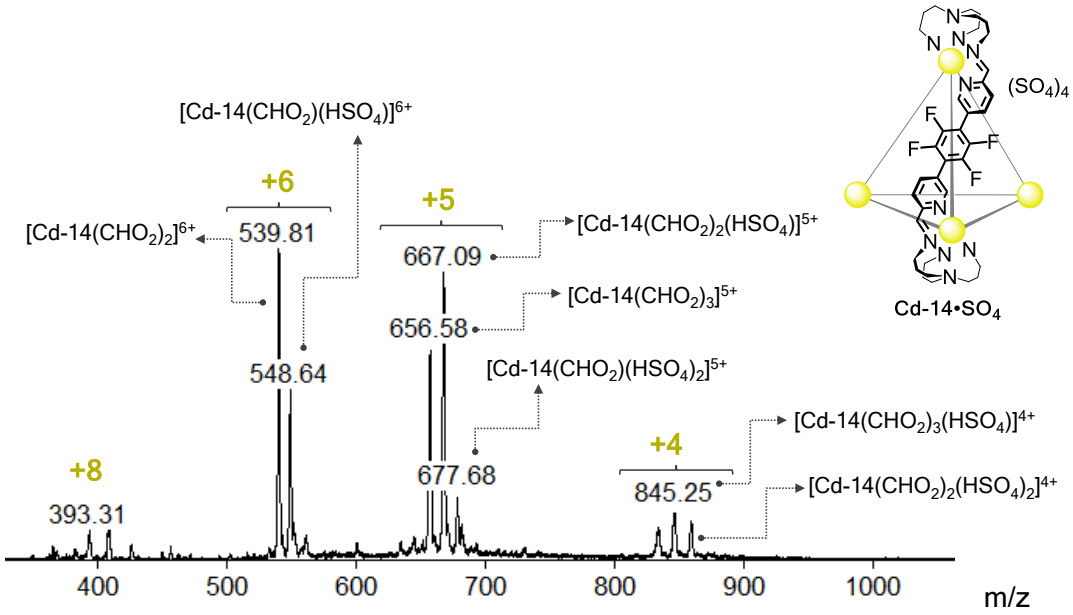

Figure S67. ESI-MS spectrum of tetrahedron **Cd–14•SO$_4$** recorded in H_2O.

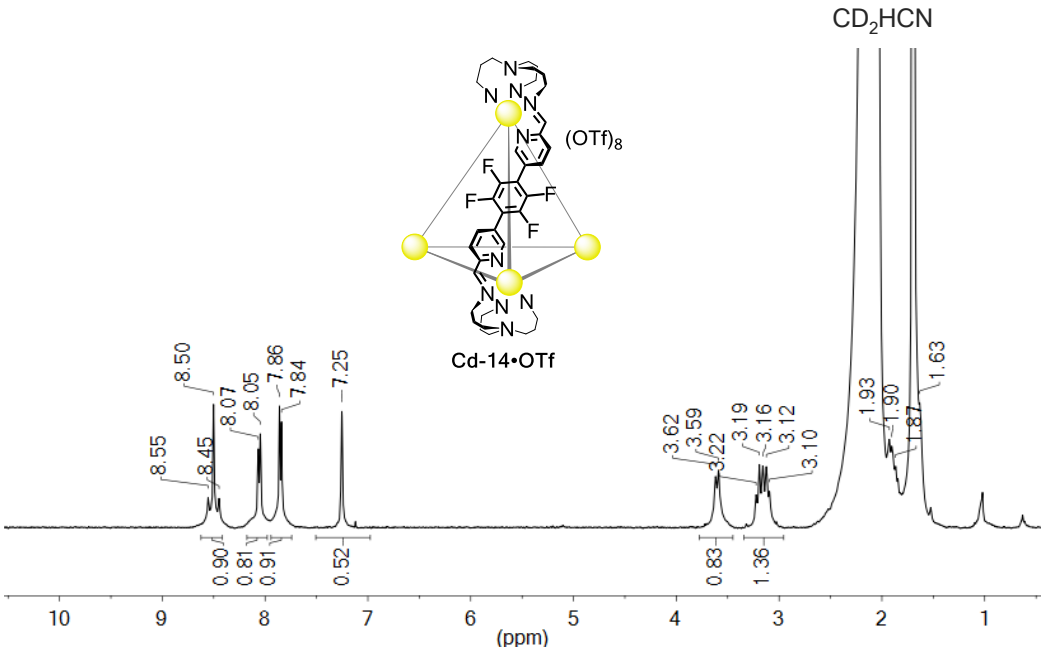

Figure S68. ^{1}H NMR spectrum (400 MHz, CD_3CN, 298 K) of tetrahedron **Cd–14•OTf**, sample obtained upon anion exchange with LiOTf from water-soluble cage **Cd–14•SO_4**.

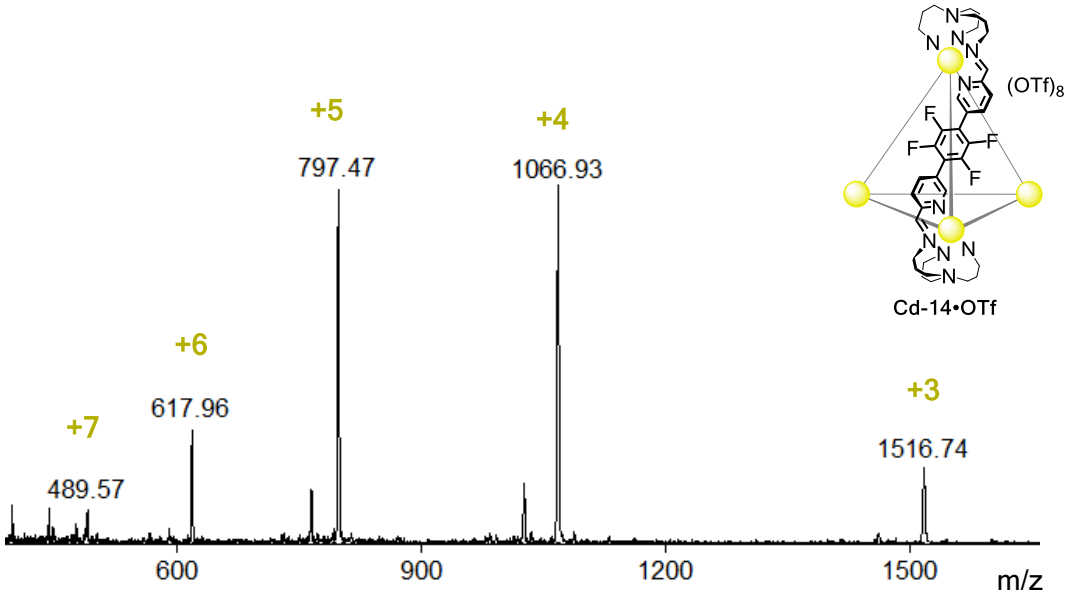

Figure S69. ESI-MS spectrum of tetrahedron **Cd–14•OTf** recorded in CH_3CN; sample obtained upon anion exchange with LiOTf from water-soluble cage **Cd–14•SO_4**.

*5.5 Reactions of aldehyde **D** to form tetrahedra **Zn–10•SO$_4$** and **Cd–15•SO$_4$***

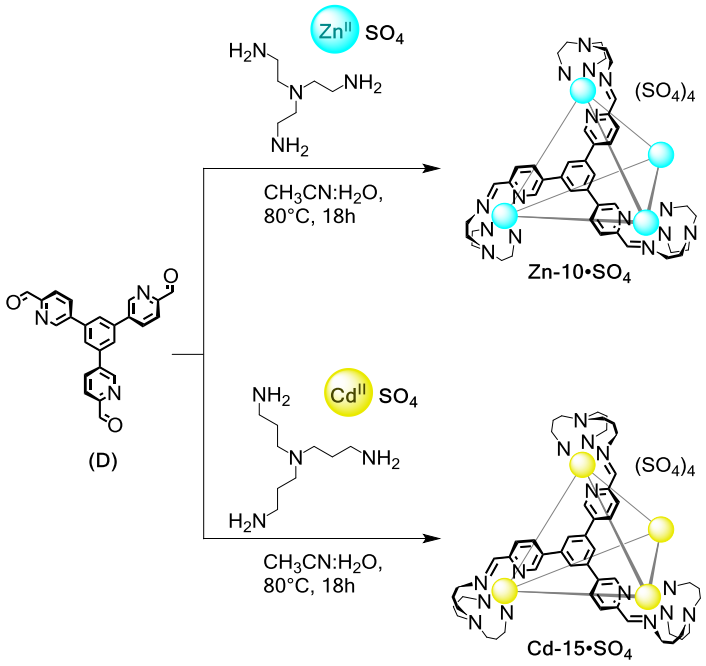

Subcomponent **D** (7.2 mg, 0.018 mmol, 4 equiv), tris(2-aminoethyl)amine (TREN) (2.8 µL, 0.018 mmol, 4 equiv), zinc(II) sulfate heptahydrate (5.2 mg, 0.018 mmol, 4 equiv), and 1.8 mL of 1:1 CH_3CN/H_2O were placed in a Schlenk flask. The mixture was degassed by three evacuation/nitrogen fill cycles, sonicated for 20 minutes and heated at 85°C overnight yielding a light yellow solution mixed with a small amount of insoluble material. This solid was removed by filtration using a small column with celite, and excess of CH_3CN was added to the bright yellow liquor leading to precipitation of a creamy solid. The mixture was centrifuged and the supernatant CH_3CN/H_2O was decanted. To remove the excess of unreacted aldehyde **D** and TREN, the solid was washed with CH_2Cl_2, centrifuged and the supernatant decanted; this process was carried out a second time with Et_2O, and a two times more with CH_3CN. Finally, the excess of solvents was removed by a gentle flow of N_2 gas yielding cage **Zn-10•SO$_4$** as a microcrystalline white solid (10.8 mg, yield 91%). ^{1}H NMR (400 MHz, D_2O, 298 K): δ = 9.01 (s, 12H, imine-H*a*), 8.47 (m, 12H, Py-H*c*), 8.46 (m, 12H, Py-H*b*), 7.37 (s, 12H, Py-H*h*), 7.26 (s, 12H, Py-H*c*), 4.03 (m, 12H, TREN-H*e*), 3.82 (d, $^2J_{1H–1H}$ = 10.1 Hz, 12H, TREN-H*e*), 3.36 (d, $^2J_{1H–1H}$ = 12.3 Hz, 12H, TREN-H*f*), 3.09 (m, 12H, TREN-H*f*). ^{13}C NMR (100 MHz, D_2O, 298 K): δ = 163.1, 148.0, 145.6, 137.6, 137.5,

136.7, 129.7, 124.7, 56.9, 54.9. DOSY Diffusion coefficient = 1.85 × 10^{-10} m^2/s. ESI-MS (H_2O): *m/z* = 275.5 [**Zn-10**]$^{+8}$, 336.1 [**Zn-10**(OTf)]$^{+7}$, 383.2 [**Zn-10**(SO_4)]$^{+6}$, 428.3 [**Zn-10**(BF_4)(NTf_2)]$^{+6}$, 502.9 [**Zn-10**(BF_4)($TFA)_2$]$^{+5}$, 598.9 [**Zn-10**($SO_4)_2$]$^{+4}$, 665.1 [**Zn-10**($TFA)_4$]$^{+4}$. Elemental analysis (%) calcd for $C_{120}H_{108}N_{28}O_{16}S_4Zn_4$•$4H_2O$•$CH_3CN$: C 54.25, H 4.44, N 15.04; found: C 54.38, H 4.56, N 15.12.

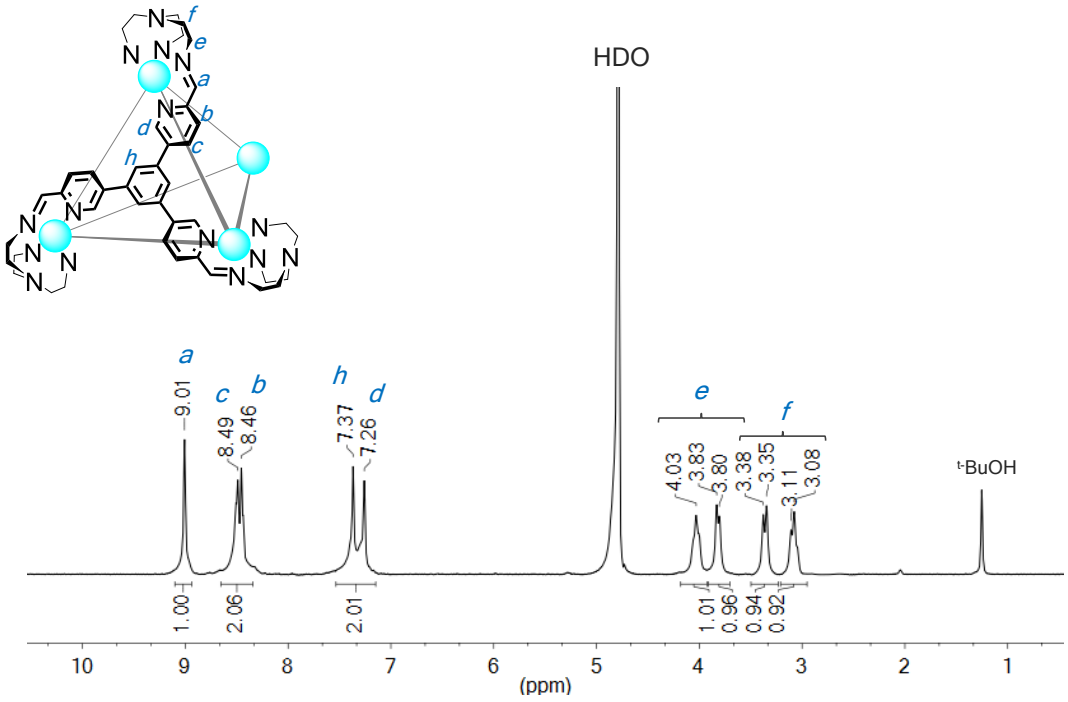

Figure S70. ^{1}H NMR spectrum (400 MHz, D_2O, 298 K) of tetrahedron **Zn–10•SO_4**.

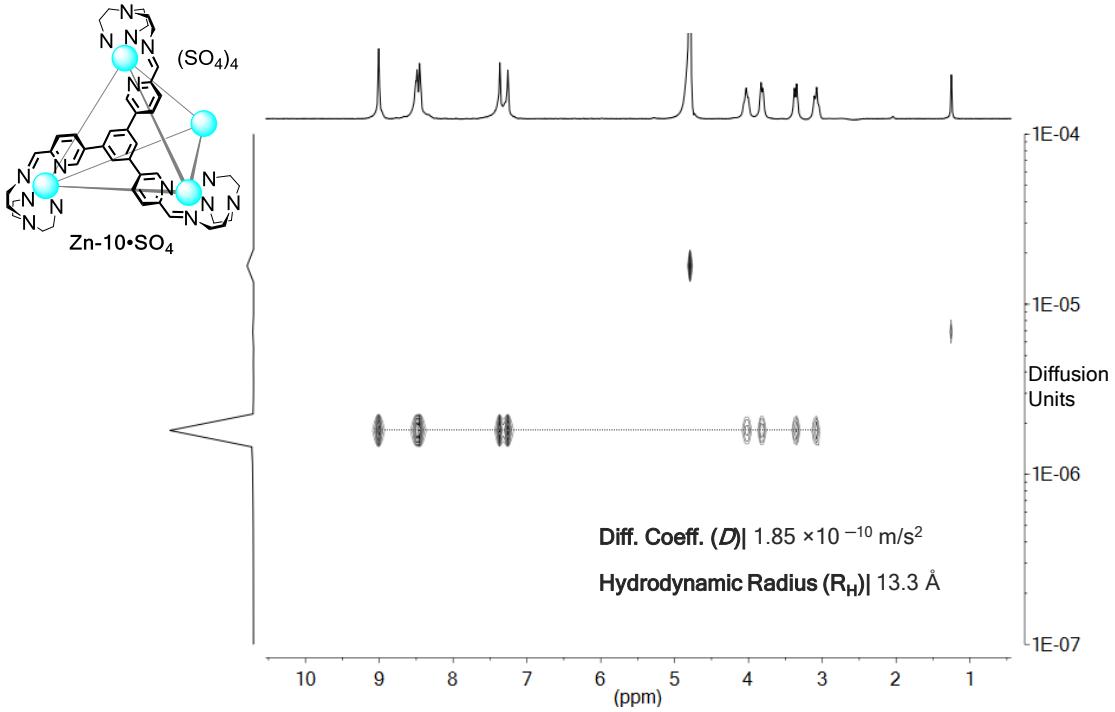

Figure S71. ^{1}H DOSY NMR spectrum (400 MHz, D_2O, 298 K) of tetrahedron **Zn–10•SO$_4$**.

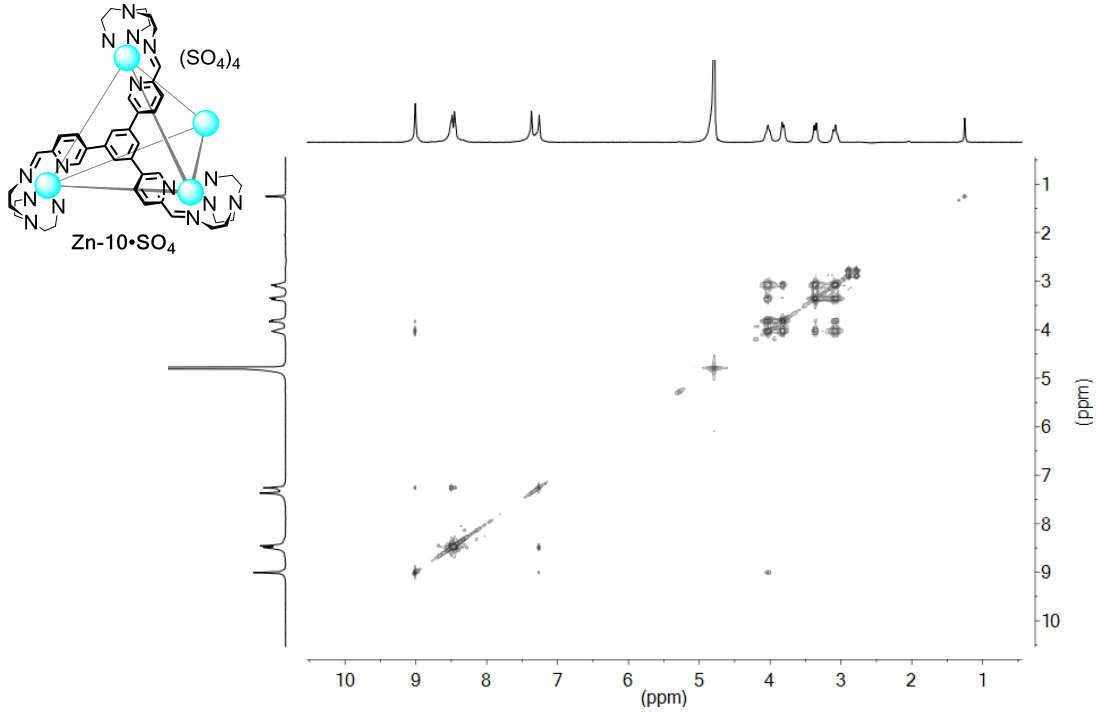

Figure S72. ^{1}H–^{1}H COSY NMR spectrum (400 MHz, D_2O, 298 K) of tetrahedron **Zn–10•SO$_4$**.

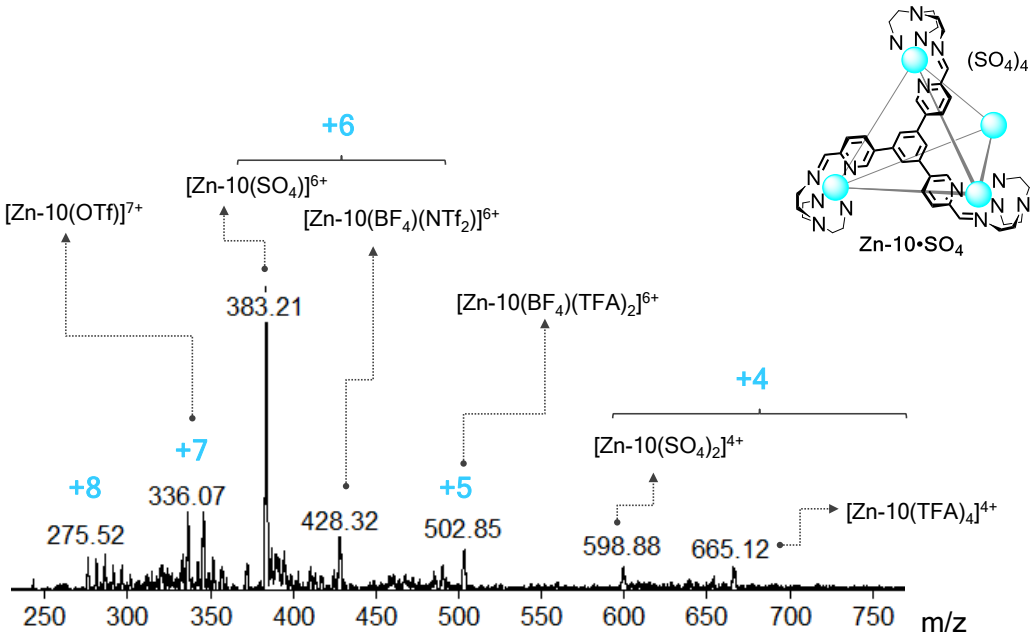

Figure S73. ESI-MS spectrum of tetrahedron **Zn–10•SO_4** recorded in H_2O.

Subcomponent **D** (6.0 mg, 0.015 mmol, 4 equiv), tris(3-aminopropyl)amine (TRPN) (2.9 μL, 0.015 mmol, 4 equiv), cadmium(II) sulfate (3.2 mg, 0.015 mmol, 4 equiv), and 2.0 mL of 1:1 CH_3CN/H_2O were placed in a Schlenk flask. The mixture was degassed by three evacuation/nitrogen fill cycles, sonicated for 20 minutes and heated at 80°C overnight yielding a light yellow solution mixed with a small amount of insoluble material. This solid was removed by filtration using a small column with celite, and excess of CH_3CN was added to the bright yellow liquor leading to precipitation of a yellow solid. The mixture was centrifuged and the supernatant CH_3CN/H_2O was decanted. To remove the excess of unreacted aldehyde **D** and TRPN, the solid was washed with CH_2Cl_2, centrifuged and the supernatant decanted; this process was carried out a second time with Et_2O, and two times more with CH_3CN. Finally, the excess of solvents was removed by a gentle flow of N_2 gas yielding cage **Cd-15•SO_4** as a microcrystalline yellow solid (9.5 mg, yield 85%). ^{1}H NMR (400 MHz, D_2O, 298 K): δ = 8.97 (s, $^3J_{1H–113Cd}$ = 21.1 Hz, 12H, imine-H*a*), 8.48 (m, 12H, Py-H*c*), 8.43 (m, 12H, Py-H*b*), 7.39 (s, 12H, Py-H*d*), 7.21 (s, 12H, Py-H*h*), 4.01 (d, $^2J_{1H–1H}$ = 10.9 Hz, 12H, TRPN-H*e*), 3.71–3.55 (m, 24H, TRPN-H*e*, H*f*), 2.46 (m, 12H, TRPN-H*f*), 2.31 (d, $^2J_{1H–1H}$ = 12.4 Hz, 12H, TRPN-H*g*), 2.02 (d, $^2J_{1H–1H}$ = 12.7 Hz, 12H, TRPN-H*g*).

^{13}C NMR (100 MHz, D_2O, 298 K): δ = 162.5, 148.2, 145.7, 137.3, 137.0, 129.5, 123.8, 62.8, 59.0, 26.1. DOSY Diffusion coefficient = 1.67 × 10^{-10} m^2/s. ESI-MS (H_2O): *m/z* = 319.8 [**Cd-15**]$^{+8}$, 371.0 [**Cd-15**(Cl)]$^{+7}$, 442.6 [**Cd-15**(SO_4)]$^{+6}$, 532.4 [**Cd-15**($Cl)_3$]$^{+5}$, 668.1 [**Cd-15** ($SO_4)_2$]$^{+4}$. Elemental analysis (%) calcd for $C_{132}H_{132}Cd_4N_{28}O_{16}S_4$•5.5$H_2O$: C 52.09, H 4.74, N 12.89; found: C 52.19, H 4.68, N 12.70.

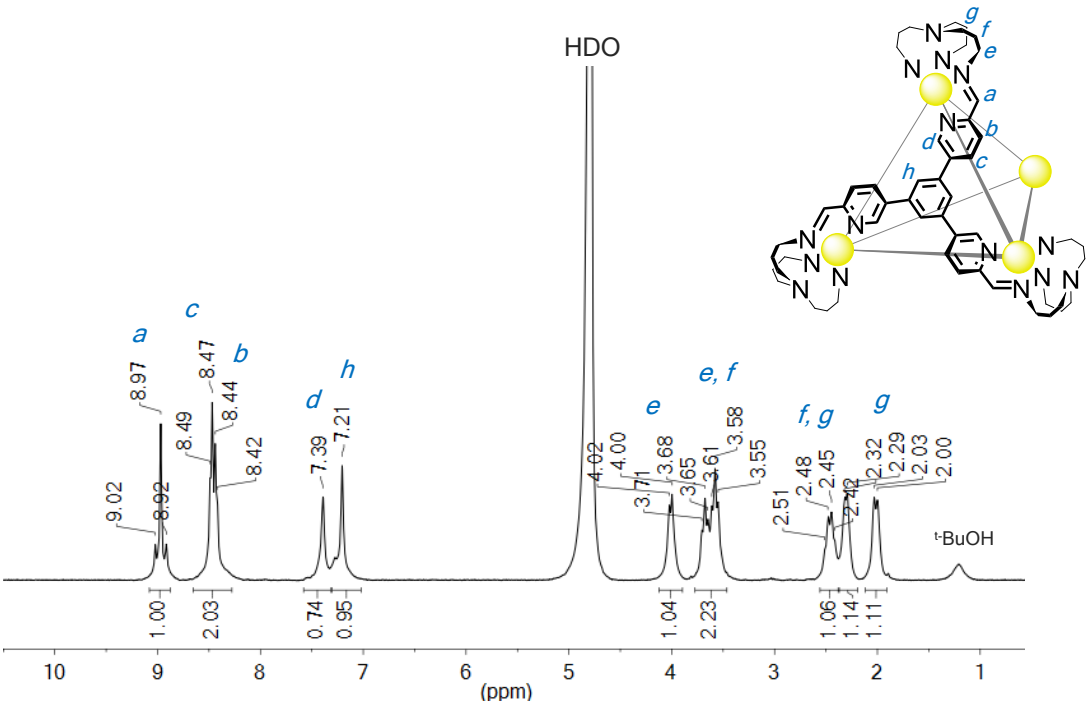

Figure S74. ^{1}H NMR spectrum (400 MHz, D_2O, 298 K) of tetrahedron **Cd–15•SO_4**.

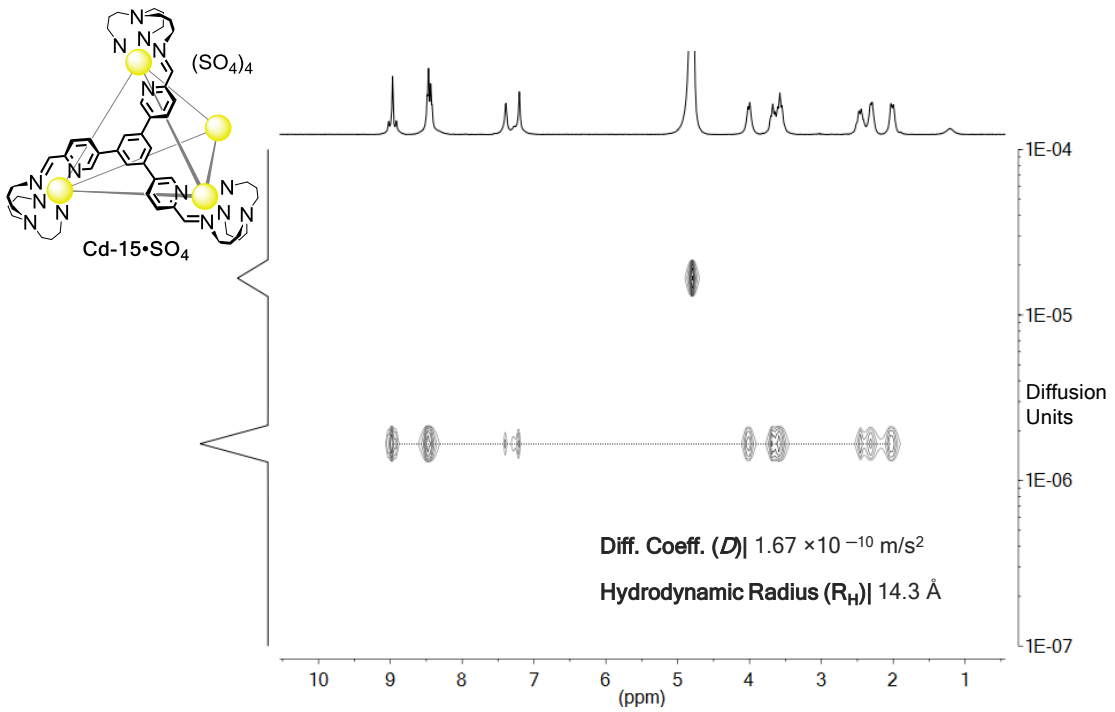

Figure S75. ^{1}H DOSY NMR spectrum (400 MHz, D_2O, 298 K) of tetrahedron **Cd–15•SO$_4$**.

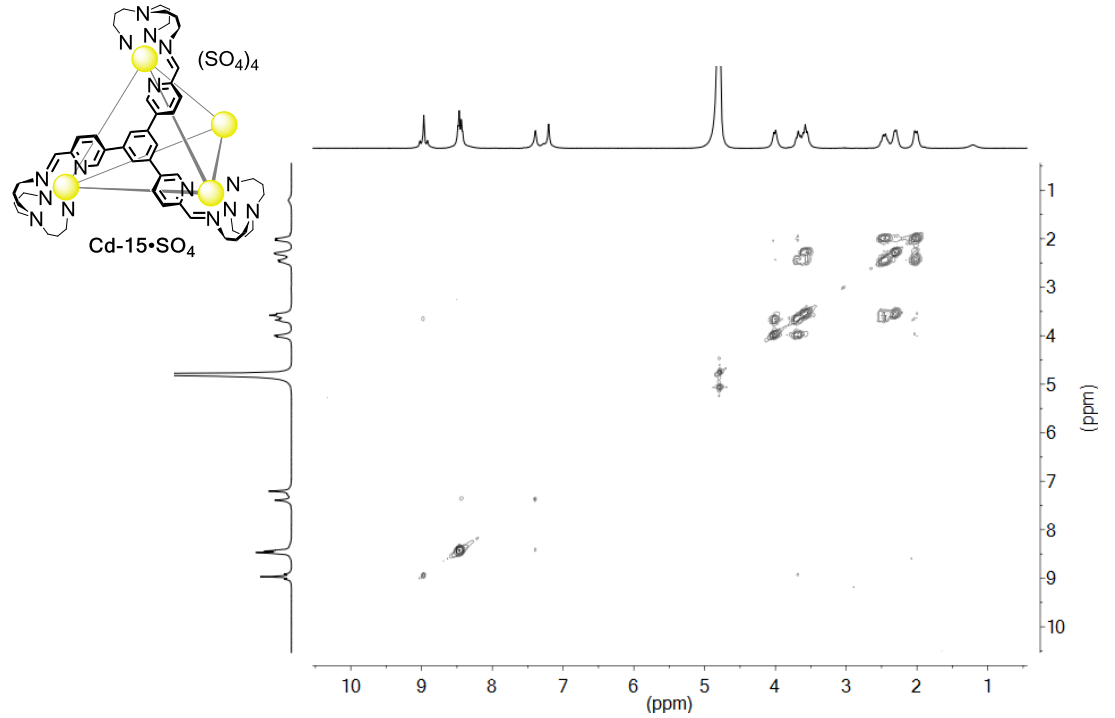

Figure S76. ^{1}H–^{1}H COSY NMR spectrum (400 MHz, D_2O, 298 K) of tetrahedron **Cd–15•SO$_4$**.

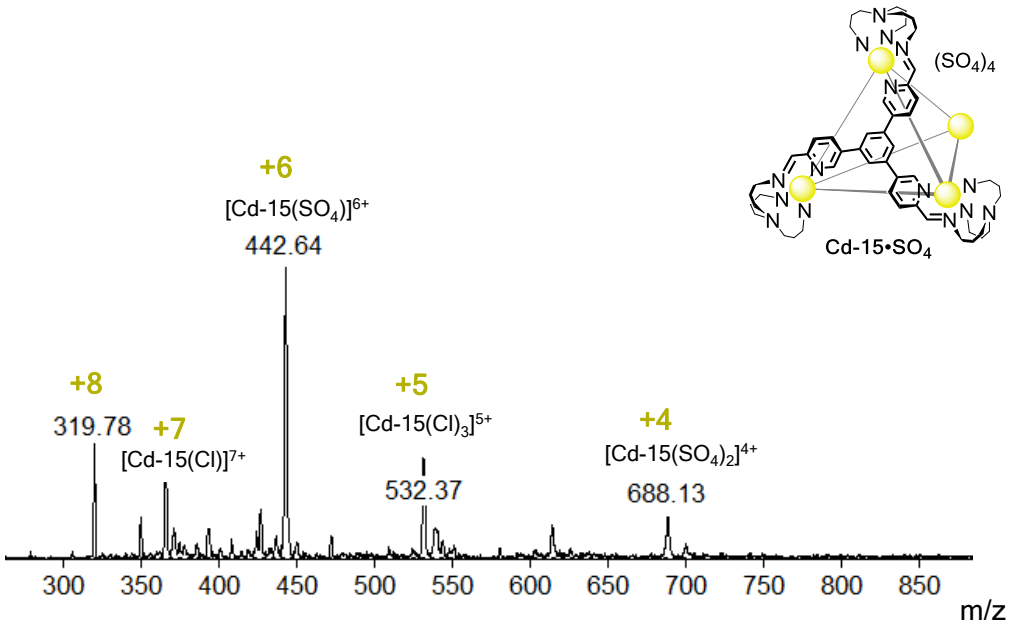

Figure S77. ESI-MS spectrum of tetrahedron **Cd–15•SO$_4$** recorded in H_2O.

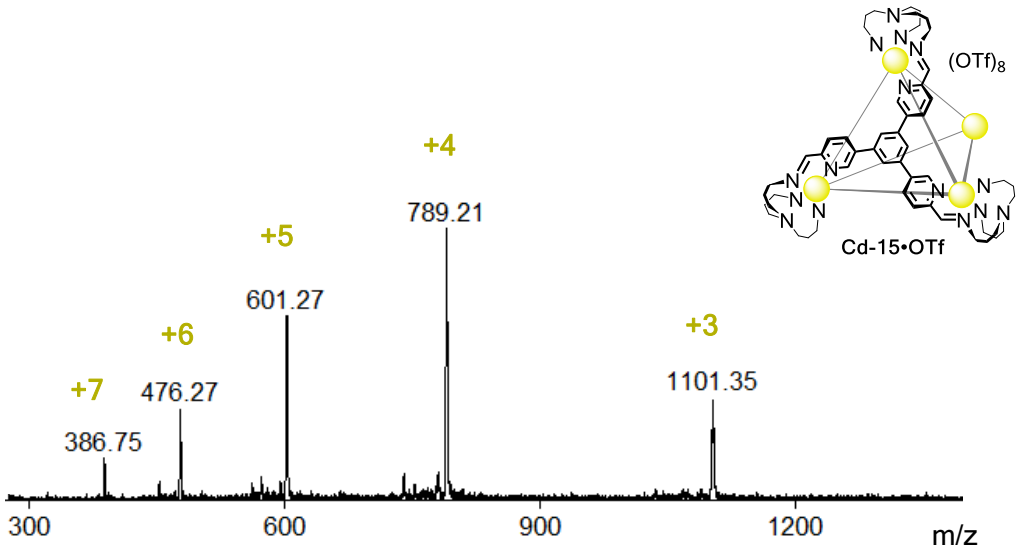

Figure S78. ESI-MS spectrum of tetrahedron **Cd–15•OTf** recorded in CH_3CN. Sample obtained upon anion exchange with LiOTf from water-soluble cage **Cd–15•SO$_4$**.

6. X–ray Crystallography

All attempts to obtain suitable crystals for X-ray diffraction studies from aqueous solutions of the water-soluble sulfate capsules were unsuccessful; all crystalline samples were obtained from acetonitrile solutions of cages. Generally, sulfate cages were dissolved in pure water and subjected to anion metathesis reactions with LiOTf, the resulting triflate coordination capsules were purified, dried and dissolved and these solutions were used to grow crystals. Notably, the obtained crystallographic evidence confirms the presence of the diverse self-assembled frameworks within the original sulfate compounds and the robustness of the structures prepared that can travel through solution–solid phases within a system.

Data were collected either using a Bruker D8 VENTURE equipped with high-brilliance IμS Cu-Kα radiation (1.54178 Å), with ω and ψ scans at 180(2) K or at Beamline I19 of Diamond Light Source employing silicon double crystal monochromated synchrotron radiation (0.6889 Å) with ω scans at 100(2) K.[13] Data integration and reduction were undertaken with SAINT and XPREP[14] or Xia2.[15] Subsequent computations were carried out using the WinGX-32 graphical user interface.[16] Multi-scan empirical absorption corrections were applied to the data using SADABS[14] or the AIMLESS tool in the CCP4 suite. Structures were solved by direct methods using SHELXT-2016[17] then refined and extended with SHELXL-2016.[18] In general, non-hydrogen atoms with occupancies greater than 0.5 were refined anisotropically. Carbon-bound hydrogen atoms were included in idealized positions and refined using a riding model. Disorder was modelled using standard crystallographic methods including constraints, restraints and rigid bodies where necessary. Crystallographic data along with specific details pertaining to the refinement follow. Crystallographic data have been deposited with the CCDC (1837541-1837547).

*6.1 Crystallographic data and refinement details for cube **Co–1***

$[Co_8L_6]\cdot 16OTf\cdot 11.5MeCN\cdot 16C_6H_6\cdot 5.75H_2O$

Formula| $C_{543}H_{406}Co_8F_{48}N_{83.50}O_{53.75}S_{16}Zn_6$, M = 11249.11, Tetragonal, space group P 4/n (#85), a 34.300(5), b 34.300(5), c 27.428(6) Å, V = 32269(11) $Å^3$, D_c 1.158 g cm^{-3}, Z 2, crystal size 0.050 by 0.050 by 0.010 mm, colour brown, habit block, temperature 100(2) K, λ(Synchrotron) 0.6889 Å, μ(Synchrotron) 0.500 mm^{-1}, T(Analytical)$_{min,max}$ 0.952391076963, 1.0, $2\theta_{max}$ 45.00, *hkl* range -38 38, -36 36, -30 27, N 130101, N_{ind} 22840(R_{merge} 0.0341), N_{obs} 16227(I > 2σ(I)), N_{var} 2077, residuals* $R1(F)$ 0.1019, $wR2(F^2)$ 0.3215, GoF(all) 1.078, $\Delta\rho_{min,max}$ -1.698, 1.678 e^- $Å^{-3}$.

*$R1 = \Sigma||F_o| - |F_c||/\Sigma|F_o|$ for $F_o > 2\sigma(F_o)$; $wR2 = (\Sigma w(F_o^2 - F_c^2)^2/\Sigma(wF_c^2)^2)^{1/2}$ all reflections

$w=1/[\sigma^2(F_o^2)+(0.2000P)^2+35.0000P]$ where $P=(F_o^2+2F_c^2)/3$

Refinement details| The crystals of $[Co_8L_6]\cdot 16OTf\cdot 11.5MeCN\cdot 16C_6H_6\cdot 5.75H_2O$ were grown by diffusion of benzene into an acetonitrile solution of $[Co_8L_6]\cdot 16OTf$. The crystals immediately lost solvent after removal from the mother liquor and rapid handling prior to flash cooling in the cryostream was required to collect data. Despite these measures and the use of synchrotron radiation few reflections at greater than 0.9 Å resolution were observed. The asymmetric unit was found to contain one quarter of a Co_8L_6 assembly and associated counterions and solvent molecules. The anions within the structure show evidence of substantial disorder. All triflate anions were modelled as disordered over up to four locations and some anions were modelled with partial occupancy. The occupancies of these partial occupancy anions were allowed to refine freely and then fixed at the obtained values. Any additional minor occupancy positions of these anions could not be located in the electron density map due to the limited resolution of the data. Many of the solvent molecules were also modelled as disordered and/or with partial occupancy. Substantial

bond length and thermal parameter restraints were applied to facilitate a reasonable refinement of the disordered triflate anions and solvent molecules and most low occupancy disordered groups were modelled with isotropic thermal parameters. Thermal parameter restraints (SIMU, RIGU) were also applied to all atoms except for cobalt and zinc. The hydrogen atoms of some water molecules could not be located in the electron density map and were therefore not included in the model.

Further reflecting the solvent loss and poor diffraction properties there is a significant amount of void volume in the lattice containing smeared electron density from disordered solvent. Consequently the SQUEEZE[19] function of PLATON[20] was employed to remove the contribution of the electron density associated with this highly disordered solvent, which gave a potential solvent accessible void of 5547 $Å^3$ per unit cell (a total of approximately 1621 electrons). Since the diffuse solvent molecules could not be assigned conclusively to acetonitrile or benzene only those solvent molecules that could be modelled with discrete atom positions were included in the formula. Consequently, the molecular weight and density given above are likely to be underestimated. The remaining electron density peaks and holes (up to 1.678 $e^{-}Å^3$) are close to the zinc centres reflecting absorption effects or a small amount of unresolved disorder.

CheckCIF gives one A and five B level alerts. The A level alert arises from irregular bond lengths in a benzene molecule located on a special position for which some additional minor disorder was not modelled. The B level alerts arise from the limited resolution of the data, further disorder in some solvent molecules and formula discrepancies arising from minor occupancy positions of disordered anions that could not be modelled as described above.

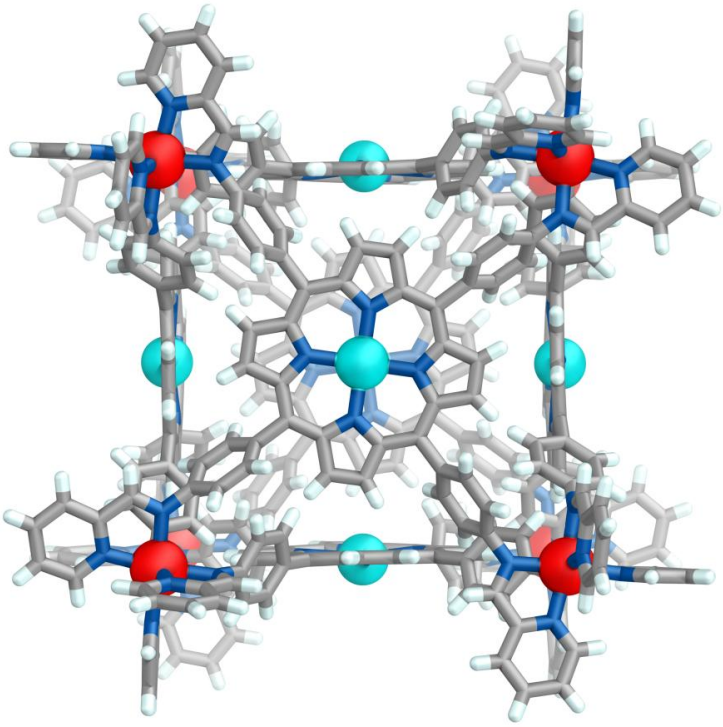

Figure S79. Cationic part of the crystal structure of cube **Co–1**, as viewed down a face. Counterions, solvents and disordered fragments are omitted for clarity. Co^{II} and Zn^{II} centres are coloured dark orange and cyan respectively.

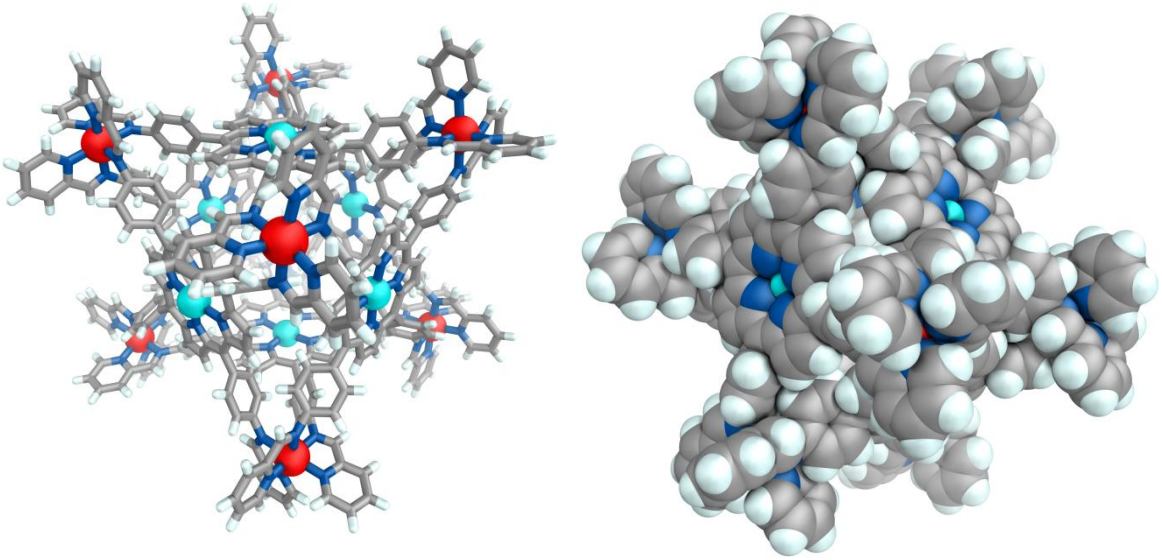

Figure S80. View of the cationic part of the crystal structure of cube **Co–1**, as viewed down a Co^{II} corner (*left*) and space-filling view of **Co–1**, as viewed down an edge (*right*). Counterions, solvents and disordered fragments are omitted for clarity. Co^{II} and Zn^{II} centres are coloured dark orange and light blue respectively.

*6.2 Crystallographic data and refinement details for cube **Ni–1***

$[Ni_8L_6]\cdot16OTf\cdot10.25MeCN\cdot14.5C_6H_6\cdot5.25H_2O$

Formula $C_{531.50}H_{392.25}F_{48}N_{82.25}Ni_8O_{53.25}S_{16}Zn_6$, *M* 11069.86, Tetragonal, space group P 4/n (#85), *a* 34.210(5), *b* 34.210(5), *c* 27.215(5) Å, *V* = 31852(11) $Å^3$, D_c 1.154 g cm^{-3}, *Z* 2, crystal size 0.040 by 0.020 by 0.020 mm, colour green brown, habit block, temperature 100(2) K, λ(Synchrotron) 0.6889 Å, μ(Synchrotron) 0.531 mm^{-1}, *T*(Analytical)$_{min,max}$ 0.952391076963, 1.0, $2\theta_{max}$ 40.72, *hkl* range -34 34, -34 34, -27 27, *N* 109166, N_{ind} 17157(R_{merge} 0.0428), N_{obs} 11538(I > 2σ(I)), N_{var} 2025, residuals* *R*1(*F*) 0.1211, *wR*2(F^2) 0.3533, GoF(all) 1.054, $\Delta\rho_{min,max}$ -0.743, 0.832 $e^- Å^{-3}$.

*$R1 = \Sigma||F_o| - |F_c||/\Sigma|F_o|$ for $F_o > 2\sigma(F_o)$; $wR2 = (\Sigma w(F_o^2 - F_c^2)^2/\Sigma(wF_c^2)^2)^{1/2}$ all reflections

$w=1/[\sigma^2(F_o^2)+(0.2000P)^2+50.0000P]$ where $P=(F_o^2+2F_c^2)/3$

Refinement details| The crystals of $[Ni_8L_6]\cdot16OTf\cdot10.25MeCN\cdot14.5C_6H_6\cdot5.25H_2O$ were grown by diffusion of benzene into an acetonitrile solution of $[Ni_8L_6]\cdot16OTf$. The crystals immediately lost solvent after removal from the mother liquor and rapid handling prior to flash cooling in the cryostream was required to collect data. Despite these measures and the use of synchrotron radiation few reflections at greater than 0.99 Å resolution were observed. The asymmetric unit was found to contain one quarter of a Ni_8L_6 assembly and associated counterions and solvent molecules. The crystals were isomorphous to those of $[Co_8L_6]\cdot16OTf\cdot11.5MeCN\cdot16C_6H_6\cdot5.75H_2O$ except for the occupancies of some disordered anions and solvent molecules. The anions within the structure show evidence of substantial disorder. All triflate anions were modelled as disordered over up to four locations and some anions were modelled with partial occupancy. The occupancies of these partial occupancy anions were allowed to refine freely and then fixed at the obtained values. Any additional minor occupancy positions of these anions could not be located in

the electron density map due to the limited resolution of the data. Many of the solvent molecules were also modelled as disordered and/or with partial occupancy. Substantial bond length and thermal parameter restraints were applied to facilitate a reasonable refinement of the disordered triflate anions and solvent molecules and most low occupancy disordered groups were modelled with isotropic thermal parameters. Thermal parameter restraints (SIMU, RIGU) were also applied to all atoms except for nickel and zinc. The hydrogen atoms of some water molecules could not be located in the electron density map and were therefore not included in the model.

Further reflecting the solvent loss and poor diffraction properties there is a significant amount of void volume in the lattice containing smeared electron density from disordered solvent. Consequently the SQUEEZE[19] function of PLATON[20] was employed to remove the contribution of the electron density associated with this highly disordered solvent, which gave a potential solvent accessible void of 5222 $Å^3$ per unit cell (a total of approximately 1148 electrons). Since the diffuse solvent molecules could not be assigned conclusively to acetonitrile or benzene only those solvent molecules that could be modelled with discrete atom positions were included in the formula. Consequently, the molecular weight and density given above are likely to be underestimated.

CheckCIF gives three A and fourteen B level alerts. These alerts (both A and B level) result from the limited data resolution and thermal motion and/or unresolved disorder of some anions and solvent molecules as described above.

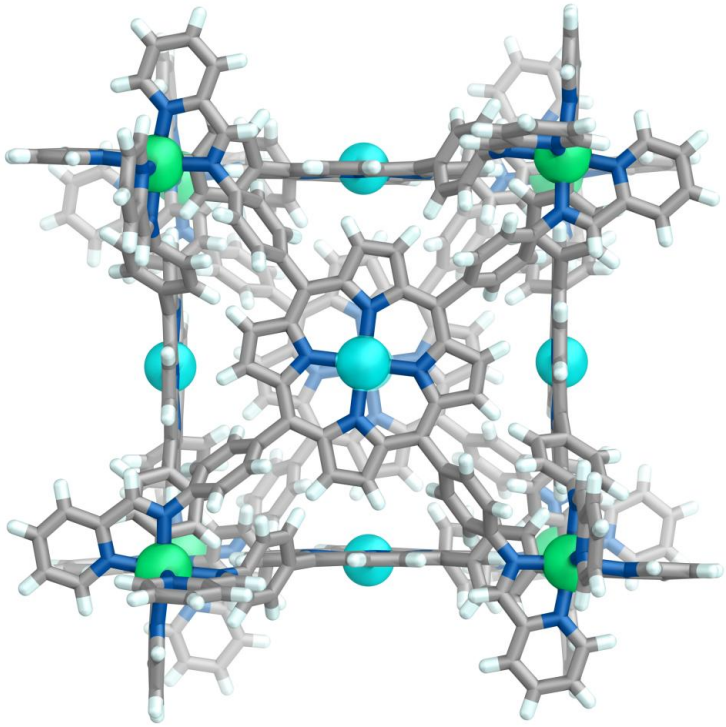

Figure S81. Cationic part of the crystal structure of cube **Ni–1**, as viewed down a face. Counterions, solvents and disorder are omitted for clarity. Ni^{II} and Zn^{II} centres are coloured green and light blue respectively.

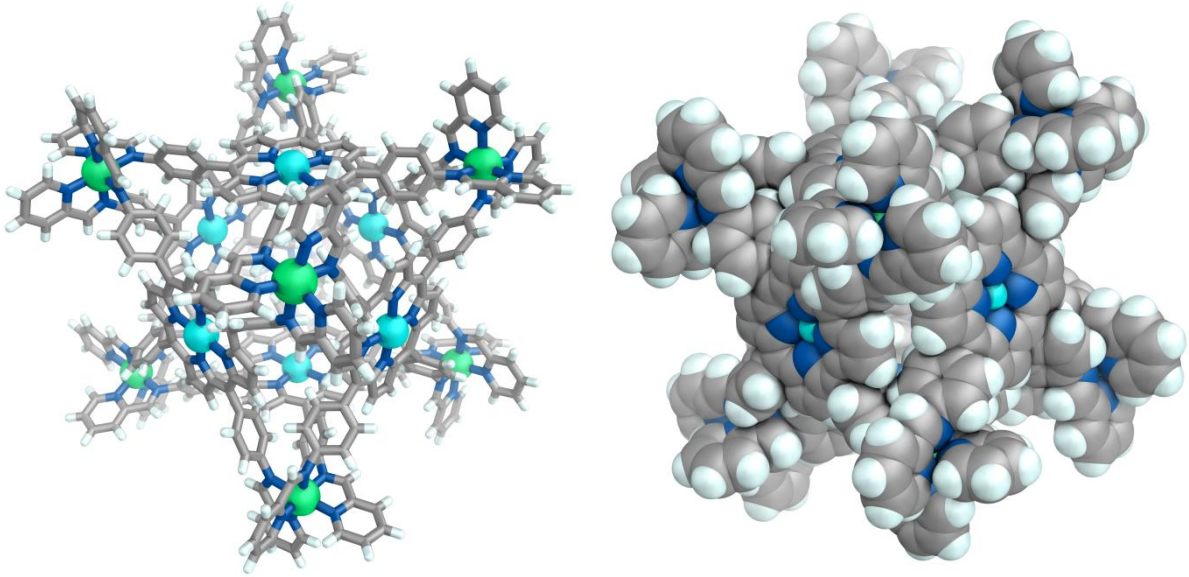

Figure S82. View of the cationic part of the crystal structure of cube **Ni–1**, as viewed down a Ni^{II} corner (*left*) and space-filling view of **Ni–1**, as viewed down an edge (*right*). Counterions, solvents and disordered fragments are omitted for clarity. Ni^{II} and Zn^{II} centres are coloured green and light blue respectively.

*6.3 Crystallographic data and refinement details for tetrahedron **Ni–3***

$[Ni_4L_6]\cdot 5OTf\cdot 3BF_4\cdot 5.25MeCN\cdot 0.25Et_2O$

Formula $C_{160.50}H_{126.25}B_3F_{27}N_{29.25}Ni_4O_{15.25}S_5$, M = 3649.22, Monoclinic, space group C 2/c (#15), a 34.257(7), b 18.552(4), c 54.149(11) Å, β 97.09(3), V = 34150(12) $Å^3$, D_C 1.420 g cm^{-3}, Z 8, crystal size 0.005 by 0.001 by 0.001 mm, colour pale yellow, habit plate, temperature 100(2) K, λ(Synchrotron) 0.6889 Å, μ(Synchrotron) 0.543 mm^{-1}, T(Analytical)$_{min,max}$ 0.982524939378, 1.0, $2\theta_{max}$ 47.22, *hkl* range -39 38, -21 21, -56 62, N 113743, N_{ind} 27632(R_{merge} 0.0445), N_{obs} 18606(I > 2σ(I)), N_{var} 2489, residuals* $R1(F)$ 0.0817, $wR2(F^2)$ 0.2765, GoF(all) 1.075, $\Delta\rho_{min,max}$ -0.741, 0.899 e^- $Å^{-3}$.

*$R1 = \Sigma||F_o| - |F_c||/\Sigma|F_o|$ for $F_o > 2\sigma(F_o)$; $wR2 = (\Sigma w(F_o^2 - F_c^2)^2/\Sigma(wF_c^2)^2)^{1/2}$ all reflections

$w=1/[\sigma^2(F_o^2)+(0.2000P)^2]$ where $P=(F_o^2+2F_c^2)/3$

Refinement details| The crystals of $[Ni_4L_6]\cdot 5OTf\cdot 3BF_4\cdot 5.25MeCN\cdot 0.25Et_2O$ were grown by diffusion of diethyl ether into an acetonitrile solution of $[Ni_4L_6]\cdot 8OTf$ containing $LiBF_4$. The crystals immediately lost solvent after removal from the mother liquor and rapid handling prior to flash cooling in the cryostream was required to collect data. The asymmetric unit was found to contain one complete Ni_4L_6 assembly and associated counterions and solvent molecules.

The triflate anions within the structure show evidence of substantial disorder. Four triflate anions were modelled as disordered over multiple locations and/or with partial occupancy; one of these anions was also further disordered over a special position. Two acetonitrile molecules were modelled as disordered over three locations each and a further partial occupancy solvent molecule was modelled as a mixture of acetonitrile and diethyl ether. Substantial bond length and thermal parameter restraints were applied to facilitate a

reasonable refinement of the disordered triflate anions and solvent molecules and most low occupancy disordered groups were modelled with isotropic thermal parameters. Thermal parameter restraints (SIMU, RIGU) were also applied to all atoms except for nickel.

CheckCIF gives five B level alerts. These alerts all result from thermal motion and/or minor unresolved disorder of some anions.

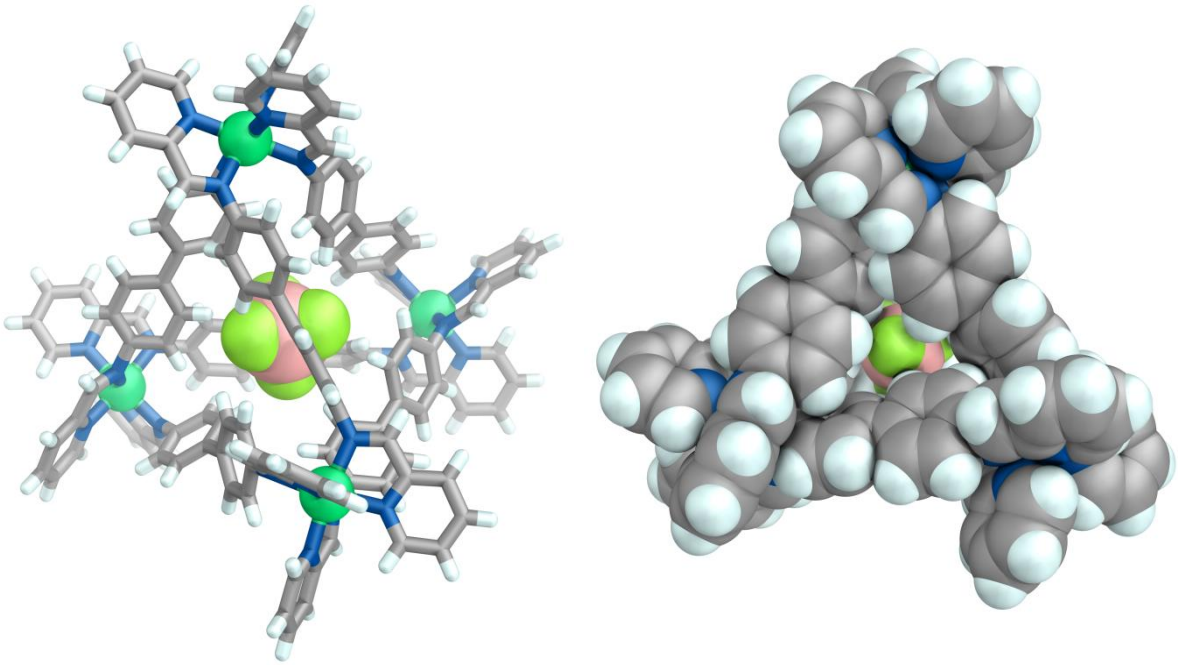

Figure S83. View of the cationic part of the crystal structure of tetrahedron **Ni–3** showing an encapsulated BF_4^- anion, as viewed down an edge (*left*) and as space-filling representation viewed down a face (*right*). Counterions, solvents and disorder are omitted for clarity.

*6.4 Crystallographic data and refinement details for helicate **Zn–7***

$[Zn_2L_3]\cdot 2.5SbF_6\cdot 1.5OTf\cdot 1.5MeCN$

Formula $C_{70.50}H_{64.50}F_{19.50}N_{15.50}O_{4.50}S_{1.50}Sb_{2.50}Zn_2$, M = 2054.58, Monoclinic, space group C 2 (#5), a 32.3977(13), b 31.6390(13), c 22.0583(9) Å, β 123.314(2), V = 18894.9(14) $Å^3$, D_c 1.444 g cm^{-3}, Z 8, crystal size 0.390 by 0.300 by 0.030 mm, colour colourless, habit plate, temperature 180(2) K, λ(CuKα) 1.54178 Å, μ(CuKα) 7.258 mm^{-1}, $T(\text{SADABS})_{min,max}$ 0.3713, 0.7522, $2\theta_{max}$ 117.86, *hkl* range -34 35, -34 35, -24 21, N 56673, N_{ind} 25343(R_{merge} 0.0533), N_{obs} 19795(I > 2σ(I)), N_{var} 2229, residuals* $R1(F)$ 0.0751, $wR2(F^2)$ 0.2177, GoF(all) 1.036, $\Delta\rho_{min,max}$ -1.348, 0.898 e^- $Å^{-3}$.

*$R1 = \Sigma||F_o| - |F_c||/\Sigma|F_o|$ for $F_o > 2\sigma(F_o)$; $wR2 = (\Sigma w(F_o^2 - F_c^2)^2/\Sigma(wF_c^2)^2)^{1/2}$ all reflections

$w=1/[\sigma^2(F_o^2)+(0.1277P)^2+64.5576P]$ where $P=(F_o^2+2F_c^2)/3$

Refinement details| The crystals of $[Zn_2L_3]\cdot 2.5SbF_6\cdot 1.5OTf\cdot 1.5MeCN$ were grown by diffusion of diisopropyl ether into an acetonitrile solution of $[Zn_2L_3]\cdot 4OTf$ containing excess $KSbF_6$. The crystals immediately lost solvent after removal from the mother liquor and rapid handling prior to flash cooling in the cryostream was required to collect data. Despite these measures and the use of a high intensity laboratory source few reflections at greater than 0.9 Å resolution were observed. Nevertheless, the quality of the data is far more than sufficient to establish the connectivity of the structure. The asymmetric unit was found to contain two complete Zn_2L_3 assemblies and associated counterions and solvent molecules. Due to the limited resolution bond lengths and angles within pairs of chemically identical organic ligands were restrained to be similar to each other and thermal parameter restraints (SIMU, RIGU) were applied to all atoms except for zinc and antimony.

The anions within the structure show evidence of substantial disorder. All anions were modeled as disordered over up to four locations and some anions were modelled with partial occupancy. Some anion lattice sites were modelled as a disordered mixture of

hexafluoroantimonate and triflate. The occupancies of partial occupancy anions were allowed to refine freely and then fixed at the obtained values. Any additional minor occupancy positions of these anions could not be located in the electron density map due to the limited resolution of the data and high levels of disorder. The acetonitrile solvent molecules were also modelled as disordered over two or three locations. Substantial bond length and thermal parameter restraints were applied to facilitate a reasonable refinement of the disordered anions and solvent molecules and most low occupancy disordered groups were modelled with isotropic thermal parameters.

Further reflecting the solvent loss and poor diffraction properties there is a significant amount of void volume in the lattice containing smeared electron density from disordered solvent. Consequently the SQUEEZE[19] function of PLATON[20] was employed to remove the contribution of the electron density associated with this highly disordered solvent, which gave a potential solvent accessible void of 3156 $Å^3$ per unit cell (a total of approximately 1127 electrons). Since the diffuse solvent molecules could not be assigned conclusively to acetonitrile or diisopropyl ether only those solvent molecules that could be modelled with discrete atom positions were included in the formula. Consequently, the molecular weight and density given above are likely to be underestimated.

CheckCIF gives one A and four B level alerts. These alerts (both A and B level) result from the limited data resolution and thermal motion and/or unresolved disorder of some anions and solvent molecules as described above.

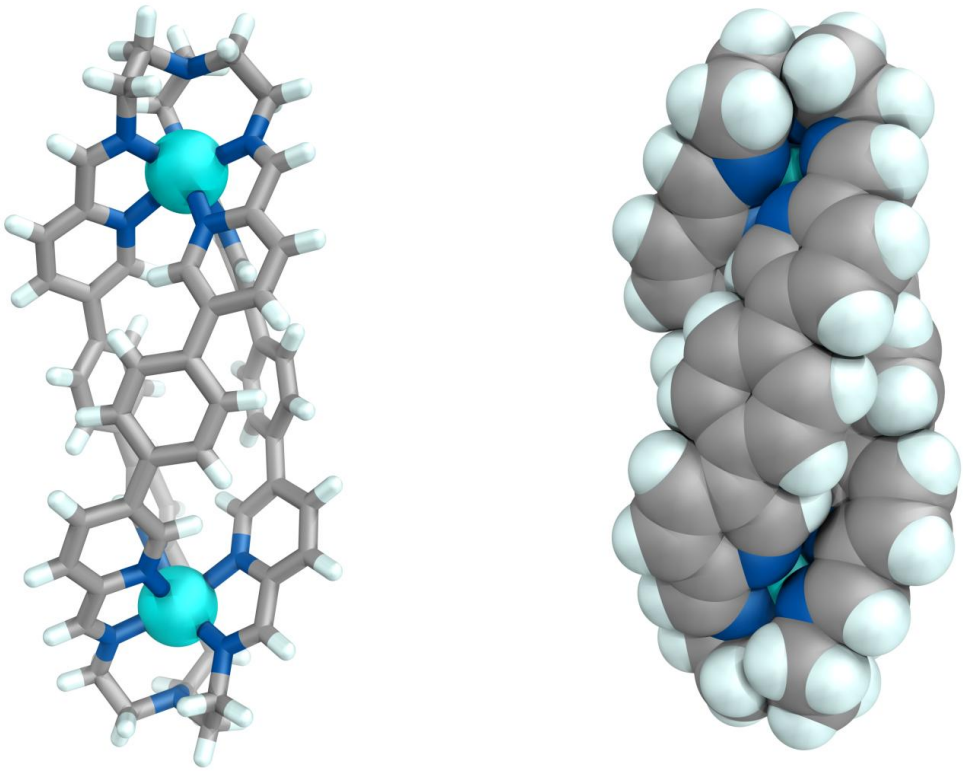

Figure S84. Two views of the cationic part of the crystal structure of helicate **Zn–7**, stick (*left*) and space-filling (*right*) representations. Counterions, solvents and disorder are omitted for clarity.

*6.5 Crystallographic data and refinement details for helicate **Zn–8***

$[Zn_2L_3]\cdot SbF_6\cdot 3.833OTf\cdot 1.5MeCN\cdot 0.833K$

Formula $C_{78.83}H_{76.50}F_{17.50}K_{0.83}N_{15.50}O_{11.50}S_{3.83}SbZn_2$, M = 2165.52, Trigonal, space group R -3 (#148), a 14.930(2), b 14.930(2), c 68.868(14) Å, γ 120º, V = 13294(5) $Å^3$, D_c 1.623 g cm^{-3}, Z 6, crystal size 0.005 by 0.003 by 0.002 mm, colour colourless, habit prism, temperature 100(2) K, λ(Synchrotron) 0.6889 Å, μ(Synchrotron) 0.980 mm^{-1}, $T(\text{Analytical})_{min,max}$ 0.987425612782, 1.0, $2\theta_{max}$ 58.94, *hkl* range -21 16, -16 21, -97 94, N 38333, N_{ind} 8890(R_{merge} 0.0688), N_{obs} 7682(I > 2σ(I)), N_{var} 539, residuals* $R1(F)$ 0.0516, $wR2(F^2)$ 0.1639, GoF(all) 1.132, $\Delta\rho_{min,max}$ -0.636, 1.271 e^- $Å^{-3}$.

*$R1 = \Sigma||F_o| - |F_c||/\Sigma|F_o|$ for $F_o > 2\sigma(F_o)$; $wR2 = (\Sigma w(F_o^2 - F_c^2)^2/\Sigma(wF_c^2)^2)^{1/2}$ all reflections
$w=1/[\sigma^2(F_o^2)+(0.0907P)^2+9.6026P]$ where $P=(F_o^2+2F_c^2)/3$

Refinement details| The crystals of $[Zn_2L_3]\cdot SbF_6\cdot 3.833OTf\cdot 1.5MeCN\cdot 0.833K$ were grown by diffusion of diisopropyl ether into an acetonitrile solution of $[Zn_2L_3]\cdot 4OTf$ containing excess $KSbF_6$. The crystals immediately lost solvent after removal from the mother liquor and rapid handling prior to flash cooling in the cryostream was required to collect data. The asymmetric unit was found to contain one third of a Zn_2L_3 assembly and associated counterions and solvent molecules.

The anions and solvent molecules within the structure show evidence of substantial disorder. All anions were modelled as disordered over up to three locations and two anion lattice sites show further disorder around symmetry positions. Two anion lattice sites were modelled as a disordered mixture of hexafluoroantimonate and triflate. The occupancies of partial occupancy anions and potassium cations were allowed to refine freely. The additional minor occupancy positions of the anions required for charge balance could not be located in the electron density map due to their low occupancy and high levels of disorder resulting in a small discrepancy between the calculated and reported molecular weights. Substantial bond length and thermal parameter restraints were applied to facilitate a reasonable refinement of the disordered anions and solvent molecules and most low occupancy disordered groups were modelled with isotropic thermal parameters.

CheckCIF gives two A and one B level alerts. These alerts (both A and B level) result from anion disorder and formula discrepancies arising from minor occupancy positions of disordered anions that could not be modelled as described above.

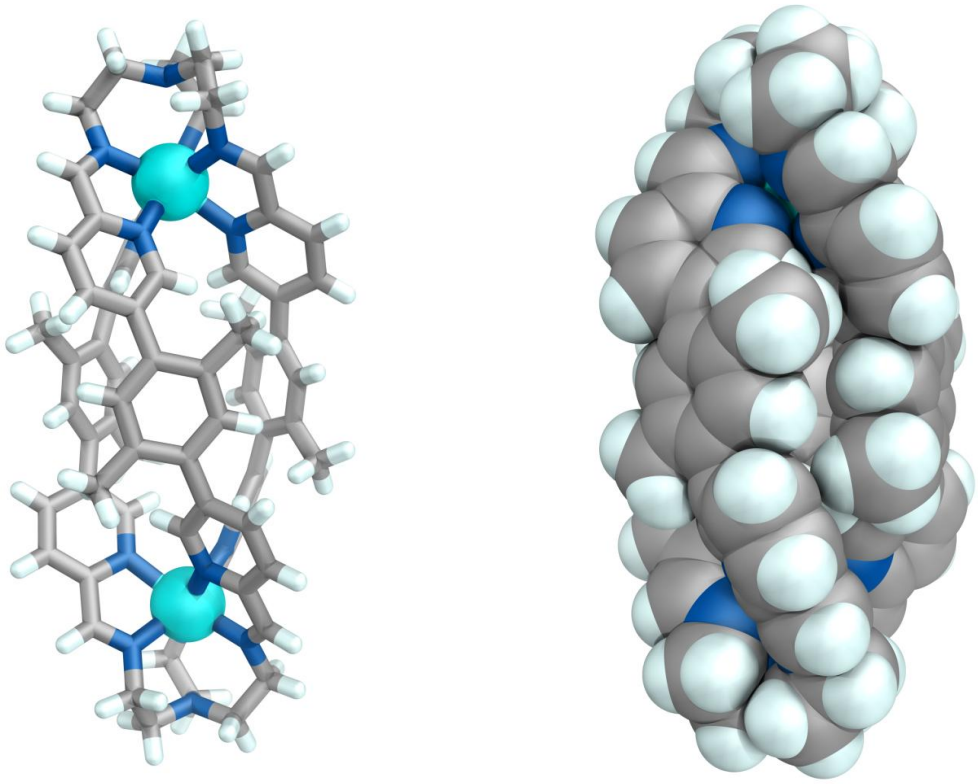

Figure S85. Two views of the cationic part of the crystal structure of helicate **Zn–8**, stick (*left*) and space-filling (*right*) representations. Counterions, solvents and disorder are omitted for clarity.

6.6 Crystallographic data and refinement details for tetrahedron ***Cd–12***

$[Cd_4L_6]\cdot 8OTf$

Formula $C_{152}H_{144}Cd_4F_{24}N_{28}O_{24}S_8$, M = 3909.02, Cubic, space group F -4 3 c (#219), a 34.3297(7), b 34.3297(7), c 34.3297(7) Å, V = 40459(2) $Å^3$, D_c 1.284 g cm^{-3}, Z 8, crystal size 0.170 by 0.160 by 0.160 mm, colour colourless, habit prism, temperature 180(2) K, λ(CuKα) 1.54178 Å, μ(CuKα) 4.817 mm^{-1}, $T(SADABS)_{min,max}$ 0.6306, 0.7528, $2\theta_{max}$ 133.57, *hkl* range -40 40, -38 40, -40 28, N 29643, N_{ind} 2961(R_{merge} 0.0287), N_{obs} 2668(I > 2σ(I)), N_{var} 149, residuals* $R1(F)$ 0.0400, $wR2(F^2)$ 0.1103, GoF(all) 1.043, $\Delta\rho_{min,max}$ -0.553, 0.254 e^- $Å^{-3}$.

*$R1 = \Sigma||F_o| - |F_c||/\Sigma|F_o|$ for $F_o > 2\sigma(F_o)$; $wR2 = (\Sigma w(F_o^2 - F_c^2)^2/\Sigma(wF_c^2)^2)^{1/2}$ all reflections

$w=1/[\sigma^2(F_o^2)+(0.0543P)^2+105.4221P]$ where $P=(F_o^2+2F_c^2)/3$

Refinement details| The crystals of $[Cd_4L_6]\cdot 8OTf$ were grown by diffusion of diisopropyl ether into an acetonitrile solution of the complex. The crystals immediately lost solvent after removal from the mother liquor and rapid handling prior to flash cooling in the cryostream was required to collect data. The asymmetric unit was found to contain one twelfth of a Cd_4L_4 assembly. The central phenyl ring of the ligand was modelled as disordered over a special position with the occupancy of each part fixed at 0.5 by symmetry. Some bond length restraints (DFIX) were required in order to obtain a reasonable model for the organic portion of the structure and thermal parameter restraints (SIMU, RIGU) were applied to all atoms except for cadmium. The anions and solvent within the lattice were significantly disordered and despite numerous attempts at modelling, including with rigid bodies no satisfactory model for the electron-density associated with them could be found. Therefore the SQUEEZE[19] function of PLATON[20] was employed to account for these highly disordered solvent and anions, which gave a potential solvent accessible void of 17857 $Å^3$ per unit cell (a total of approximately 3768 electrons). Since the diffuse solvent molecules could not be assigned conclusively to acetonitrile or diisopropyl ether they were not included in the formula. Consequently, the molecular weight and density given above are likely to be underestimated.

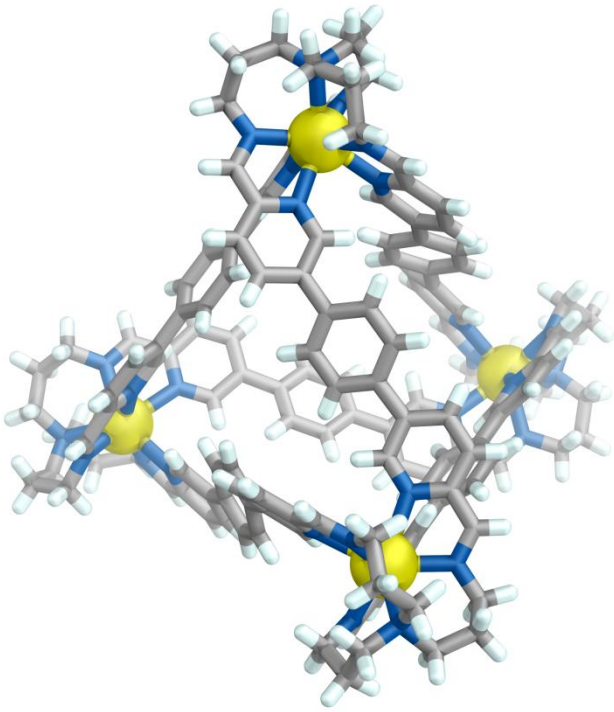

Figure S86. View of the cationic part of the crystal structure of tetrahedron **Cd–12**, as viewed down an edge. Counterions, solvents and disorder are omitted for clarity.

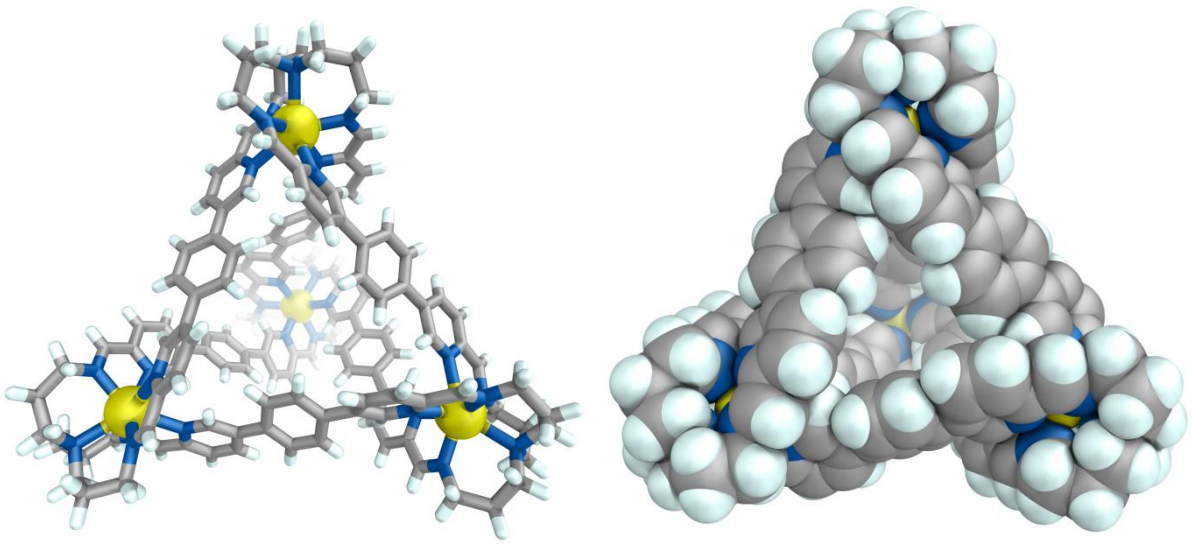

Figure S87. Two views of the cationic part of the crystal structure of tetrahedron **Cd–12**, as viewed down a face in stick (*left*) and space-filling (*right*) representations. Counterions, solvents and disorder are omitted for clarity.

*6.7 Crystallographic data and refinement details for tetrahedron **Cd–14***

$[Cd_4L_6]\cdot 7SbF_6\cdot OTf\cdot 4MeCN$

Formula $C_{153}H_{132}Cd_4F_{69}N_{32}O_3SSb_7$, M = 5111.81, Cubic, space group P 21 3 (#198), a 26.441(3), b 26.441(3), c 26.441(3) Å, V = 18487(6) $Å^3$, D_c 1.837 g cm^{-3}, Z 4, crystal size 0.006 by 0.005 by 0.004 mm, colour colourless, habit prism, temperature 100(2) K, λ(Synchrotron) 0.6889 Å, μ(Synchrotron) 1.448 mm^{-1}, T(Analytical)$_{min,max}$ 0.959411743808, 1.0, $2\theta_{max}$ 54.66, *hkl* range -34 35, -35 31, -35 28, N 148304, N_{ind} 15319(R_{merge} 0.1187), N_{obs} 13422(I > 2σ(I)), N_{var} 819, residuals* $R1(F)$ 0.0654, $wR2(F^2)$ 0.1983, GoF(all) 1.024, $\Delta\rho_{min,max}$ -2.718, 2.272 e^- $Å^{-3}$.

*$R1 = \Sigma||F_o| - |F_c||/\Sigma|F_o|$ for $F_o > 2\sigma(F_o)$; $wR2 = (\Sigma w(F_o^2 - F_c^2)^2/\Sigma(wF_c^2)^2)^{1/2}$ all reflections

$w=1/[\sigma^2(F_o^2)+(0.1637P)^2]$ where $P=(F_o^2+2F_c^2)/3$

Refinement details| The crystals of $[Cd_4L_6]\cdot 7SbF_6\cdot OTf\cdot 4MeCN$ were grown by diffusion of diethyl ether into an acetonitrile solution of $[Cd_4L_6]\cdot 8OTf$ containing excess $KSbF_6$. The crystals immediately lost solvent after removal from the mother liquor and rapid handling prior to flash cooling in the cryostream was required to collect data. The asymmetric unit was found to contain one third of a Cd_4L_4 assembly and associated counterions and solvent molecules. One anion lattice site was modelled as a disordered mixture of triflate and hexafluoroantimonate with bond length and thermal parameter restraints applied to the disordered moieties in order to facilitate a reasonable refinement. Thermal parameter restraints (SIMU, RIGU) were also applied to all atoms except for cadmium and antimony.

CheckCIF gives three B level alerts. These alerts all result from thermal motion and/or minor unresolved disorder of some anions.

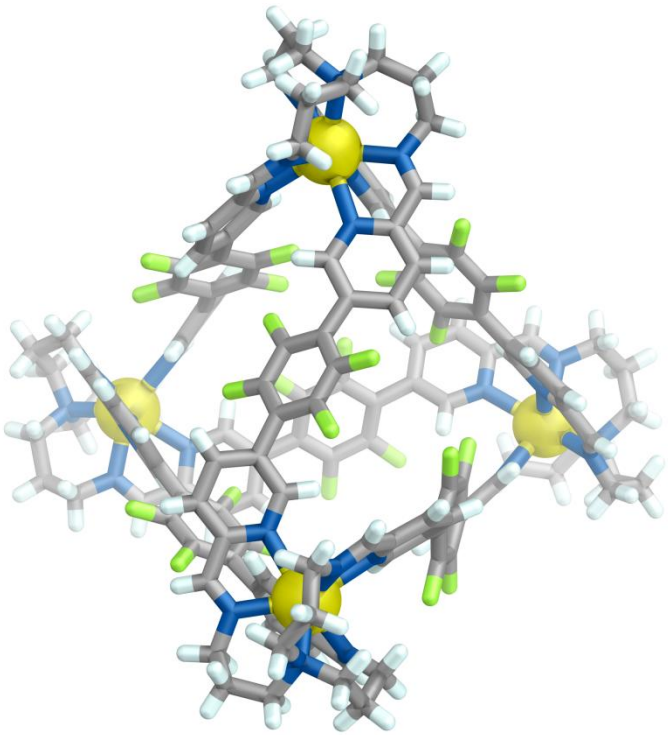

Figure S88. View of the cationic part of the crystal structure of tetrahedron **Cd–14**, as viewed down an edge. Counterions, solvents and disorder are omitted for clarity.

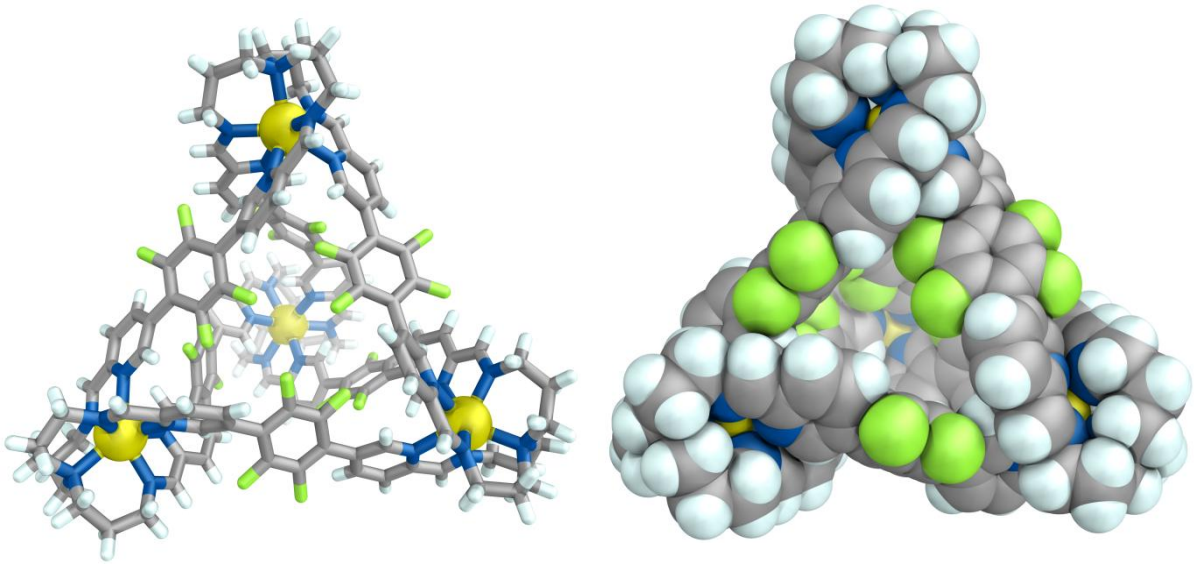

Figure S89. Two views of the cationic part of the crystal structure of tetrahedron **Cd–14**, as viewed down a face in stick (*left*) and space-filling (*right*) representations. Counterions, solvents and disorder are omitted for clarity.

7. Volume calculations

In order to determine the available void space within the water-soluble cubes, VOIDOO calculations based on their crystal structures were performed. We only carried out calculations[21] on the **Co-1** and **Ni-1** cubes since these systems remain intact in water solution unlike the **Zn-1** and **Cd-1** cubes. A virtual probe of 1.4 Å (set by default, water-sized) was employed, and the standard parameters tabulated below were used.

Maximum number of volume-refinement cycles |	30
Minimum size of secondary grid |	3
Grid for plot files |	0.1
Primary grid spacing |	0.1
Plot grid spacing |	0.2

The volume was thus calculated to be 1331 and 1324 $Å^3$ for the **Co-1** and **Ni-1** cubes, respectively. The void volume for the **Fe-1** cube was previously informed by our group.[3]

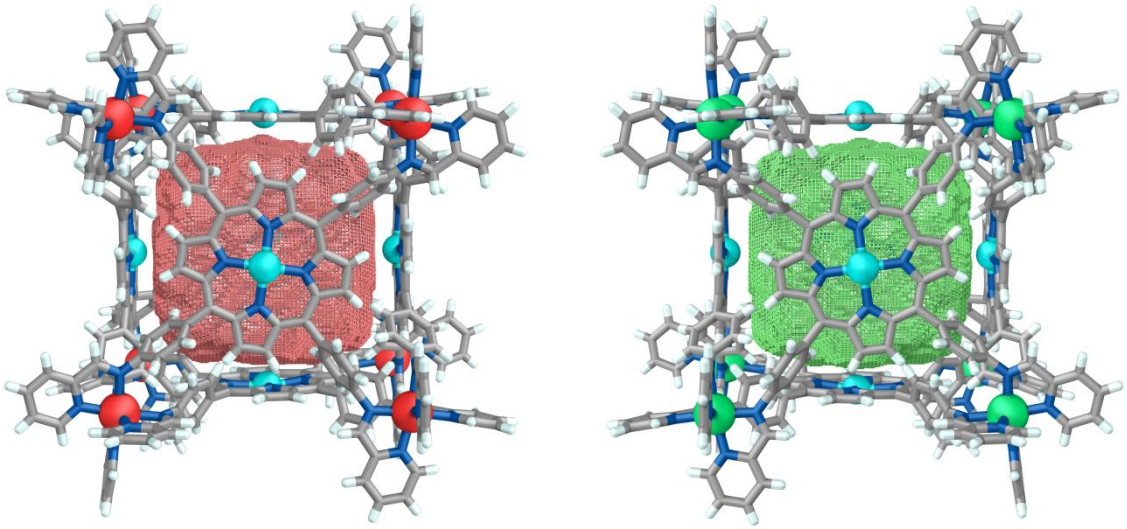

Figure S90. VOIDOO calculated void space (shown in mesh) within the **Co-1** (*left*) and **Ni-1** (*right*) cubes obtained from the corresponding crystal structures.

8. References

(1) I. A. Riddell, M. M. J. Smulders, J. K. Clegg, Y. R. Hristova, B. Breiner, J. D. Thoburn and J. R. Nitschke, *Nat. Chem.*, 2012, **4**, 751.

(2) F. Rizzuto and J. R. Nitschke, *Nat. Chem.*, 2017, **9**, 903.

(3) W. Meng, B. Breiner, K. Rissanen, J. D. Thoburn, J. K. Clegg and J. R. Nitschke, *Angew. Chem. Int. Ed.*, 2011, **50**, 3479.

(4) R. A. Bilbeisi, J. K. Clegg, N. Elgrishi, X. de Hatten, M. Devillard, B. Breiner, P. Mal and J. R. Nitschke, *J. Am. Chem. Soc.*, 2012, **134**, 5110.

(5) J. K. Clegg, J. Cremers, A. J. Hogben, B. Breiner, M. M. J. Smulders, J. D. Thoburn and J. R. Nitschke, *Chem. Sci.*, 2013, **4**, 68.

(6) A. M. Castilla, N. Ousaka, R. A. Bilbeisi, E. Valeri, T. K. Ronson and J. R. Nitschke, *J. Am. Chem. Soc*., 2013, **135**, 17999.

(7) Y. R. Hristova, M. M. J. Smulders, M. M. J.; Clegg, J. K.; Breiner, B.; Nitschke, J. R. *Chem. Sci.*, 2011, **2**, 638.

(8) S. Ma, M. M. J. Smulders, Y. R. Hristova, J. K. Clegg, T. K. Ronson, S. Zarra and J. R. Nitschke, *J. Am. Chem. Soc.*, 2013, **135**, 5678.

(9) N. Ousaka, S. Grunder, A. M. Castilla, A. C. Whalley, J. F. Stoddart and J. R. Nitschke, *J. Am. Chem. Soc.*, 2012, **134**, 15528.

(10) M. Kieffer, B. S. Pilgrim, T. K. Ronson, D. A. Roberts, M. Aleksanyan and J. R. Nitschke, *J. Am. Chem. Soc*., 2016, **138**, 6813.

(11) T. K. Ronson, W. Meng and J. R. Nitschke, *J. Am. Chem. Soc.*, 2017, **139**, 9698.

(12) I. A. Riddell, Y. R. Hristova, J. K. Clegg, C. S. Wood, B. Breiner and J. R. Nitschke, *J. Am. Chem. Soc.*, 2013, **135**, 2723.

(13) D. Allan, H. Nowell, S. Barnett, M. Warren, A. Wilcox, J. Christensen, L. Saunders, A. Peach, M. Hooper, L. Zaja, S. Patel, L. Cahill, R. Marshall, S. Trimnell, A. Foster, T.

Bates, S. Lay, M. Williams, P. Hathaway, G. Winter, M. Gerstel, R. A. Wooley, *Crystals*, 2017, **7**, 336.

(14) Bruker-Nonius, *APEX*, *SAINT and XPREP*. Bruker AXS Inc.: Madison, Wisconsin, USA, 2013.

(15) (a) Collaborative Computational Project, N., The CCP4 suite: programs for protein crystallography. *Acta Cryst.*, 1994, **D50**, 760. (b) P. Evans, *Acta Cryst.*, 2006, **D62**, 72. (c) G. Winter, *J. Appl. Crystallogr.*, 2010, **43**, 186.

(16) L. Farrugia, *J. Appl. Crystallogr.*, 2012, **45**, 849.

(17) G. Sheldrick, *Acta. Cryst.*, 2015, **A71**, 3.

(18) G. M. Sheldrick, *Acta. Cryst.*, 2015, **C71**, 3.

(19) P. van der Sluis, A. L. Spek, *Acta Cryst.*, 1990, **A46**, 194.

(20) A. L. Spek, *PLATON: A Multipurpose Crystallographic Tool*. Utrecht University: Utrecht, The Netherlands, 2008.

(21) G. J. Kleywegt, T. A. Jones, *Acta Cryst.*, 1994, **D50**, 178.